UC Berkeley
UC Berkeley Electronic Theses and Dissertations

Title
Synthesis, Reactivity and Catalytic Applications of Two-Coordinate First Row Transition Metal Complexes

Permalink
https://escholarship.org/uc/item/7mh1k115

Author
Lipschutz, Michael Isaac

Publication Date
2015

Peer reviewed|Thesis/dissertation

eScholarship.org Powered by the California Digital Library
University of California

Synthesis, Reactivity and Catalytic Applications of Two-Coordinate First Row Transition Metal Complexes

by

Michael Isaac Lipschutz

A dissertation submitted in partial satisfaction of the
requirements for the degree of
Doctor of Philosophy
in
Chemistry
in the
Graduate Division
of the
University of California, Berkeley

Committee in charge:
Professor T. Don Tilley, Chair
Professor K. Peter C. Vollhardt
Professor Richard A. Andersen
Professor Alexander Katz

Spring 2015

Abstract
Synthesis, Reactivity and Catalytic Applications of Two-coordinate
First Row Transition Metal Complexes

Michael Isaac Lipschutz
Doctor of Philosophy in Chemistry
University of California, Berkeley
Professor T. Don Tilley, Chair

Chapter 1. A strictly two-coordinate nickel(II) bis(amido) complex has been prepared and its reactivity towards a variety of small molecules is described. $Ni[N(SiMe_3)(DIPP)]_2$ reacts with DMAP and acetonitrile to form T-shaped three-coordinate compounds, and preliminary results show that $Ni[N(SiMe_3)(DIPP)]_2$ is a catalyst for the hydrosilation of olefins with secondary silanes at ambient temperature. Lipschutz, M. I.; Tilley, T. D. *Chem. Commun.* **2012**, *48*, 7146.

Chapter 2. A structurally persistent bis-amido ligand framework capable of supporting nickel compounds in three different oxidation states has been identified. A highly unusual, isolable Ni(III) alkyl species has been prepared and characterized via a rare example of a two-electron oxidative addition of MeI to Ni(I). Lipschutz, M. I.; Yang, X.; Chatterjee, R.; Tilley, T. D. *J. Am. Chem. Soc.* **2013**, *135*, 15298.

Chapter 3. Recently, the development of more sustainable catalytic systems based on abundant first-row metals, especially nickel, for cross-coupling reactions has attracted significant interest. One of the key intermediates invoked in these processes is a Ni^{III}–alkyl species, but no such species that is part of a competent catalytic cycle has yet been isolated. Herein, we report a carbon–carbon cross-coupling system based on a two-coordinate Ni^{II}–bis(amido) complex in which a Ni^{III}–alkyl species can be isolated and fully characterized. This study details compelling experimental evidence of the role played by this Ni^{III}–alkyl species as well as those of other key Ni^{I} and Ni^{II} intermediates. The catalytic cycle described herein is also one of the first examples of a two-coordinate complex that competently catalyzes an organic transformation, potentially leading to a new class of catalysts based on the unique ability of first-row transition metals to accommodate two-coordinate geometries. Lipschutz, M. I.; Tilley, T. D. *Angew. Chem. Int. Ed.* **2014**, *53*, 7290.

Chapter 4. A convenient method of preparing two- and three-coordinate Ni(I) complexes of the form $L–Ni^{I}–X$ ($L = P^tBu_3$, P^iPr_3, DPPE, NHC; $X = -N(SiMe_3)(2,6\text{-}^iPr\text{-}C_6H_3)$, $-O(2,6\text{-}^tBu_2\text{-}4\text{-}Me\text{-}C_6H_2)$) is reported. Protonation of the easily prepared anionic Ni(I) bis(amido) compound $K\{Ni[N(SiMe_3)(2,6\text{-}^iPr\text{-}C_6H_3)]_2\}$ in the presence of an appropriate L-type ligand results in loss of $HN(SiMe_3)(2,6\text{-}^iPr\text{-}C_6H_3)$ and trapping of the resulting neutral Ni(I)-amido fragment to yield neutral, paramagnetic, two- and three-coordinate Ni(I) complexes. Protonation by the bulky phenol $HO(2,6\text{-}^tBu_2\text{-}4\text{-}Me\text{-}C_6H_2)$ results in loss of the second amido moiety and trapping by the resulting phenoxide to yield $Ni(I)\text{-}O(2,6\text{-}^tBu_2\text{-}4\text{-}Me\text{-}C_6H_2)$ complexes. The hapticity of the phenoxide ligand is influenced by the π-accepting ability of L. Where $L = P^tBu_3$, a poor π-acceptor, the phenoxide acts as a π-acceptor and adopts a η^5-bonding mode through dearomatization of the phenyl ring. When L = NHC, a competent π-acceptor, the phenoxide acts

as a π-donor, adopting a η^1-bonding mode through the O atom. The modular nature of this synthetic strategy allows variation of both the L- and X-type ligands of the complex in a stepwise fashion and should be extendable to a wide variety of ligand types for new Ni(I) complexes. Lipschutz, M. I.; Tilley, T. D. *Organometallics* **2014**, *33*, 5566.

Chapter 5. The amido ligand –N(Si^{i}Pr$_3$)DIPP (DIPP = 2,6-diisopropylphenyl) has been used to prepare two-coordinate complexes of Cr^{I}, Cr^{II}, and Cr^{III}. The Cr^{II} species was converted to a three-coordinate Cr^{III} iodide complex, which can be used to access a stable Cr^{III} methyl species. Cai, I. C.; Lipschutz, M. I.; Tilley, T. D. *Chem. Commun.* **2014**, *50*, 13062.

Chapter 6. The synthesis of the first heteroleptic, two-coordinate Fe^{I} complex IPr–Fe–N(SiMe$_3$)DIPP (IPr = 1,3-bis(2,6-diisopropylphenyl)imidazol-2-ylidene; DIPP = 2,6-^{i}Pr$_2$-C$_6$H$_3$) is reported. Protonation of the Fe^{II} bis(amido) compound Fe[N(SiMe$_3$)DIPP]$_2$ followed by addition of IPr and reduction by potassium graphite in a one-pot reaction results in good yields of IPr–Fe–N(SiMe$_3$)DIPP. The redox activity of IPr–Fe–N(SiMe$_3$)DIPP and comparison with its reduction product by ^{57}Fe Mössbauer spectroscopy is discussed, and the reduction was found to be metal-based rather than ligand-based. The activity of IPr–Fe–N(SiMe$_3$)DIPP towards the catalytic cyclotrimerization of terminal and internal alkynes is described.

Synthesis, Reactivity and Catalytic Applications of Two-coordinate First Row Transition Metal Complexes

Table of Contents

Table of Contents i

Acknowledgements iii

Chapter 1. Synthesis and Reactivity of a Conveniently Prepared Two-coordinate Bis(amido) Nickel(II) Complex 1
- Introduction 2
- Results and Discussion 2
- Conclusion 6
- Experimental 6
- References 9
- Appendix 11

Chapter 2. A Structurally Rigid Bis(amido) Ligand Framework in Low-Coordinate Ni(I), Ni(II) and Ni(III) Analogues Provides Access to a Ni(III) Methyl Complex *via* Oxidative Addition 16
- Introduction 17
- Results and Discussion 17
- Conclusion 21
- Experimental 21
- References 25
- Appendix 27

Chaper 3. Carbon-carbon cross-coupling reactions catalyzed by a two-coordinate nickel(II) bis(amido) complex *via* observable Ni^{I}, Ni^{II} and Ni^{III} intermediates 43
- Introduction 44
- Results and Discussion 44
- Conclusion 50
- Experimental 50
- References 55
- Appendix 57

Chapter 4. A Useful Method for the Preparation of Low-coordinate Ni(I) Complexes *via* Transformations of the Ni(I) Bis(amido) Complex $K\{Ni[N(SiMe_3)(2,6\text{-}^{i}Pr_2\text{-}C_6H_3)]_2\}$ 63
- Introduction 64
- Results and Discussion 64
- Conclusion 69
- Experimental 70
- References 73
- Appendix 75

Chapter 5. A Bis(amido) Ligand Set That Supports Two-coordinate Chromium in the +1, +2, and +3 Oxidation States 87
Introduction 88
Results and Discussion 88
Conclusion 93
Experimental 93
References 97
Appendix 100

Chapter 6. Synthesis, Characterization and Alkyne Trimerization Catalysis of a Heteroleptic Two-Coordinate Fe^{I} Complex 113
Introduction 114
Results and Discussion 114
Conclusion 122
Experimental 122
References 126
Appendix 128

Acknowledgements

Research is rarely, if ever, a solitary endeavor. Many people contributed greatly to my success in graduate school and I would like to acknowledge their contributions here (in no particular order):

My advisor, Professor T. Don Tilley: in my time at Berkeley, he afforded me tremendous freedom to pursue the projects in which I was interested and to follow the chemistry where it led me. Without this unusual level of flexibility, none of the two-coordinate research would have been possible. Additionally, his unique perspectives on my research forced me to think outside the box (sometimes very far outside) on some key questions.

Rosemary Tilley: as Don's administrative assistant, her tireless efforts kept the group running, us paid, chemicals on the shelves, nitrogen in the dewars and graduate students from getting lost in the massive bureaucracy that is UC Berkeley. Her tremendous powers of persuasion and resolve also tamed a rouge agent of the National Park Service and for this I am especially greatful.

Dr. Meg Fasulo: as a senior graduate student when I joined the group, she was an invaluable resource for me. She taught me most of what I know about X-ray crystallography and her institutional knowledge about the department and about Berkeley helped me avoid many pitfalls and made my experience here a positive one.

Dr. Antonio DiPasquale: as head of the X-ray crystallographic facility, he taught me many great tricks and helped solve some really difficult and strange crystal structures.

Allegra Liberman-Martin: inorganic chemistry for the color-blind is no picnic. Allegra provided a consistent basis for determining the color of countless compounds, solutions and reaction mixtures. All reports of colors in the range of green, blue or purple in the following chapters are based on her assessment.

Marisa Whitchurch, Javier Farjado and Yuyang Dong: in my time at Berkeley, I have had the opportunity to mentor these three undergraduate students while they performed their own independent research projects. Mentoring these students provided me with valuable experience communicating esoteric scientific concepts and teaching similarly esoteric laboratory skills.

My wife, Kourtney Imburgia: As a "normal person" (read: non-chemist), she has shown remarkable tolerance and patience with the crazy hours and strange habits associated with graduate school. Without her support I probably would've burnt out some time ago.

The Parking and Transportation department: I worked an uncountable number of late nights in the lab by parking illegally behind the Chemistry department and were it not for their negligence in writing tickets, I would not have finished my PhD.

Finally, Birch, Gigi and Feynman: they are cats. They are warm and fuzzy.

Chapter 1. Synthesis and Reactivity of a Conveniently Prepared Two-coordinate Bis(amido) Nickel(II) Complex

INTRODUCTION

Two-coordinate metal complexes are a relatively small class of compounds with unusual structural, electronic, and chemical properties.[1] The low coordination number and inherently electron deficient nature of these compounds suggest that they should display a rich reaction chemistry associated with activations and conversions of a wide array of substrates. However, chemical reactions of two-coordinate complexes have not been extensively investigated. Low-coordinate complexes have been shown to mediate interesting chemical transformations such as nitrene- and phosphinidine-group transfer to ethylene,[2] and the activation of small molecules such as N_2O.[3] Two-coordinate compounds have also been shown to activate CO_2.[4] Most importantly, two-coordinate bis(amido) $M[N(SiMe_3)_2]_2$ complexes of first row metals have found wide utility as convenient starting materials for inorganic and organometallic compounds.[5] Metal bis(amido) complexes are also used as precursors in nanoparticle synthesis.[6] In these laboratories, the recent discovery that $Fe[N(SiMe_3)_2]_2$ is a catalyst precursor for the efficient hydrosilation of organic carbonyl compounds[7] prompted further investigations of the reaction chemistry of two-coordinate amido complexes of the first row metals.

While two-coordinate, bis(amido) complexes of iron, cobalt and manganese are well known,[8] related nickel(II) species have only recently been reported.[9] One such compound, $Ni\{HN[2,6\text{-}(2,6\text{-diisopropylphenyl})]\}_2$, may be described as pseudo-four-coordinate, in that the solid-state structure contains two additional close contacts between the nickel center and aryl groups of the amido ligand.[9a] Herein we report the synthesis and characterization of $Ni[N(SiMe_3)DIPP]_2$ (**1**), a strictly two-coordinate nickel(II) bis(amido) complex, its reactivity towards small molecules and preliminary results on its activity as a catalyst in the hydrosilation of olefins.

RESULTS AND DISCUSSION

Compound **1** was synthesized by reaction of $Ni(DME)Br_2$ with 1.9 equiv of $Li[N(SiMe_3)(2,6\text{-}^iPr_2C_6H_3)]$ in benzene over 6 hours at ambient temperature. Workup of the reaction mixture afforded dark purple crystals of **1** from hexanes in 86% yield. The X-ray analysis of **1** (Fig. 1) reveals a perfectly linear structure, with a crystallographically imposed 180º N–Ni–N bond angle. The 1.7987(11) Å Ni–N bond length is the shortest Ni–N(amido) distance yet observed. For comparison, related compounds bearing bulky terphenyl groups, synthesized by Cui and Power, possess Ni–N bond lengths of 1.818(3) Å and 1.8284(15) Å, respectively.[9a,b] The two amido ligands adopt an eclipsed configuration whereby both substituents on the two trigonal planar nitrogen atoms occupy the same plane. This is in contrast to the staggered, allene-like structure adopted by the similar iron compound $Fe[N(SiMe_3)_2]_2$ in its monomeric state.[8] The eclipsed conformation is also adopted by the Ni(II) bis(amido) complexes of Cui and Power and appears to be the most stable, even in the absence of secondary interactions between the metal and pendent aryl groups on the ligand. The ^1H NMR spectrum exhibits strongly paramagnetic shifts that are assigned by integration (see Experimental Section). The magnetic moment of 2.67 μB, determined by Evans's method,[10] is consistent with two unpaired electrons per nickel.

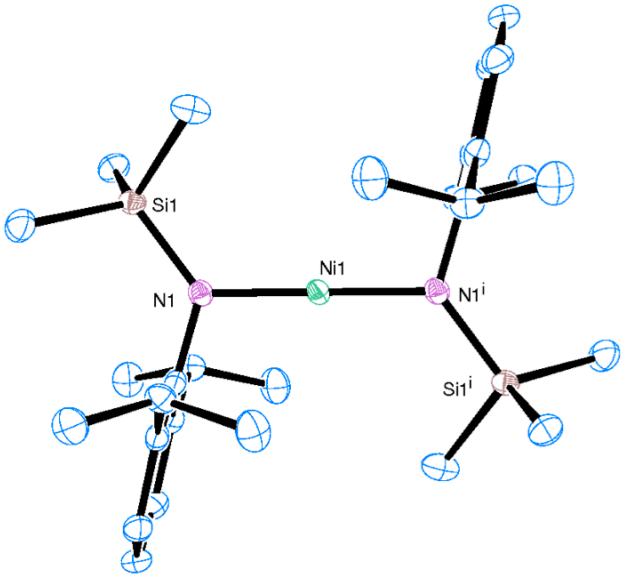

Figure 1. ORTEP diagram of **1**. Thermal ellipsoids shown at 50% probability. Bond lengths (Å) and angles (deg): Ni-N = 1.7987(11); N-Ni-N = 180.00(8).

Compound **1** reacts with the nitrogen donor compounds p-dimethylaminopyridine (**DMAP**) and acetonitrile to produce three-coordinate, nearly T-shaped complexes Ni[N(SiMe$_3$)DIPP]$_2$(DMAP) (**2**) and Ni[N(SiMe$_3$)DIPP]$_2$(MeCN) (**3**), respectively (Fig. 2). Reaction of 1 with 1 equiv of DMAP in pentane for 20 minutes at ambient temperature, and subsequent evaporation of the solvent results in quantitative formation of the analytically pure compound **2**. Recrystallization from pentane afforded **2** as red crystals in 89% yield.

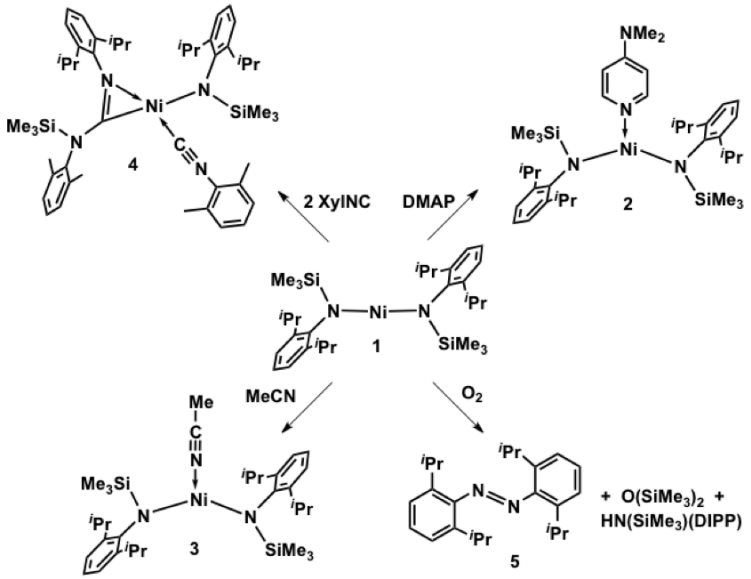

Figure 2. Reactions of Ni[N(SiMe$_3$)DIPP]$_2$ (**1**).

The structures of both **2** and **3** exhibit significant distortions from an ideal trigonal planar geometry. The N–Ni–N bond angles in these compounds are 155.07(7)º and 161.26(6)º, respectively, resulting in a nearly T-shaped coordination environment (Fig. 3). Interestingly, despite the added steric hindrance, the eclipsed conformation of the two amido substituents in compound **1** is almost entirely conserved in both **2** and **3**. Furthermore, the plane occupied by the substituents of both amido ligands contains the ligand field, which would seem to maximize steric interactions between the three ligands on the metal center and their substituents.

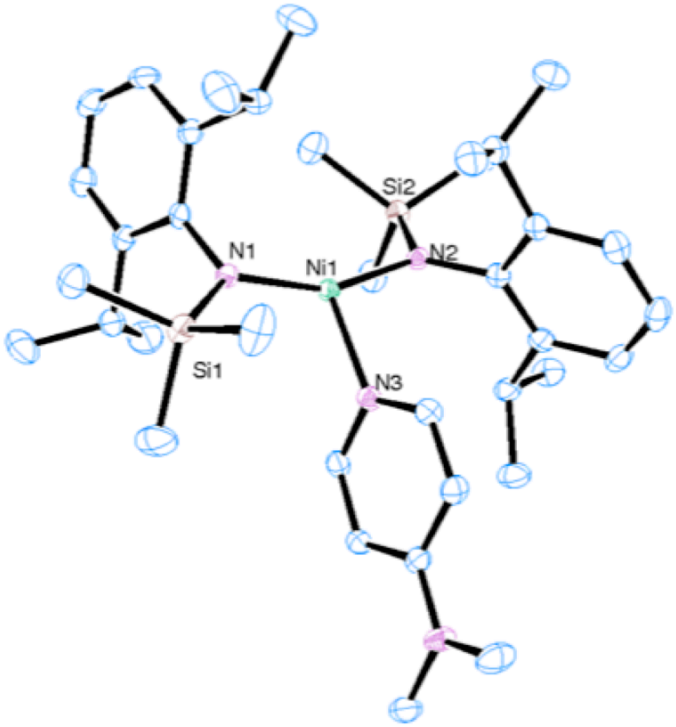

Figure 3. ORTEP diagram of **2**. Thermal ellipsoids shown at 50% probability. Bond lengths (Å) and angles (deg): Ni-N1 = 1.8614(15); Ni-N2 = 1.8717(15); Ni-N3 = 2.0187(16); N1-Ni-N2 = 155.07(7); N1-Ni1-N3 = 103.71(6); N2-Ni1-N3 = 100.47(6).

Reaction of compound **1** with 2 equiv of 2,6-dimethylphenylisocyanide in benzene at ambient temperature over 30 minutes resulted in formation of the diamagnetic insertion product **4** in 96% yield, as determined by ^{1}H NMR spectroscopy (Fig. 4). Reaction of **1** with 1 equiv of 2,6-dimethylphenylisocyanide led to the formation of 0.5 equiv of **4** and unreacted starting material. Interestingly, the product arises from insertion of an isonitrile into an Ni–N bond, accompanied by cleavage of a Ni–Si bond via 1,3-migration of the trimethylsilyl group from the amido nitrogen to a nitrogen atom originating from the isonitrile reactant (Scheme 1). The diamagnetic nature of **4** suggests that the structure is best regarded as a distorted, square planar Ni(II) d^8 species. The coordinated C–N bond distance is 1.278(2) Å, which is slightly longer than expected for a C–N double bond, but somewhat shorter than similar, less sterically crowded ligands in related insertion products of zirconium (1.299–1.315 Å).[11] While there is significant

double bond character between the carbon and nitrogen bound to the metal center, the π-system of that bond is oriented perpendicular to the plane formed by the carbon, nitrogen and nickel atoms, resulting in no interaction between the π-system and the metal center. Rather, the ligand is a bidentate XL-type donor, and isoelectronic with an acyl group.

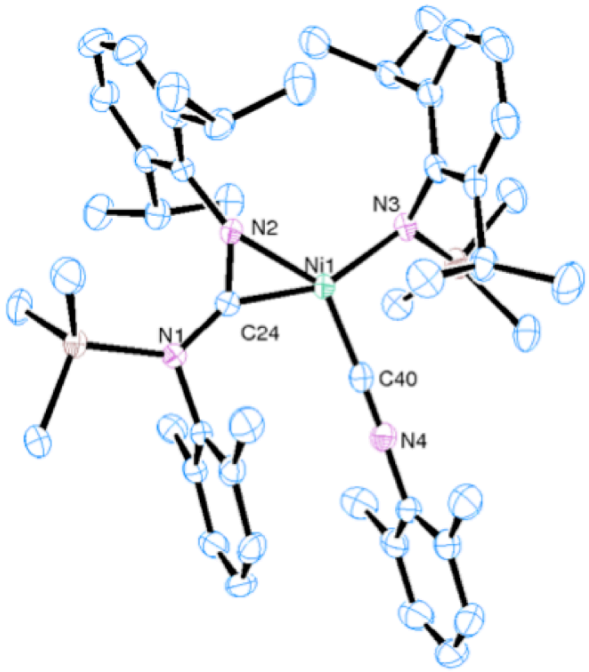

Figure 4. ORTEP diagram of **4**. Thermal ellipsoids shown at 50% probability. Bond lengths (Å) and angles (deg): Ni1-N2 = 1.9699(16); Ni1-C24 = 1.8181(19); N2-C24 = 1.278(2); N2-Ni1-C24 = 39.16(7).

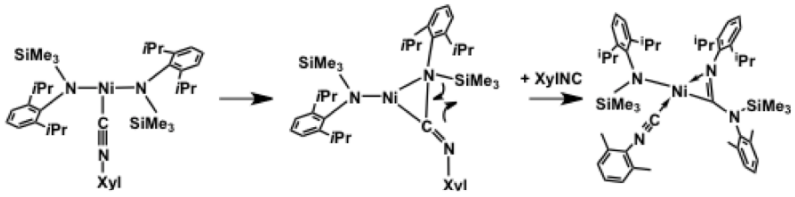

Scheme 1. Formation of insertion product **4**.

Reactions of bis(silylamido) complexes of Co and Fe with oxygen have been utilized in effective preparations of metal oxide nanoparticles.[6] In this context, the stoichiometric reaction of **1** with dioxygen, which also results in N–Si bond cleavage, was examined. Reaction of **1** under 1 atm of O_2 (99.99% pure) produced a mixture of the amine $HN(SiMe_3)DIPP$ and the diazo compound $(2,6\text{-}^{i}Pr_2C_6H_3)_2N_2$ (**5**) in an approximately 4 to 1 molar ratio (by ^1H NMR spectroscopy). The diazo compound was characterized by X-ray diffraction, NMR spectroscopy and high-resolution mass spectrometry.

Formation of the diazo compound is accompanied by loss of $-SiMe_3$ groups to form 0.5 equiv of $(Me_3Si)_2O$ per equivalent of **5** (as determined by ^1H and ^{13}C NMR spectroscopy) and an insoluble brown powder. This powder proved difficult to characterize, due to its insolubility in all solvents including 6M HCl. Infrared spectroscopy revealed no notable features and the material was determined to be amorphous by powder XRD. Elemental analysis (CHN) showed that the powder contained carbon, nitrogen and hydrogen in a ratio which closely matches that of a $-N(SiMe_3)(DIPP)$ group (C, 39.08%; H, 6.30%; N, 3.29%) and the observed stoichiometry is consistent with the incorporation of one amido group per Ni into this powder. Reaction of **1** with 1 equivalent of O_2 per Ni center resulted in incomplete consumption of the starting material and a mixture of the free amine and **5** as before, but in an approximately 7 to 1 ratio. Presumably, the nitrogen-bound proton of the observed $HN(SiMe_3)DIPP$ product arises from the amido moiety which becomes incorporated into the insoluble powder. Further, based on the increase in the production of the amine relative to the diazo product when using sub-stoichiometric amounts of oxygen, it seems likely that the amine is formed initially, and is subsequently oxidized to form the diazo compound **5**. This oxidation may be catalyzed by the transient Ni species remaining from initial reaction with oxygen before formation of the insoluble Ni-containing material occurs.

Given the observed activity of $Fe[N(SiMe_3)_2]_2$ as a catalyst for the hydrosilation of carbonyl compounds,[7] complex **1** was investigated as a catalyst for the hydrosilation of olefins with secondary silanes. Reaction of **1** with 55 equivalents of 1-octene and 50 equivalents of diphenylsilane in d_6-benzene at room temperature over 2 hours resulted in formation of the anti-Markovnikov addition product (n-octyl)diphenylsilane in >95% yield with no observed isomerization of the olefin to internal isomers (eqn (1)). Ongoing investigations are addressing the scope, utility and mechanism of this reaction type in various hydrosilations.

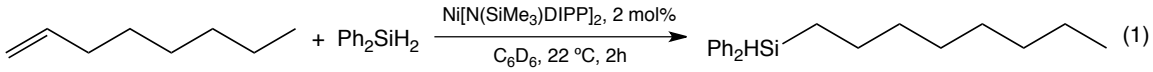

(1)

CONCLUSION

In summary, **1** represents a stable, conveniently prepared bis(amido) complex containing two-coordinate nickel(II). Initial reactivity studies indicate that **1** mediates several interesting chemical transformations. These results should be of use in further investigations of **1** as a precursor to a variety of nickel-based compounds, catalysts and materials.

EXPERIMENTAL

General Considerations. Unless stated otherwise, all reactions and procedures were carried out in a VAC Atmosphere Nexus glovebox or using standard Schlenk techniques under a nitrogen atmosphere. Solvents were received from Sigma Aldrich, degassed and dried using a VAC Atmosphere Solvent Purifier system and stored over 3Å molecular sieves. Prior to drying, toluene, benzene and pentane were treated to remove thiophenes and olefins as appropriate, using standard techniques.[12] Acetonitrile was dried by stirring over CaH_2 and was then distilled under a nitrogen atmosphere. C_6D_6 was purchased from Cambridge Isotope Laboratories, dried

over Na/K alloy, and then degassed by several freeze-pump-thaw cycles. All silanes were purchased from Gelest, stored under nitrogen and used as received. 2,6-dimethylphenylisocyanide and 4-(N,N-dimethylamino)pyridine were purchased from Sigma Aldrich and used as received. Oxygen gas was purchased from Praxair and used without additional purification or drying. Lithium (trimethylsilyl)(2,6-diisopropylphenyl) amide[13] was prepared according to a literature procedure. Molecular sieves were activated by evacuation overnight at approximately 200ºC. GC-MS analysis was performed using an Agilent Technologies 6890N GC system equipped with an HP-5MS column and an Agilent Technologies 5973 Network Mass Selective detector. All NMR spectra were collected at ambient temperature (ca. 23°C) on Bruker AVB-400, AV-500, AV-600 or AVQ-400 NMR spectrometers equipped with a 5 mm BB probe, as appropriate and referenced to the residual proteo solvent signals. Solution magnetic susceptibilities were determined by ^{1}H NMR spectroscopy using Evans's method.[10] X-ray analyses were carried out at UC Berkeley CHEXRAY crystallographic facility. Measurements of **1-5** were made on an APEX CCD area detector with graphite-monochromated Mo Kα radiation (λ = 0.71073 Å). IR spectra were collected on a Bruker Alpha-P FT-IR Spectrometer equipped with a "Platinum" Attenuated Total Reflection sample module.

Ni[N(SiMe$_3$)DIPP]$_2$ (1). To a 100 mL round bottom Schlenk flask was added lithium (trimethylsilyl)(2,6-diisopropylphenyl)amide (1.005 g, 3.935 mmol) and nickel(II) bromide dimethoxyethane adduct (0.640 g, 2.077 mmol). Approximately 25 mL of benzene was added to form a dark suspension that quickly became dark purple. The mixture was stirred at ambient temperature for 6 h. The volatile components were then removed under reduced pressure, and to the resulting residue was added 50 mL of hexanes and the mixture was stirred for 1 h. The mixture was filtered, and the filtrate cooled to -78°C for 17 h, yielding 0.945 g (86%) of **1** as dark purple block-like crystals. ^{1}H NMR (400 MHz, C_6D_6, 23°C) δ 65.63 (m-Ar-*H* or Me_2C-*H*, 4H), 56.28 (m-Ar-*H* or Me_2C-*H*, 4H), 41.27 (HC(C*H*$_3$)$_2$, 12H), 11.79 (HC(C*H*$_3$)$_2$, 12H), 6.40 (Si(C*H*$_3$)$_3$, 18H), -91.70 (p-Ar-*H*, 2H). μ_{eff} = 2.67 μB (C_6D_6, 22°C, Evans's method). MP = 164.5-166ºC. Anal. Calcd. for $C_{30}H_{52}N_2NiSi_2$: C, 64.85%; H, 9.43%; N, 5.04%. Found: C, 64.96%; H, 9.26%; N, 4.98%. Crystals suitable for X-ray diffraction were obtained from the workup described above.

Ni[N(SiMe$_3$)DIPP]$_2$(DMAP) (2). To a 20 mL scintillation vial was added **1** (0.0350 g, 0.063 mmol) which was dissolved in approximately 4 mL of pentane to form a dark purple solution. To this solution was added DMAP (4-(N,N-dimethylamino)pyridine) (0.0077 g, 0.063 mmol) and the mixture was manually shaken for approximately 3 min, during which the color changed to dark red. The volatile components were removed under reduced pressure and the resulting red solid residue was extracted with 2 mL of pentane and the extracts were filtered and placed in the freezer at -35ºC overnight, yielding 0.038 g (89%) of **2** as dark red crystals. μ_{eff} = 3.07 μB (C_6D_6, 21°C, Evans's method) Anal. Calcd. for $C_{37}H_{62}N_4NiSi_2$: C, 65.57%; H, 9.22%; N, 8.27%. Found: C, 65.42%; H, 9.25%; N, 8.19%. Crystals suitable for X-ray diffraction were obtained from the workup described above. ^{1}H NMR spectra of **2** exhibited extremely broad signals that were difficult to integrate. We attribute this to the paramagnetism of **2**.

Ni[N(SiMe$_3$)DIPP]$_2$(MeCN) (3). To a 20 mL scintillation vial was added **1** (0.0996 g, 0.174 mmol) which was dissolved in approximately 4 mL of pentane forming a dark purple solution. To this solution was added 10 drops of acetonitrile and the solution was stirred

vigorously for 20 min, during which the color changed to dark red. The volatile components were removed under reduced pressure and the resulting red solid residue was redissolved in approximately 1 mL of hexanes and the resulting solution was placed in the freezer at -20ºC overnight, yielding 0.080g (77%) of **3** as dark red crystals. μ_{eff} = 2.86 μB (C_6D_6, 20°C, Evans's method) Anal. Calcd. for $C_{32}H_{55}N_3NiSi_2$: C, 64.42%; H, 9.29%; N, 7.04%. Found: C, 64.47%; H, 9.26%; N, 6.96%. IR (neat solid, cm^{-1}) 2959 m, 1424 m sh, 1310 w sh, 1239 m sh, 1189 m sh, 899 m sh, 878 m sh, 822 s, 783 s sh, Crystals suitable for X-ray diffraction were obtained from the workup described above. ^{1}H NMR spectra of **3** exhibited extremely broad signals that were difficult to integrate. We attribute this to the paramagnetism of **3**.

[N,N-(SiMe$_3$)(2,6-dimethylphenyl)-N`-(DIPP)carbamimidoyl]Ni[N(SiMe$_3$)(DIPP)][CN(2,6-dimethylphenyl)] (4). To a 20 mL scintillation vial was added **1** (0.100 g, 0.180 mmol), 2,6-dimethylphenylisocyanide (0.0472 g, 0.360 mmol) and 8 mL of benzene, to form a dark red solution. The mixture was stirred at ambient temperature for 30 min, during which the color changed to a lighter red. The volatile components were removed under reduced pressure, yielding 0.147 g of **4** as a red powder that was 96% pure by ^{1}H NMR spectroscopy. Extremely pure samples of **4** were obtained by recrystallization of this red powder from 2 mL of hexanes at -35°C, to yield 0.032 g (22%) of **4** as red crystals. ^{1}H NMR (500 MHz, C_6D_6, 23°C) δ 7.04 (d, 7.4Hz, 2H, Ar-*H*), 6.94 (m, 4H, Ar-*H*), 6.71 (m, 1H, Ar-*H*), 6.63 (m, 4H, Ar-*H*), 6.45 (t, 7.6Hz, 1H, Ar-*H*), 4.47 (sep, 5.3Hz, 2H, Me_2C-*H*), 3.22 (spt, 5.3Hz, 2H, Me_2C-*H*), 2.42 (s, 6H, Ar- C*H$_3$*), 1.94 (s, 6H, Ar-C*H$_3$*), 1.68 (d, 6.8Hz, 6H, HC(C*H$_3$*)$_2$), 1.46 (d, 6.9Hz, 6H, HC(C*H$_3$*)$_2$), 1.38 (d, 6.9Hz, 6H, HC(C*H$_3$*)$_2$), 1.07 (d, 6.9Hz, 6H, HC(C*H$_3$*)$_2$), 0.18 (s, 9H, Si(C*H$_3$*)$_3$), -0.23 (s, 9H, Si(C*H$_3$*)$_3$). ^{13}C NMR (600 MHz, C_6D_6, 22°C) δ 159.55, 159.03, 146.16, 145.28, 142.30, 138.67, 134.39, 132.66, 128.74, 128.35, 127.71, 127.57, 127.51, 126.17, 124.17, 122.68, 119.58, 28.79, 27.83, 25.89, 25.55, 25.03, 23.44, 19.71, 19.60, 4.92, 1.52. Anal. Calcd. for $C_{48}H_{70}N_4NiSi_2$: C, 70.48%; H, 8.63%; N, 6.85%. Found: C, 70.42%; H, 8.31%; N, 7.22%. IR (neat solid, cm^{-1}) 2958 m, 2138 m sh, 1656 m sh, 1461 m sh, 1421 m sh, 1236 m sh, 837 s sh, 766 s sh. Crystals suitable for X-ray diffraction were obtained by slow cooling of a saturated solution in hexanes at -35ºC.

(DIPP)$_2$N$_2$ (5). To a 50 mL Chemglass Air-Free teflon-stoppered flask was added **1** (0.106 g, 0.191 mmol) and 15 mL of benzene, to form a dark purple solution. The solution was frozen with liquid nitrogen, and the headspace of the flask was evacuated and refilled with oxygen gas. The flask was sealed and the solution was allowed to thaw and was stirred for 20 min, by which time the solution had changed to dark orange. The volatile materials were removed under reduced pressure, to leave a dark orange residue. The residue was extracted with two portions of 4 mL of pentane and the extracts were filtered. The filtrate was combined and the volatile materials were removed under reduced pressure to give a gooey orange solid. Recrystallization of this solid from hexanes at -35°C yielded orange crystals of **5** (0.08g, 24%). Crystals suitable for X-ray diffraction were obtained by the method described above. ^{1}H NMR (600 MHz, C_6D_6, 23 °C) δ 7.24-7.14 (m, 6H, Ar-*H*), 3.49 (spt, 6.7Hz, 4H, Me_2C-*H*), 1.21 (d, 6.7Hz, 24H, HC(C*H$_3$*)$_2$). ^{13}C NMR (600 MHz, C_6D_6, 22°C) δ 141.26, 129.13, 128.59, 124.28, 28.00, 28.45. HRMS *m/z* Calcd. for $C_{24}H_{34}N_2$: 350.2722. Found: 350.2732.

Procedure for Reaction of Ni[N(SiMe$_3$)DIPP]$_2$ (1) with 1 equiv of O$_2$ Gas. To a 20 mL scintillation vial was added **1** (0.0350 g, 0.063 mmol) and $Si(SiMe_3)_4$ (0.0040 g, 0.012

mmol) as an internal standard. The contents of the vial were dissolved in approximately 0.7 mL of C_6D_6 and transferred to a J-Young NMR tube equipped with a Teflon valve. The tube was attached to a 45 mL calibrated bulb and the entire apparatus was attached to a Schlenk line. The solution was frozen and the headspace above the tube was evacuated along with the calibrated bulb. The tube was then isolated from the bulb via a Teflon valve. The vacuum manifold of the Schlenk line and the bulb were isolated from the vacuum pump and refilled with O_2 gas to a pressure of 6-7 mm Hg. The bulb was then isolated from the Schlenk line via a Teflon valve, and the valve was isolated the J-young tube from the bulb was opened. The tube was then submerged in liquid nitrogen for 2 h, after which the tube was sealed and allowed to thaw. When melted, the contents of the tube were shaken for several min. The solution was then filtered and analysis of the products was conducted by ^{1}H NMR spectroscopy.

Procedure for Reaction of Ni[N(SiMe$_3$)DIPP]$_2$ (1) with 1 atm of O_2 Gas and Isolation of the Insoluble Precipitate. To a 100 mL Chemglass Air-Free Teflon-stoppered flask was added **1** (0.4010 g, 0.720 mmol) and 50 mL of benzene, to form a purple solution. The flask was attached to a Schlenk line, the solution was frozen with liquid nitrogen and the headspace was evacuated. The vacuum manifold was isolated from the vacuum pump and refilled with 1 atm of O_2 gas. The solution was then thawed and upon fully melting, the flask was sealed and the solution was stirred for 2 days, during which the color changed from purple to brown. After 2 days, the solution was filtered through a Bucher funnel and the dark brown powder was collected on the filter. The powder was washed three times with 10 mL of hexanes and then dried under vacuum, to give 0.165 g of a tan/brown powder. Anal. Found: C, 39.08%; H, 6.30%; N, 3.29%.

REFERENCES

(1) (a) Power, P. P. *Comments Inorg. Chem.* **1989**, *8*, 177. (b) Chen, H.; Bartlett R. A.; Olmstead, M. M.; Power P. P.; Shoner, S. C. *J. Am. Chem. Soc.* **1990**, *112*, 1048. (c) Kays D. L.; Cowley, A. R. *Chem. Commun.* **2007**, *10*, 1053. (d) Holland, P. L. *Angew. Chem. Int. Ed.* **2011**, *50*, 6213.
(2) Waterman R.; Hillhouse, G. L. *J. Am. Chem. Soc.* **2003**, *125*, 13350.
(3) Harrold, N. D.; Waterman, R.; Hillhouse G. L.; Cundari, T. R. *J. Am. Chem. Soc.* **2009**, *131*, 12872.
(4) Sita, L. R.; Babcock J. R.; Xi, R. *J. Am. Chem. Soc.* **1996**, *118*, 10912.
(5) (a) Frazier, B. A.; Wolczanski, P. T.; Lobkovsky E. B.; Cundari, T. R. *J. Am. Chem. Soc.* **2009**, *131*, 3428. (b) Nikolaides, K. R.; Hoffmann S. D.; Eppinger, J. J. *J. Organomet. Chem.* **2008**, *693*, 2223. (c) Gosink, H.; Roesky, H. W.; Schmidt, H.; Noltemeyer, M.; Irmer E.; Herbst-Inner, R. *Organometallics* **1994**, *13*, 3420. (d) Weymann, C.; Danapolous A. A.; Wilkinson, G. *Polyhedron* **1996**, *15*, 3605. (e) Deschner, T.; Tornroos, K. W.; Anwander, R. *Inorg. Chem.* **2011**, *50*, 7217. (f) Anwander, R. *Chem. Mater.* **2011**, *13*, 4419.
(6) Kahn, M. L.; Glaria, A.; Pages, C.; Monge, M.; Macary, L. S.; Maisonnat, A.; Chaudret, B. *J. Mater. Chem.* **2009**, *19*, 4044.
(7) Yang J.; Tilley, T. D. *Angew. Chem. Int. Ed.* **2010**, *49*, 10186.
(8) Andersen, R. A.; Faegri, K.; Green, J. C.; Haaland, A.; Lappert, M. F.; Leung, W. P.; Rypdal, K. *Inorg. Chem.* **1988**, *27*, 1782.
(9) (a) Li, J.; Song, H.; Cui, C.; Cheng, J. *Inorg. Chem.* **2008**, *47*, 3468. (b) Bryan, A. M.; Merrill, W. A.; Reiff, W. M.; Fettinger, J. C.; Power, P. P. *Inorg. Chem.* **2012**, *51*, 3366.
(10) Evans, D. F. *J. Chem. Soc.* **1959**, 2003.

(11) Wu, Z.; Diminnie, J.; Xue, Z. *Organometallics* **1999**, *18*, 1002.
(12) Armarego, W. L. F.; Chai, C. L. L. Purification of Organic Chemicals. *Purification of Laboratory Chemicals,* 6th Edition; Butterworth-Heinemann; Oxford, UK; 2009; p. 236.
(13) Chao, Y.-W.; Wexler, P. A.; Wigley, D. E. *Inorg. Chem.* **1989**, *28*, 3860.

Chapter 1 Appendix

X-RAY DATA TABLES

Compound **1**:

Empirical formula	C30 H52 N2 Ni Si2	
Formula weight	555.62	
Temperature	100(2) K	
Wavelength	0.71073 Å	
Crystal system	Triclinic	
Space group	P-1	
Unit cell dimensions	a = 8.9248(4) Å	a= 102.092(2)º.
	b = 9.1680(4) Å	b= 92.571(2)º.
	c = 10.9493(5) Å	g = 114.391(2)º.
Volume	789.11(6) $Å^3$	
Z	1	
Density (calculated)	1.169 Mg/m^3	
Absorption coefficient	0.711 mm^{-1}	
F(000)	302	
Crystal size	0.12 x 0.08 x 0.08 mm^3	
Theta range for data collection	1.92 to 25.39º.	
Index ranges	-10<=h<=10, -11<=k<=11, -13<=l<=13	
Reflections collected	15509	
Independent reflections	2891 [R(int) = 0.0307]	
Completeness to theta = 25.00º	99.7 %	
Absorption correction	Semi-empirical from equivalents	
Max. and min. transmission	0.9453 and 0.9196	
Refinement method	Full-matrix least-squares on F^2	
Data / restraints / parameters	2891 / 0 / 167	
Goodness-of-fit on F^2	1.061	
Final R indices [I>2sigma(I)]	R1 = 0.0241, wR2 = 0.0645	
R indices (all data)	R1 = 0.0260, wR2 = 0.0658	
Largest diff. peak and hole	0.380 and -0.199 $e.Å^{-3}$	

Compound **2**:

Empirical formula	C37 H62 N4 Ni Si2	
Formula weight	677.80	
Temperature	100(2) K	
Wavelength	0.71073 Å	
Crystal system	Triclinic	
Space group	P-1	
Unit cell dimensions	a = 10.5555(4) Å	a= 84.922(2)º.
	b = 12.6703(5) Å	b= 74.854(2)º.
	c = 16.2859(6) Å	g = 69.522(2)º.
Volume	1969.57(13) $Å^3$	
Z	2	

Density (calculated)	1.143 Mg/m^3
Absorption coefficient	0.582 mm^{-1}
F(000)	736
Crystal size	0.18 x 0.10 x 0.06 mm^3
Theta range for data collection	1.30 to 25.40º.
Index ranges	-12<=h<=12, -15<=k<=14, -19<=l<=19
Reflections collected	37916
Independent reflections	7213 [R(int) = 0.0479]
Completeness to theta = 25.00º	100.0 %
Absorption correction	Semi-empirical from equivalents
Max. and min. transmission	0.9659 and 0.9025
Refinement method	Full-matrix least-squares on F^2
Data / restraints / parameters	7213 / 0 / 398
Goodness-of-fit on F^2	1.046
Final R indices [I>2sigma(I)]	R1 = 0.0333, wR2 = 0.0788
R indices (all data)	R1 = 0.0423, wR2 = 0.0839
Largest diff. peak and hole	0.314 and -0.275 $e.Å^{-3}$

Compound **3**:

Empirical formula	C32 H55 N3 Ni Si2	
Formula weight	596.68	
Temperature	100(2) K	
Wavelength	0.71073 Å	
Crystal system	Triclinic	
Space group	P-1	
Unit cell dimensions	a = 9.6047(3) Å	a= 97.4630(10)º.
	b = 11.1888(4) Å	b= 97.333(2)º.
	c = 17.6838(5) Å	g = 110.211(2)º.
Volume	1737.61(10) $Å^3$	
Z	2	
Density (calculated)	1.140 Mg/m^3	
Absorption coefficient	0.650 mm^{-1}	
F(000)	648	
Crystal size	0.16 x 0.07 x 0.06 mm^3	
Theta range for data collection	1.97 to 25.36º.	
Index ranges	-11<=h<=11, -13<=k<=13, -21<=l<=21	
Reflections collected	29585	
Independent reflections	6356 [R(int) = 0.0279]	
Completeness to theta = 25.00º	99.5 %	
Absorption correction	Semi-empirical from equivalents	
Max. and min. transmission	0.9620 and 0.9031	
Refinement method	Full-matrix least-squares on F^2	
Data / restraints / parameters	6356 / 0 / 358	
Goodness-of-fit on F^2	1.034	

Final R indices [I>2sigma(I)]	R1 = 0.0280, wR2 = 0.0666
R indices (all data)	R1 = 0.0337, wR2 = 0.0694
Largest diff. peak and hole	0.359 and -0.224 e.Å^{-3}

Compound **4**:

Empirical formula	C48 H70 N4 Ni Si2	
Formula weight	817.97	
Temperature	100(2) K	
Wavelength	0.71073 Å	
Crystal system	Orthorhombic	
Space group	Pna2(1)	
Unit cell dimensions	a = 16.3178(4) Å	a= 90º.
	b = 20.8353(5) Å	b= 90º.
	c = 13.7272(3) Å	g = 90º.
Volume	4667.06(19) Å^3	
Z	4	
Density (calculated)	1.164 Mg/m^3	
Absorption coefficient	0.503 mm^{-1}	
F(000)	1768	
Crystal size	0.24 x 0.18 x 0.15 mm^3	
Theta range for data collection	1.59 to 25.34º.	
Index ranges	-19<=h<=19, -23<=k<=25, -16<=l<=16	
Reflections collected	39140	
Independent reflections	8159 [R(int) = 0.0265]	
Completeness to theta = 25.00º	99.9 %	
Absorption correction	Semi-empirical from equivalents	
Max. and min. transmission	0.9284 and 0.8889	
Refinement method	Full-matrix least-squares on F^2	
Data / restraints / parameters	8159 / 1 / 514	
Goodness-of-fit on F^2	1.031	
Final R indices [I>2sigma(I)]	R1 = 0.0268, wR2 = 0.0636	
R indices (all data)	R1 = 0.0305, wR2 = 0.0658	
Absolute structure parameter	-0.007(8)	
Largest diff. peak and hole	0.297 and -0.159 e.Å^{-3}	

Compound **5**:

Empirical formula	C24 H34 N2	
Formula weight	350.53	
Temperature	100(2) K	
Wavelength	0.71073 A	
Crystal system, space group	Monoclinic, C2/c	
Unit cell dimensions	a = 16.2978(9) A	alpha = 90 deg.
	b = 9.4465(5) A	beta = 100.003(2) deg.
	c = 13.7560(8) A	gamma = 90 deg.

Volume	2085.6(2) A^3
Z, Calculated density	4, 1.116 Mg/m^3
Absorption coefficient	0.065 mm^-1
F(000)	768
Crystal size	0.15 x 0.06 x 0.04 mm
Theta range for data collection	2.50 to 25.37 deg.
Limiting indices	-19<=h<=19, -11<=k<=11, -16<=l<=16
Reflections collected / unique	13521 / 1914 [R(int) = 0.0448]
Completeness to theta = 25.00	99.8 %
Absorption correction	Multi-scan
Max. and min. transmission	0.9974 and 0.9904
Refinement method	Full-matrix least-squares on F^2
Data / restraints / parameters	1914 / 0 / 122
Goodness-of-fit on F^2	1.026
Final R indices [I>2sigma(I)]	R1 = 0.0392, wR2 = 0.0901
R indices (all data)	R1 = 0.0553, wR2 = 0.0991
Largest diff. peak and hole	0.177 and -0.180 e.A^-3

Chapter 2. A Structurally Rigid Bis(amido) Ligand Framework in Low-Coordinate Ni(I), Ni(II) and Ni(III) Analogues Provides Access to a Ni(III) Methyl Complex *via* Oxidative Addition

INTRODUCTION

Due to their comparatively low toxicity, minimal cost and high abundance, catalysts based on first-row transition metals are attracting considerable interest.[1] Many attempts to develop such catalysts are based on well-known mechanisms associated with second- and third-row metals; however, alternative design strategies might leverage the chemical transformations and properties that are unique to the 3*d* metals. Among the many features that distinguish first row metals from their heavier congeners is their ability to adopt very low coordination numbers (e.g., two and three) that are associated with electrophilic metal centers and high reactivity.[2a-h]

Whereas a number of low-coordination number complexes are known, for example with Cr, Mn, Fe, Co and Ni, the reaction chemistry associated with this structural type is relatively unexplored.[2a] Exceptions are found in the research of Hillhouse and coworkers, who have explored a number of novel transformations for low-coordinate, neutral Ni(I) and Ni(0) complexes.[3a-f] Applications of such complexes to catalysis are less well studied, but this laboratory has recently described use of the precatalyst $Fe[N(SiMe_3)_2]_2$ for hydrosilations of carbonyl compounds,[4] and $Ni[N(SiMe_3)DIPP]_2$ (**1**, DIPP = 2,6-diisopropylphenyl) as an alkene hydrosilation catalyst.[5] In this chapter, we describe the redox chemistry of **1**, and demonstrate that this nickel bis(amido) framework readily supports low-coordinate complexes in three different oxidations states, Ni(I/II/III), and accommodates a two-electron oxidative addition to anionic $\{Ni[N(SiMe_3)DIPP]_2\}^-$ (**2**) to produce the unusual nickel(III) alkyl complex $(Me)Ni[N(SiMe_3)DIPP]_2$ (**3**).

RESULTS AND DISCUSSION

Previous reactivity studies of **1** demonstrated that simple two-electron donors such as MeCN and 4-(N,N-dimethylamino)pyridine add rapidly to form three-coordinate, T-shaped adducts.[5] However, the more sterically demanding N-heterocyclic carbene IPr (N,N'-1,3-bis(2,6-diisopropylphenyl)imidazol-2-ylidene) reacted with **1** upon heating at 80 °C to form the yellow nickel(I) species $(IPr)Ni[N(SiMe_3)DIPP]$ (**4**) in 61% isolated yield (Scheme 1). This interesting redox process, which formally involves displacement of $\bullet N(SiMe_3)DIPP$, represents a convenient route to low-coordinate Ni(I) amido complexes, which have been used as precursors to Ni-imido complexes by Hillhouse and coworkers.[3d] The unusual redox process associated with this reaction prompted an examination of **1** by cyclic voltammetry (CV), which reveals fully reversible Ni(I/II) and Ni(II/III) couples at -1.28 V ($E_{1/2}$ vs. Fc/Fc^+, $ip_a/ip_c = 0.98$) and +0.18 V ($E_{1/2}$ vs. Fc/Fc^+, $ip_a/ip_c = 0.97$; see Experimental Section). The relatively low and reversible reduction potential for **1** suggested that the corresponding, anionic Ni(I) complex might be isolable.

The reduction of **1** by 1.1 equiv of KC_8 in toluene occurred over 20 minutes at -30 °C and workup of the solution provided $K\{Ni[N(SiMe_3)DIPP]_2\}$ (**2a**) as light yellow crystals in 89% yield (Scheme 1). The X-ray structure of **2a** reveals that the complex maintains a linear geometry about nickel with a N-Ni-N bond angle of 178.05(9)° (Scheme 1) and a Ni-N bond distance of 1.8436(2) Å. The potassium atom in this complex is sandwiched *via* η^6-coordination to aryl rings of both amido ligands (Scheme 1). The potassium was exchanged for tetrabutylammonium ($N^nBu_4^+$) by reaction of **2a** with $[N^nBu_4]Br$ in THF to give $N^nBu_4\{Ni[N(SiMe_3)DIPP]_2\}$ (**2b**) as yellow crystals in 70% yield. As shown by the crystal structure (Scheme 1), **2** exists as a rigorously two-coordinate bis(amido) complex with metrical parameters similar to those of **2a**

and both of these complexes exhibit an eclipsed conformation of the planar amido substituents. The solution magnetic moments of **2a**,**b**, determined by Evans's method,[6] are 1.66 and 2.03 μ_B, respectively, and are consistent with one unpaired electron as expected for a d^9 configuration.

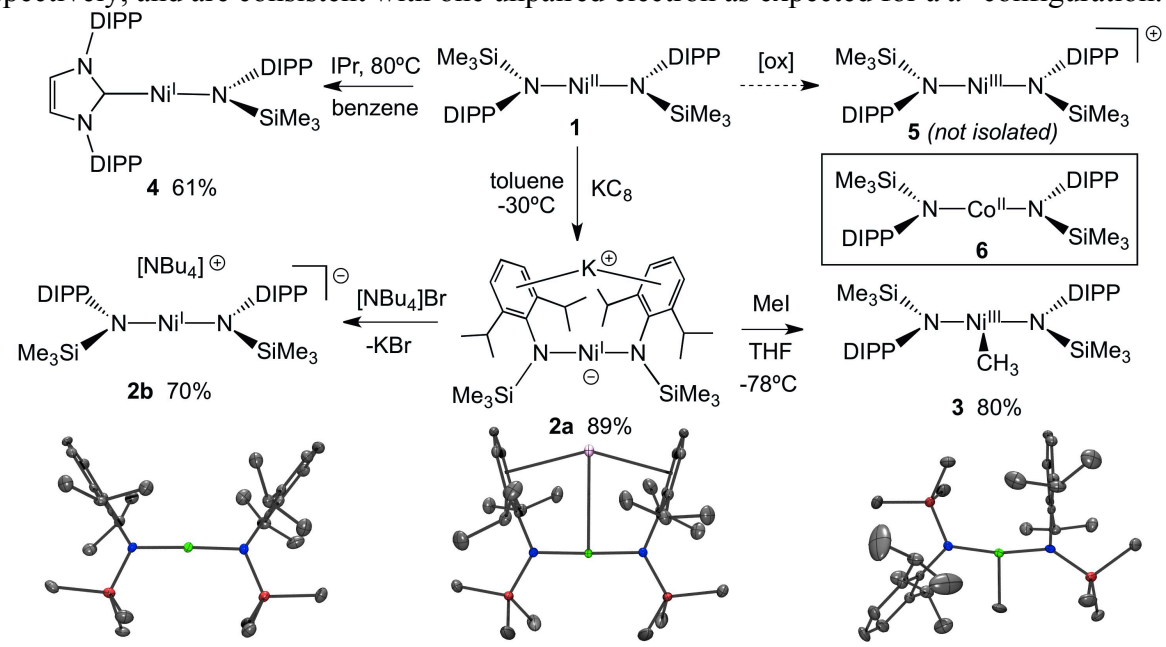

Scheme 1. Reactions of Ni bis(amido) complexes.

To better understand the electronic configuration of this eclipsed, bis-amido structural motif, DFT calculations were performed on **1** and **2b**, using both the hybrid functional ωB97XD[7] and the pure functional revTPSS,[8] since these functionals treat open-shell spin states in fundamentally different ways. The optimized structures of **1** and **2b** are in close agreement with their respective crystal structures, in retaining a linear, eclipsed coordination geometry with bond lengths and angles consistent with experimental values (see Experimental Section and Appendix). In both calculations of **1**, the triplet spin state is favored over the singlet state by a considerable margin (17 and 7 kcal/mole for the ωB97XD and revTPSS calculations, respectively). This is in agreement with the magnetic moment of 2.67 μ_B observed for **1**, consistent with two unpaired electrons.

In addition to the conformational and metrical similarities between neutral **1** and anionic **2b**, the DFT calculations indicate that their electronic structures are closely related. A single qualitative MO diagram can be used to represent the electronic structures of both **1** and **2b** as shown in Figure 1. The HOMO for both complexes is a singly-occupied N-Ni-N π-antibonding orbital. This three-centered π system may be viewed as resulting from combinations of Ni d_{yz} and N p_y orbitals to give bonding, non-bonding and anti-bonding orbitals populated by a total of five electrons. Single occupancy of the π-antibonding HOMO results in a net bond order of $^1/_2$ for this π system, for both **1** and **2b**. It is difficult to assess the contribution of this π bonding to the stability of eclipsed structures for **1** and **2a**. However, it is worth noting that the conversion of **1** to **2a** is accompanied by a rotation about the Ni-N bond to place the two aryl groups *cis* to one another. That this occurs at ambient temperatures suggests that the rotational barrier is minimal and thus that the π bonding interaction is weak.

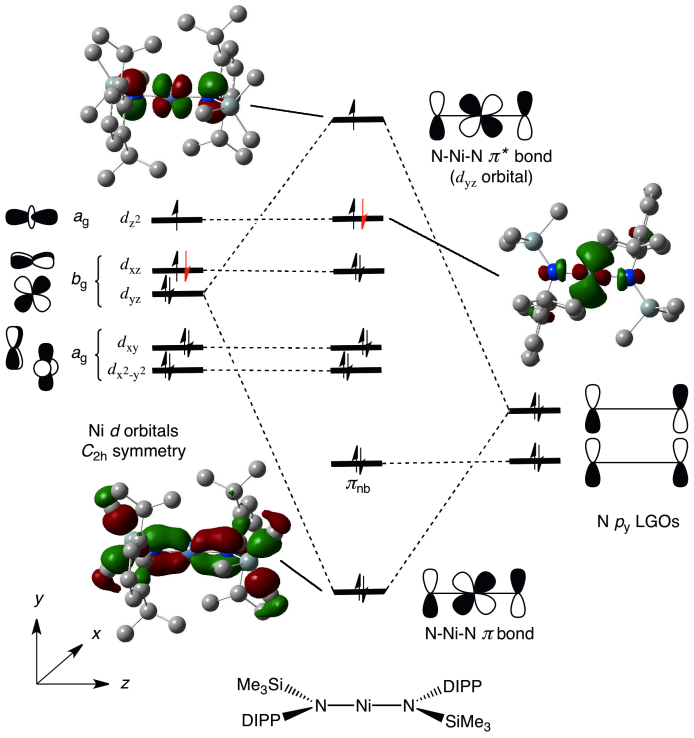

Figure 1. Qualitative MO diagram for Ni bis(amido) ligand framework with selected calculated molecular orbitals. The red electron is present only in Ni(I) d^9 species **2a**,**b**. Computed molecular orbital figures are from the hybrid calculations on compound **1**.

Given the striking similarities between the electronic structures of the two-coordinate Ni(I) and Ni(II) complexes **1** and **2b**, it was of interest to synthetically access the analogous Ni(III) (d^7) cation. The optimized geometry of the Ni(III) cation $\{Ni[N(SiMe_3)DIPP]_2\}^+$ (**5**), calculated by the DFT methods described above,[9] is predicted to feature an eclipsed conformation and a linear coordination geometry. The more electrophilic metal center in this case results in a canting of the aryl groups within the coordination plane to provide close aryl-Ni interactions and a smaller Ni-N-C_{ipso} bond angle (88.15° compared to 106.66(9)º for **1** and 121.62(19)° for **2b**, see Appendix). The hybrid calculation also predicts that the doublet spin state is favored over the quartet spin state by 14 kcal/mole.

Observation of the reversible oxidation wave for **1** at +0.18 V suggested that the Ni(III) cation might be chemically accessible. However, this wave lies close to an irreversible event at *ca.* 0.67 V (E_p vs. Fc/Fc^+), with an onset potential of *ca.* 0.40 V. The close proximity of these two oxidation events places upper and lower bounds on the oxidation potential for the oxidant required to isolate the Ni(III) cation. Attempts to observe the oxidation of **1** with Ag(I) reagents led to an intractable mixture of Ni-containing products $(Ag(Et_2O)[B(C_6F_5)_4]$ and $Ag[CH_6B_{11}Br_6])$ or no reaction at 60 °C (AgOTf, $AgBF_4$ and $AgNTf_2$).

Given these results, the isoelectronic d^7 Co bis(amido) complex $Co[N(SiMe_3)DIPP]_2$ (**6**) was obtained by a procedure analogous to that used for **1** (see Experimental Section). This complex was isolated as red crystals with a solution μ_{eff} value of 5.67 μ_B, reflecting a high-spin configuration with strong spin-orbit coupling, as previously observed for related two-coordinate

Co(II) bis-amido complexes.[10] Complexes **1** and **6** are isostructural, with an eclipsed conformation of the amido substituents. There are several structural and electronic differences between the calculated properties of **5** and the observed properties of **6**, but this comparison is convoluted by the difference in charge and the strong spin-orbit coupling interactions observed in **6**.

Further analysis of the calculated electronic structures of **1** and **2b** suggested an alternative route to complexes with the Ni(III) oxidation state. The HOMO-1 orbital of both compounds is the σ-antibonding d_z2 orbital, in which most of the electron density has been pushed into the torus of the d_z2 orbital. Substantial mixing between d_z2 and $d_{x^2-y^2}$, expected for the C_{2h} symmetry of **1** and **2b**, results in electron density being distributed along the "in-plane" molecular x-axis instead of in a radially symmetrical fashion (Figure 1). This creates a much more directional orbital, which is more amenable to bond formation. Prior work with **1** has shown that this orbital, depicted in Figure 1 (and derived from d_z^2), acts as an acceptor for neutral, two-electron donors.[5] However, in **2b**, this orbital is doubly occupied, suggesting it may instead serve as a reasonable nucleophile toward a small, organic substrate.

The reaction of **2a** with methyl iodide occurred over 35 minutes starting at -78ºC and warming to room temperature. Workup of the reaction mixture and recrystallization from pentane afforded the unusual Ni(III) alkyl complex (Me)Ni[N(SiMe$_3$)DIPP]$_2$ (**3**, Scheme 1) as green prisms in 80% yield. Compound **3** is thermally unstable, decomposing in benzene solution at ambient temperature over *ca.* 24 hours to **1**, accompanied by the formation of ethane (detected by ^{1}H and ^{13}C NMR spectroscopy). However, **3** was found to be sufficiently stable for single crystal X-ray diffraction studies and combustion analysis, and exhibited no signs of decomposition after three months as a solid at -30ºC.

Complex **3** is a rare example of a Ni(III) organometallic complex and appears to be only the third structurally characterized Ni(III) alkyl complex.[11a-d] The X-ray structure of **3** reveals two inequivalent molecules, each in a T-shaped coordination geometry, with an average N-Ni-N angle of 167.4(1)º and an average Ni-C_{Me} bond length of 1.923(4) Å. Both molecules display a close contact between the Ni center and the ipso carbon of an adjacent aryl ring, similar to the interactions predicted in the calculated structure of **5**. Although the relevant distances and angles vary by a significant amount between the two molecules (Ni-C_{ipso}: 2.377(2) Å and 2.541(2) Å, Ni-N-C_{ipso}: 94.01(1)º and 102.90(1)º, respectively), this suggests that the predicted structure of **5** is qualitatively reasonable. The Ni-C bond length of 1.923(4) Å is similar to those reported for the two previously known Ni(III) alkyl species (1.994(3) Å and 2.015(3) Å for –Me and –Et analogs, respectively), although both of these examples are five-coordinate, negatively charged species.[11a] The solution magnetic moment of **3** was determined to be 1.78 μ_B, consistent with one unpaired electron and a low spin, d^7 electronic configuration.

Efforts to better understand the electronic structure of **3** involved EPR spectroscopy and DFT calculations using the same two functionals employed in the analyses of **1** and **2a**,**b**. Both computations of **3** place the odd electron in a π* orbital bearing substantial metal character (see Appendix) supporting the assignment of **3** as Ni(III). The frozen glass EPR spectrum of **3** in toluene reveals an anisotropic signal with $g_{xx,}$ $g_{yy,}$ g_{zz} = (2.32, 2.15, 2.13), indicating that the unpaired spin resides in an orbital with significant metal character (see Appendix). The signal also displays hyperfine coupling to the two nitrogen atoms, indicating substantial delocalization of the unpaired spin density onto those nitrogen atoms, which is in agreement with the calculated HOMO of **3**. Together, the calculations and EPR data support the characterization of **3** as a Ni(III) complex rather than a Ni(II) complex with an oxidized, ligand-based radical.

While **3** is an unusual compound in and of itself, the oxidative process which gives rise to it is also quite rare. Analysis of **2a**,**b** and **3** by DFT calculations and EPR spectroscopy support the oxidation state assignments of Ni(I) (see Appendix) and Ni(III), respectively (*vide supra*)**;** thus, the formation of **3** from **2a** is formally a two-electron oxidative addition. Notably, the lack of well-defined, two-electron redox processes for first-row metal complexes is thought to represent a major impediment to the development of catalytic cycles for these metals.[1] While oxidative additions to nickel are known, they are much more commonly observed in Ni(0)/Ni(II) or Ni(II/IV) couples. Well defined Ni(I)/Ni(III) oxidative additions are rare,[12] but similar, ligand-assisted two-electron oxidative additions are implicated in various nickel-catalyzed cross-coupling reactions and Ni(III) alkyl complexes like **3** are proposed as intermediates in those reactions.[13,14] To the best of our knowledge, no other Ni(I)/Ni(III) oxidative additions leading to an isolable Ni(III) product are known. Remarkably, complex **3** was found to be unreactive towards both powerful electrophiles (Me_3SiOTf, triflic acid) and nucleophiles (KO^tBu, KOMe, LiSPh). No reaction was observed with the above reagents in THF at ambient temperature prior to the complete thermal decomposition of **3** (*ca.* 24 h, *via* ^1H NMR spectroscopy). Similarly, **3** (0.0035 mM in THF) was found to be unreactive towards saturated THF solutions of $[N^nBu_4]X$ (X = Cl, 0.022 mM; Br, 0.11 mM; I, 0.0050 mM), indicating that the oxidative addition of methyl iodide is not readily reversible under these conditions.

CONCLUSION

In summary, a structurally persistent bis-amido ligand framework for nickel compounds in three oxidation states has been identified and a highly unusual Ni(III) alkyl species has been prepared and characterized. Further exploration of this system should yield important mechanistic information relevant to nickel-catalyzed coupling reactions and multi-electron redox processes for first row metals.

EXPERIMENTAL

General Considerations. Unless otherwise stated, all reactions and manipulations were carried out in a VAC Atmosphere Nexus glovebox or using standard Schlenk techniques under a nitrogen atmosphere. Pentane, hexanes, benzene, toluene, and 1,2-difluorobenzene were purchased from Sigma Aldrich. Diethyl ether was purchased from Honeywell and tetrahydrofuran was purchased from Macron Chemicals. Pentane, toluene, tetrahydrofuran, diethyl ether and 1,2-difluorobenzene were dried using a JC Meyers Phoenix SDS solvent purification system. Benzene and hexane were dried and degassed using a Vacuum Atmosphere solvent purifier system. Prior to drying, benzene was dethiophenated using standard techniques.[15] C_6D_6 was purchased from Cambridge Isotope Laboratories, dried over Na/K alloy and then degassed by four freeze-pump-thaw cycles. Tetrabutylammonium salts, trimethylsilyl triflate, triflic acid, silver tetrafluoroborate and silver triflate were purchased from Sigma Aldrich and used as received. $[Li(Et_2O)_n][B(C_6F_5)_4]$ (n is assumed to be 3) was purchased from Boulder Scientific and used as received. Methyl iodide was purchased from Sigma Aldrich, dried over 3Å molecular sieves, degassed by three freeze-pump-thaw cycles and used as a 0.100M solution in tetrahydrofuran. Potassium graphite,[16] IPr,[17] $Ag[CH_6B_{11}Br_6]$[18] and tetrabutylammonium tetrakis(pentafluorophenyl)borate[19] were prepared by standard literature procedures. $[Ag(Et_2O)][B(C_6F_5)_4]$[20] was prepared by modified literature procedures, substituting

$[Li(Et_2O)_n][B(C_6F_5)_4]$ for $K[B(C_6F_5)_4]$. Compound **1** and $LiN(SiMe_3)DIPP$ were prepared by previously reported methods.[5] All NMR spectra were collected at ambient temperature (ca. 21°C) on Bruker AVB-400, AV-500, AV-600 or AVQ-400 NMR spectrometers, each equipped with a 5 mm BB probe, and referenced to the residual proteo solvent signals. Solution magnetic susceptibilities were determined by ^1H NMR spectroscopy using Evans's method.[6] Elemental analyses were performed by the UC Berkeley College of Chemistry Microanalytical Facility except **6** which was performed by Galbraith Laboratories. The abbreviation "IPr" refers to N,N'-1,3-bis(2,6-diisopropylphenyl)imidazol-2-ylidene and "DIPP" refers to a 2,6-diisopropylphenyl moiety.

Cyclic Voltammetry Experiments. Cyclic voltammetry experiments were conducted at ambient temperature in a Vacuum Atmospheres glovebox. Measurements employed a Bio-Logic SP-200 potentiostat with a standard three electrode configuration. The working electrode was a 3 mm diameter glassy carbon electrode purchased from ALS. Silver wire was used as a quasi-reference electrode and sublimed ferrocene was used as an internal potential reference. The counter electrode was a 1/8 inch diameter graphite rod purchased from Electron Microscopy Sciences. The glassy carbon electrode was polished with 1 μm alumina prior to each use. The graphite rod was cleaned with acetone and dried prior to each use. Analyses of **1** and **2b** were performed in a 0.1 M solution of tetrabutylammonium tetrakis(pentafluorophenyl)borate in 1,2-difluorobenzene with an analyte concentration of 1 mM at a scan rate of 100 mV/s. Solution resistance was corrected by applying *i*R compensation for each measurement. All potential values are reported as $E_{1/2}$ for reversible events and E_p for irreversible events.

X-ray Diffraction Experiments. Single crystal X-ray diffraction experiments were carried out at UC Berkeley CHEXRAY crystallographic facility. Measurements of compounds **2a**, **2b**, **3**, **4** and **6** were performed on a Bruker APEX-II CCD area detector using Mo Kα radiation (λ = 0.71073 Å) monochromated using QUAZAR multilayer mirrors. Specific details of each experiment can be found below and in the Appendix.

Experimental Details:

	Detector Distance	Image Width	Exposure Time
Compound **2a**	40mm	0.5°	10 s
Compound **2b**	45mm	0.5°	30 s
Compound **3**	40mm	0.5°	15 s
Compound **4**	60mm	0.5°	10 s
Compound **6**	40mm	0.5°	5 s

DFT Calculations. All calculations were performed using the Gaussian 09 program.[21] Geometry optimization was performed using both hybrid and pure density functional theory (DFT). Hybrid DFT calculations were performed using the ωB97XD[7] functional and pure DFT calculations were performed using revTPSS[8] functional. The basis set used for all atoms in all calculations was 6-31+G(d), using polarization and diffuse orbitals for all atoms except hydrogen. Both hybrid and pure restricted open-shell calculations were performed on **1** and **2b** starting from their respective crystal structures (the $N^nBu_4^+$ counter ion was excluded from the calculation of **2b**). Hybrid restricted open-shell calculations and pure unrestricted calculations

were performed on the hypothetical two-coordinate Ni(III) cation starting from the crystal structure of **1**. The unrestricted calculations employed the use of a quadratically convergent SCF procedure.[9] The equivalent pure, restricted open-shell calculations for the Ni(III) cation did not converge. In all cases, frequency calculations confirm that the optimized structure resides at an energetic minimum. All geometries were optimized in the gas phase.

EPR Spectroscopy. EPR spectra were collected at Lawrence Berkeley National Laboratory using a Varian E109 EPR spectrometer equipped with a Model 102 Microwave bridge. Sample temperature was regulated using an Air Products LTR liquid helium cryostat. Spectra were recorded as frozen toluene glasses at *ca.* 60 K. G-values for the spectra were derived from simulations performed using the EasySpin EPR simulation package.[22] Hyperfine coupling constants were unable to be simulated due to inhomogeneous broadening of the signal.

Solubility Measurements of NBu_4X (X = Cl, Br, I). A large excess of the NBu4X (*ca.* 500 mg) salt was placed in a 20 mL scintillation vial with approximately 4 mL of dry THF. The suspension was stirred vigorously for 24 h. The solution was then filtered and 1 mL of the filtrate was measured by syringe and transferred to a tared vial. The volatiles were evaporated under reduced pressure until a constant mass was achieved. The measured solubility was 6, 36 and 2 mg/mL for the Cl, Br and I salts, respectively.

$Ni[N(SiMe_3)DIPP]_2$ (1). Full preparation and characterization data for **1** is available in a prior publication[5] and Chapter 1. Cyclic voltammetry (1,2-difluorobenzene, $NBu_4B(C_6F_5)_4$, 100 mV/s): –1.28 V (ip_a/ip_c = 0.98), +0.18 V (ip_a/ip_c = 0.97), +0.67 V (irreversible).

$K\{Ni[N(SiMe_3)DIPP]_2\}$ (2a). To a 20 mL scintillation vial was added **1** (0.400 g, 0.720 mmol) and 12 mL of toluene, forming a purple solution. The mixture was stirred vigorously for approximately 20 min to ensure complete dissolution of **1**. The solution was then placed in a freezer at -30 °C where it was allowed to cool for 20 min. The vial containing the solution was then removed and the solution was stirred. To the stirring solution of **1** was added potassium graphite (0.107 g, 0.792 mmol) as a single aliquot. The mixture was allowed to warm to room temperature and stirring was continued for 20 min at which point no purple color was visible. The mixture was then filtered and the volatile components of the filtrate were removed under reduced pressure. The resulting residue was dissolved in 4 mL of toluene, forming a yellow solution, upon which was layered 9 mL of pentane. The vial was placed in the freezer at -30 °C overnight, yielding 0.290 g (68%) of **2a** as light yellow block-like crystals which were isolated by decantation and dried in vacuo. The supernatant was collected and the volatile components removed under reduced pressure. A second crystallization was set up in an identical fashion using the resulting residue with 1 mL of toluene and 6 mL of pentane, yielding an additional 0.093 g of **2a**. Total yield: 0.383 g (89%). The ^{1}H NMR spectrum of **2a** contains characteristic, but broad and unintegratable signals. We attribute this to the paramagnetism of **2a.** ^{1}H NMR (500 MHz, C_6D_6, 22°C) δ 16.96, 7.35, 0.71, -0.73, -6.81. μ_{eff} = 1.66 μ_B (C_6D_6, 20 °C, Evans's method). Anal. Calcd. for $C_{30}H_{52}KN_2NiSi_2$: C, 60.59%; H, 8.81%; N, 4.71%. Found: C, 60.41%; H, 8.62%; N, 4.62%. Crystals suitable for single crystal X-ray diffraction studies were obtained from the workup described above.

[N^{n}Bu$_4$]{Ni[N(SiMe$_3$)DIPP]$_2$} (2b). To a 20 mL scintillation vial was added **2a** (0.102 g, 0.171 mmol) and tetrabutylammonium bromide (0.055 g, 0.171 mmol). To the mixture of solids was added 5 mL of tetrahydrofuran, forming a light yellow suspension. The suspension was stirred at ambient temperature for 35 min, during which time most of the suspended particles dissolved, leaving a hazy yellow solution. The mixture was filtered, the filtrate was collected and the volatile components were removed under reduced pressure. The resulting residue was dissolved in 1 mL of tetrahydrofuran and 5 mL of diethyl ether were layered on top of the tetrahydrofuran solution. The vial was placed in the freezer at -30°C overnight, yielding 0.095 g (70%) of **2b** as light grey block-like crystals which were isolated by decantation and dried in vacuo. The ^{1}H NMR spectrum of **2b** contains characteristic, but broad and unintegratable signals for the Ni-containing ion and integratable signals for the tetrabutylammonium cation. We attribute this to the paramagnetism of **2b**. ^{1}H NMR (400 MHz, THF-d_8, 21°C) δ 15.21, 7.51, 3.21 (N-(CH_2)$_3$-CH$_3$, 8H), 1.68 (N-(CH_2)$_3$-CH$_3$, 8H), 1.45 (N-(CH_2)$_3$-CH$_3$, 8H), 1.06 (N-(CH$_2$)$_3$-CH_3, 12H), -0.84, -1.26. μ_{eff} = 2.03μ_B (THF-d_8, 20°C, Evans's method). Anal. Calcd. for $C_{46}H_{88}N_3NiSi_2$: C, 69.23%; H, 11.11%; N, 5.27%. Found: C, 69.17%; H, 11.07%; N, 5.26%. Cyclic voltammetry (1,2-difluorobenzene, $NBu_4B(C_6F_5)_4$, 100 mV/s): –1.28 V (ip_a/ip_c = 0.99), +0.18 V (ip_a/ip_c = 0.98), +0.67 V (irreversible). Crystals suitable for single crystal X-ray diffraction studies were obtained from the workup described above.

(Me)Ni[N(SiMe$_3$)DIPP]$_2$ (3). To a 100 mL Schlenk flask was added **2a** (0.543 g, 0.913 mmol) and 15 mL of tetrahydrofuran, forming a light yellow solution. The flask was placed in a dry ice/isopropanol bath and allowed to cool for 15 min. To this stirring, cooled solution was added methyl iodide (9.6 mL, 0.100 M, 0.960 mmol), dropwise, via syringe. The mixture was stirred at -78 °C for 5 min, then removed from the bath and allowed to warm to ambient temperature. Stirring was continued for 30 min, during which time the reaction mixture turned dark green. The volatile components were then removed under reduced pressure. The resulting residue was extracted with 12 mL of hexanes, the extracts were filtered and the volatile components of the filtrate removed under reduced pressure. The resulting residue was dissolved in 3 mL of pentane and the solution was placed in a freezer at -30°C overnight, yielding 0.417 g (80%) of **3** as green prism-shaped crystals which were isolated by decantation and dried in vacuo. The ^{1}H NMR spectrum of **3** contains characteristic, but broad and unintegratable signals. We attribute this to the paramagnetism of **3**. ^{1}H NMR (500 MHz, C_6D_6, 22°C) δ 32.20, 5.20, 4.21, 2.43, 0.80. μ_{eff} = 1.78 μ_B (C_6D_6, 20°C, Evans's method). Anal. Calcd. for $C_{31}H_{55}N_2NiSi_2$: C, 65.25%; H, 9.71%; N, 4.91%. Found: C, 65.24%; H, 9.82%; N, 4.84%. Crystals suitable for single crystal X-ray diffraction studies were obtained from the workup described above.

(IPr)Ni[N(SiMe$_3$)DIPP] (4). To a 50 mL Chemglass Teflon-stoppered flask was added **1** (0.137 g, 0.247 mmol), IPr (0.095 g, 0.244 mmol) and 15 mL of benzene, forming a dark purple solution. The flask was closed and placed in an oil bath at 80°C. The solution was stirred for 12 h, during which the color changed to dark orange. The volatile components of the solution were removed under reduced pressure and the resulting residue was washed with six portions of 2 mL of pentane cooled to -35°C. The remaining yellow powder was dried in vacuo, yielding 0.105 g (61%) of **4**. ^{1}H NMR (400 MHz, C_6D_6, 21ºC) δ 22.20 (2H), 10.93 (4H), 9.37 (2H), 8.37 (p-Ar-*H*, 1H), 4.17 (4H), 3.99 (2H), 3.82 (-Si(CH_3)$_3$, 9H), 3.56 (Ar-CH(CH_3)$_2$, 12H), 1.88 (Ar-CH(CH_3)$_2$, 12H), -0.65 (Ar-CH(CH_3)$_2$, 6H), -6.27 (Ar-CH(CH_3)$_2$, 6H), -11.69 (2H). Assignment of shifts to particular protons is given where integration allows unambiguous assignment. μ_{eff} = 2.12 μ_B

(C_6D_6, 21°C, Evans's method). Anal. Calcd. for $C_{42}H_{62}N_3NiSi_2$: C, 72.51%; H, 8.98%; N, 6.04%. Found: C, 72.27%; H, 9.26%; N, 5.77%. Crystals suitable for single crystal X-ray diffraction studies were obtained by preparing a saturated solution of **4** in toluene, layering pentane equal to four times the volume of toluene on top of the solution and placing the solution in a -30°C freezer overnight.

Co[N(SiMe$_3$)DIPP]$_2$ (6). To a 20 mL scintillation vial was added $CoBr_2$ (0.180 g, 0.823 mmol), LiN(SiMe$_3$)DIPP (0.400 g, 1.566 mmol), and 12 mL of diethyl ether. The mixture was stirred vigorously at ambient temperature for 24 h. The volatile components of the reaction mixture were then removed under reduced pressure and the resulting dark red residue was extracted with three portions of 3 mL of pentane. The combined extracts were filtered and the volatile components of the filtrate were removed under reduced pressure. The resulting red residue was dissolved in 8 mL of pentane and the solution was placed in a freezer at -30ºC overnight, yielding 0.208 g (45%) of **5** as small red crystals, which were isolated by decantation and dried in vacuo. ^{1}H NMR (500 MHz, C_6D_6, 20ºC) δ 124.14 (2H, very broad, *m*-Ar-*H* or Ar-C*H*(CH$_3$)$_2$), 64.96 (9H, Si(C*H*$_3$)$_3$), 35.65 (6H, Ar-CH(C*H*$_3$)$_2$), 32.37 (2H, *m*-Ar-*H* or Ar-C*H*(CH$_3$)$_2$), -92.47 (1H, *p*-Ar-*H*), -220.86 (6H, Ar-CH(C*H*$_3$)$_2$). μ_{eff} = 5.67 μ_B (C_6D_6, 19°C, Evans's method). Anal. Calcd. for $C_{30}H_{52}CoN_2Si_2$: C, 64.82%; H, 9.43%; N, 5.04%. Found: C, 65.13%; H, 9.58%; N, 5.07%. Crystals suitable for single crystal X-ray diffraction studies were obtained by the workup described above.

REFERENCES

(1) *Catalysts Without Precious Metals*; Bullock, R. M., Eds.; Wiley-VCH: Weinheim, Germany, 2010.
(2) (a) Power, P. P. *Chem. Rev.* **2012**, *112*, 3482. (b) Lei, H.; Fettinger, J. C.; Power, P. P. *Inorg. Chem.* **2012**, *51*, 1821. (c) Dugan, T. R.; Sun, X.; Rybak-Akimova, E. V.; Olatunji-Ojo, O.; Cundari, T. R.; Holland, P. L.; *J. Am. Chem. Soc.* **2011**, *133*, 12418. (d) Harrold, N. D.; Hillhouse, G. L. *Chem. Sci.* **2013**, *4*, 4011. (e) Nia, C.; Power. P. P. *Chem. Commun.* **2009**, 5543. (f) Danopoulos, A. A.; Braunstein, P. *Dalton Trans.* **2013**, *42*, 7276. (g) Laskowski, C. A.; Hillhouse, G. L. *Organometallics* **2009**, *28*, 6114.
(3) (a) Laskowski, C. A.; Hillhouse, G. L. *J. Am. Chem. Soc.* **2008**, *130*, 13846. (b) Laskowski, C. A.; Miller, A. J. M.; Hillhouse, G. L.; Cundari, T. R. *J. Am. Chem. Soc.* **2011**, *133*, 771. (c) Iluc, V. M.; Hillhouse, G. L. *J. Am. Chem. Soc.* **2010**, *132*, 11890. (d) Laskowski, C. A.; Morello, G. R.; Saouma, C. T.; Cundari, T. R.; Hillhouse, G. L. *Chem. Sci.* **2013**, *4*, 170. (e) Iluc, V. M.; Hillhouse, G. L. *J. Am. Chem. Soc.* **2010**, *132*, 15148. (f) Anderson, J. S.; Iluc, V. M.; Hillhouse, G. L. *Inorg. Chem.* **2010**, *49*, 10203. (g) Mindiola, D. J.; Hillhouse, G. L. *J. Am. Chem. Soc.* **2001**, *123*, 4623.
(4) Yang, J.; Tilley, T. D. *Angew. Chem. Int. Ed.* **2010**, *49*, 10186.
(5) Lipschutz, M. I.; Tilley, T. D. *Chem. Commun.* **2012**, *48*, 7146.
(6) Evans, D. F. *J. Chem. Soc.* **1959**, 2003.
(7) Chai, J. D.; Head-Gordon, M. *Phys. Chem. Chem. Phys.* **2008**, *10*, 6615.
(8) Perdew, J. P.; Ruzsinszky, A.; Csonka, G. I.; Constantin, L. A.; Sun, J. *Phys. Rev. Lett.* **2011**, *106*, 179902.
(9) Calculations of the Ni(III) cation based on the pure functional would only converge using an unrestricted, quadratically convergent SCF procedure. The optimized geometry derived from this

calculation was similar in all relevant aspects to that calculated using the hybrid-functional and the doublet spin state was also found to be the lowest energy. Backsay, G. B. *Chem. Phys.* **1988**, *61*, 385.
(10) Bryan, A. M.; Merrill, W. A.; Reiff, W. M.; Fettinger, J. C.; Power, P. P. *Inorg. Chem.* **2012**, *51*, 3366.
(11) (a) Lee, C.-M.; Chen, C.-H.; Liao, F.-X.; Hu, C.-H.; Lee, G.-H. *J. Am. Chem. Soc.* **2010**, *132*, 9256. (b) Grove, D. M.; van Koten, G.; Zoet, R.; Murrall, N. W.; Welch, A. *J. Am. Chem. Soc.* **1983**, *105*, 1379. (c) Grove, D. M.; van Koten, G.; Mul, W. P.; van der Zeijden, A.; Terheijden, J. *Organometallics* **1985**, *5*, 33 (d) Kelley, D. G.; Marchaj, A.; Bakac, A.; Espenson, J. H. *J. Am. Chem. Soc.* **1991**, *113*, 7583.
(12) Tsou, T. T.; Kochi, J. K. *J. Am. Chem. Soc.* **1979**, *101*, 7547.
(13) Hu, X. *Chem. Sci.* **2011**, *2*, 1867.
(14) Jones, G. D.; Martin, J. L.; McFarland, C.; Allen, O. R.; Hall, R. E.; Haley, A. D.; Brandon, R. J.; Konovalova, T.; Desrochers, P. J.; Pulay, P.; Vicic, D. A. *J. Am. Chem. Soc.* **2006**, *128*, 13175.
(15) Armarego, W. L. F.; Chai, C. L. L. Purification of Organic Chemicals. *Purification of Laboratory Chemicals,* 6th Edition; Butterworth-Heinemann; Oxford, UK; 2009; p. 236.
(16) Bergbreiter, D. E.; Killough, J. M. *J. Am. Chem. Soc.,* **1978**, *100*, 2126.
(17) Jafarpour, L.; Stevens, E. D.; Nolan, S. P. *J. Organomet. Chem.,* **2000**, *606*, 49.
(18) Reed, C. A. *Acc. Chem. Res.*, **2010**, *43*, 121.
(19) LeSuer, R. J.; Buttolph, C.; Geiger W. E. *Anal. Chem.,* **2004**, *76*, 6395.
(20) (a) Hayashi, Y.; Rohde, J. J.; Corey, E. J. *J. Am. Chem. Soc.*, **1996**, *118*, 5502. (b) Cintrón, M. S.; Green, O.; Burstyn, J. N. *Inorg. Chem.*, **2012**, *51*, 2737.
(21) Frisch, M. J.; Trucks, G. W.; Schlegel, H. B.; Scuseria, G. E.; Robb, M. A.; Cheeseman, J. R.; Scalmani, G.; Barone, V.; Mennucci, B.; Petersson, G. A.; Nakatsuji, H.; Caricato, M.; Li, X.; Hratchian, H. P.; Izmaylov, A. F.; Bloino, J.; Zheng, G.; Sonnenberg, J. L.; Hada, M.; Ehara, M.; Toyota, K.; Fukuda, R.; Hasegawa, J.; Ishida, M.; Nakajima, T.; Honda, Y.; Kitao, O.; Nakai, H.; Vreven, T.; Montgomery, J. A., Jr.; Peralta, J. E.; Ogliaro, F.; Bearpark, M.; Heyd, J. J.; Brothers, E.; Kudin, K. N.; Staroverov, V. N.; Kobayashi, R.; Normand, J.; Raghavachari, K.; Rendell, A.; Burant, J. C.; Iyengar, S. S.; Tomasi, J.; Cossi, M.; Rega, N.; Millam, N. J.; Klene, M.; Knox, J. E.; Cross, J. B.; Bakken, V.; Adamo, C.; Jaramillo, J.; Gomperts, R.; Stratmann, R. E.; Yazyev, O.; Austin, A. J.; Cammi, R.; Pomelli, C.; Ochterski, J. W.; Martin, R. L.; Morokuma, K.; Zakrzewski, V. G.; Voth, G. A.; Salvador, P.; Dannenberg, J. J.; Dapprich, S.; Daniels, A. D.; Farkas, Ö.; Foresman, J. B.; Ortiz, J. V.; Cioslowski, J.; Fox, D. J. Gaussian, Inc., Wallingford CT, 2009. *Gaussian 09, Revision C.01*, Gaussian, Inc.: Wallingford CT, 2009.
(22) Stoll, S.; Schweiger, A. *J. Magn. Reson.* **2006**, *178*, 42.

Chapter 2 Appendix

ENLARGED ORTEP DIAGRAMS

Carbon atoms are shown in dark grey, Potassium in pink, Nickel in green, Silicon in red and Nitrogen in blue and Cobalt in yellow in all of the following diagrams.

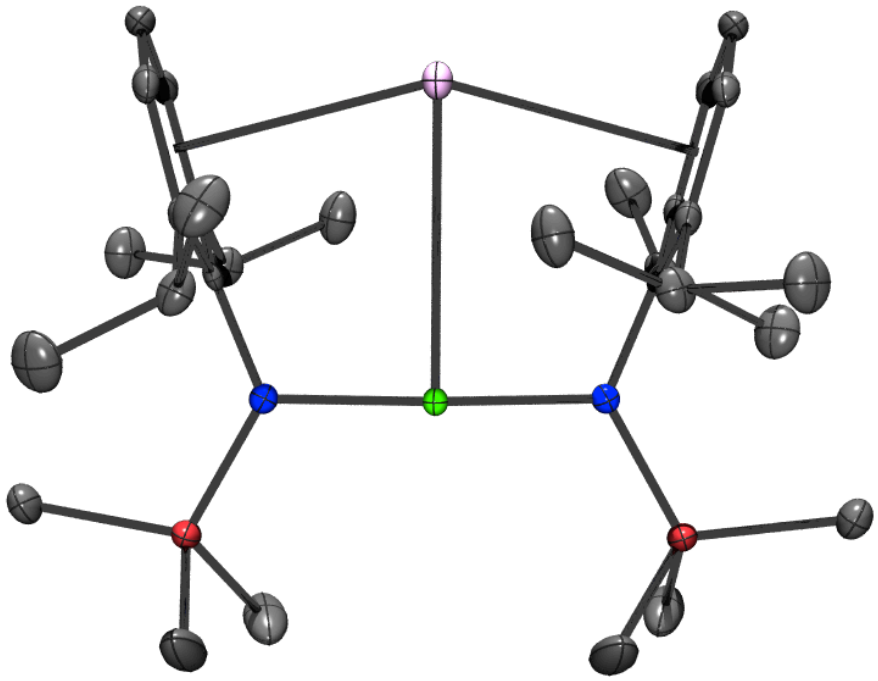

ORTEP diagram for compound **2a** (thermal ellipsoids shown at 50% probability). Ni-N: 1.8436(2) Å; N-Ni-N: 178.05(9)°

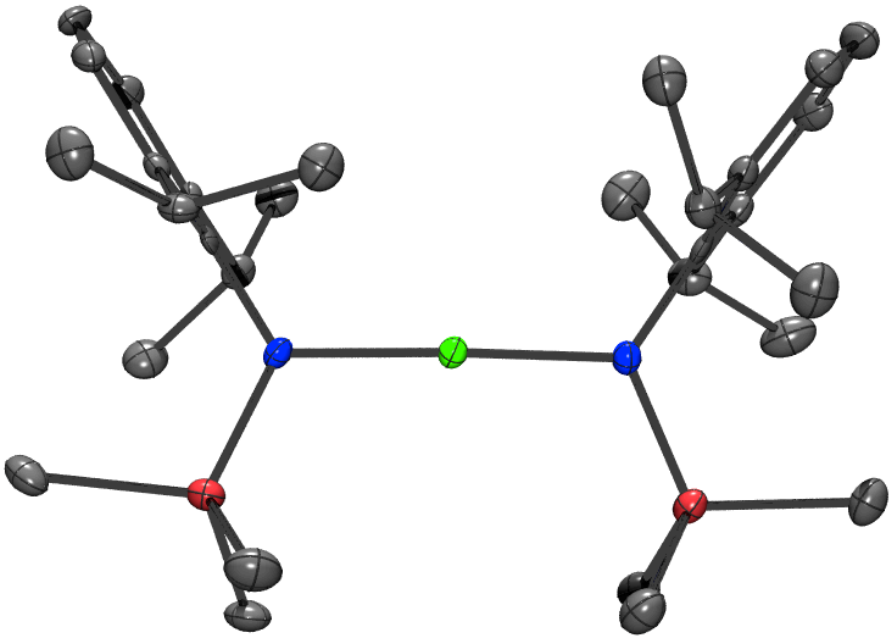

ORTEP diagram for compound **2b** (thermal ellipsoids shown at 50% probability). Ni-N: 1.8437(17), 1.8516(17) Å; N-Ni-N: 176.51(8)º

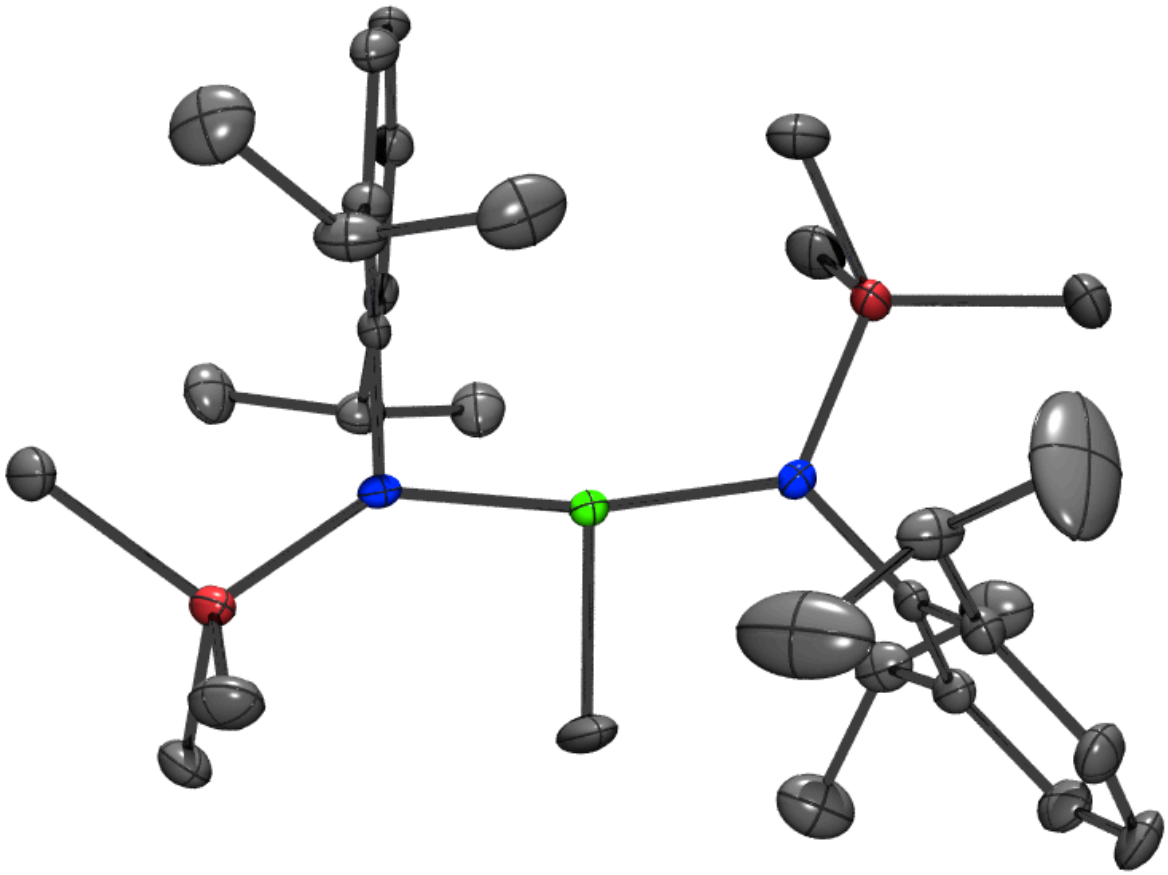

ORTEP diagram for compound **3** (thermal ellipsoids shown at 50% probability). Ni-N (close): 1.8037(18), 1.809(2) Å; Ni-N (far): 1.8249(19), 1.8156(19) Å; Ni-C: 1.923(4) Å; N-Ni-N: 167.4(1)º (where measurements differ significantly between the two crystallographically inequivalent molecules, both measurements are given sequentially).

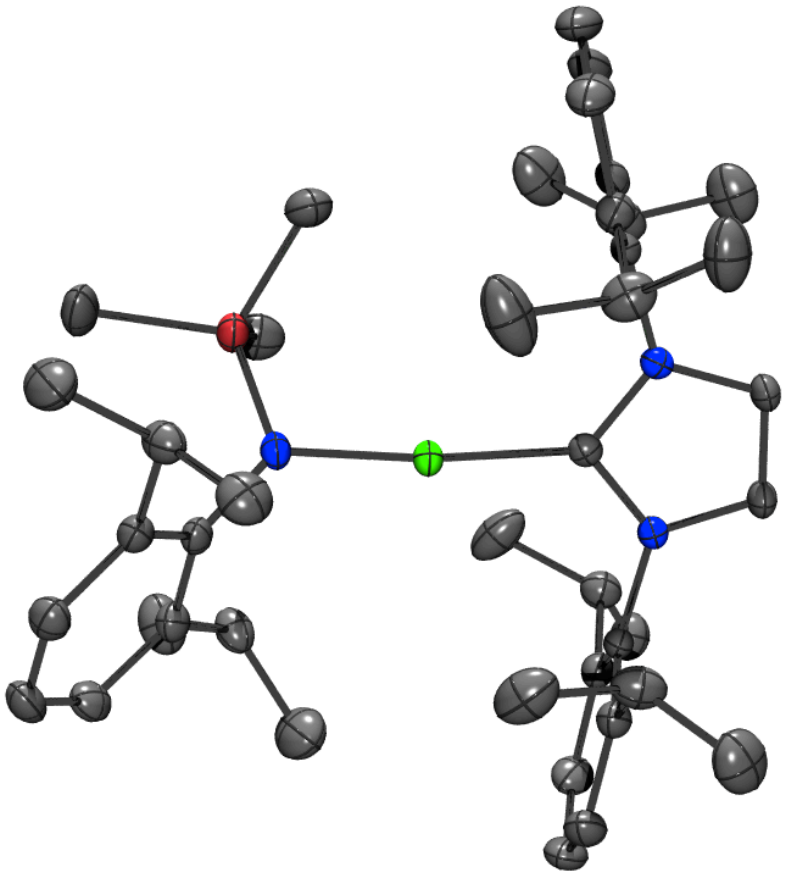

ORTEP diagram for compound **4** (thermal ellipsoids shown at 50% probability). Ni-N: 1.8271(14) Å; Ni-C: 1.9123(16) Å; N-Ni-C: 173.01(7)º

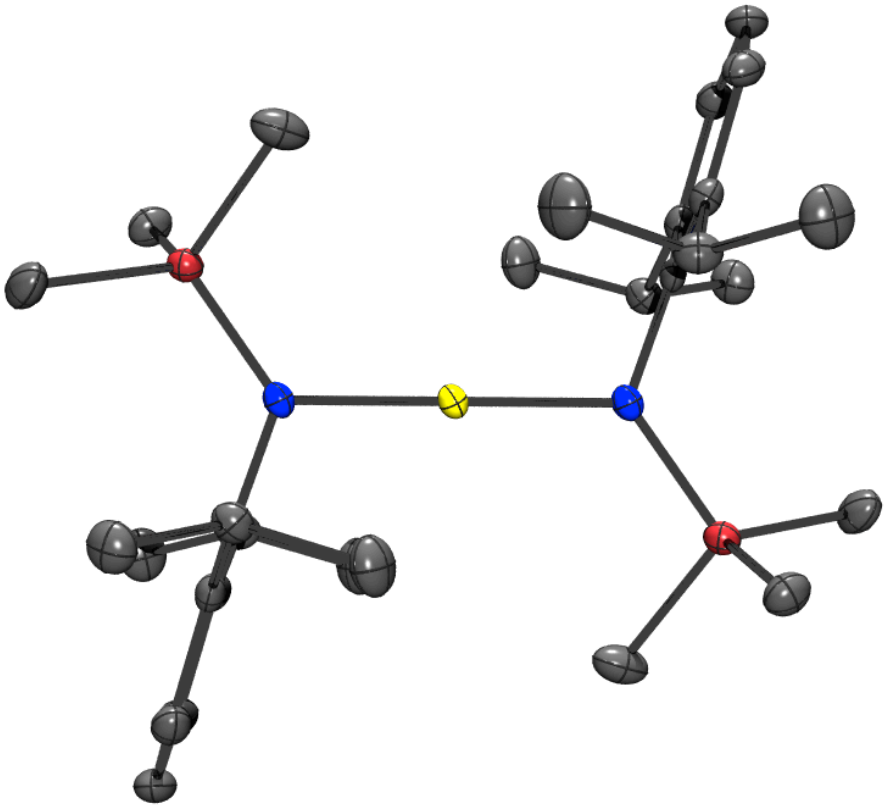

ORTEP diagram for compound **6** (thermal ellipsoids shown at 50% probability). Co-N: 1.8339(10) Å; N-Co-N: 180.00(3)º

CALCULATED GEOMETRIES AND MO FIGURES

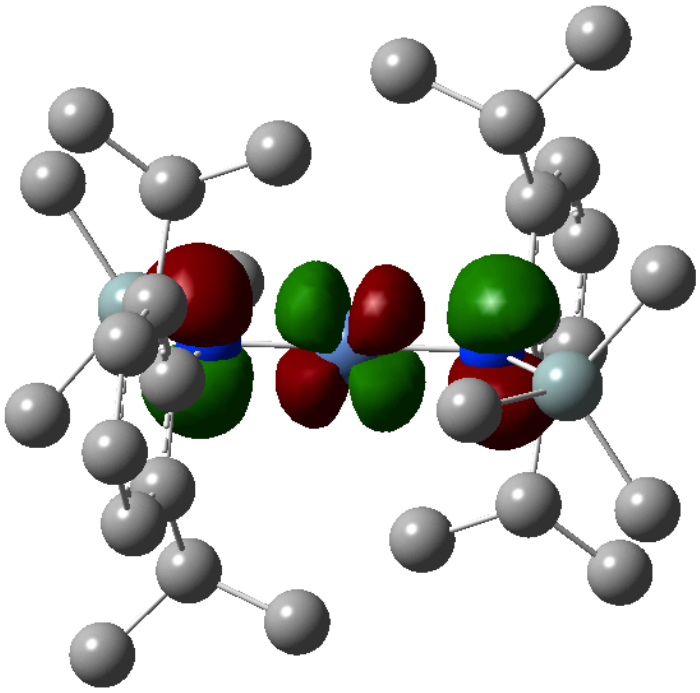

Calculated HOMO (π-antibonding) for **1** using hybrid functional.

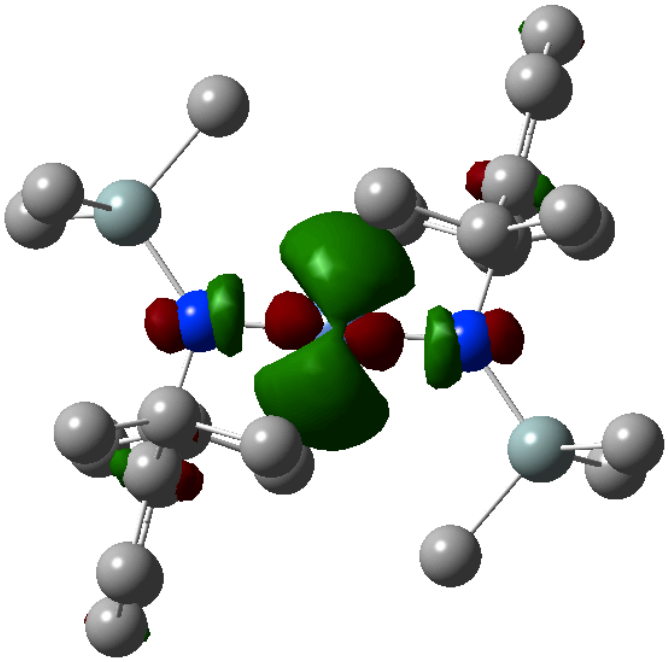

Calculated HOMO - 1 for **1** using hybrid functional.

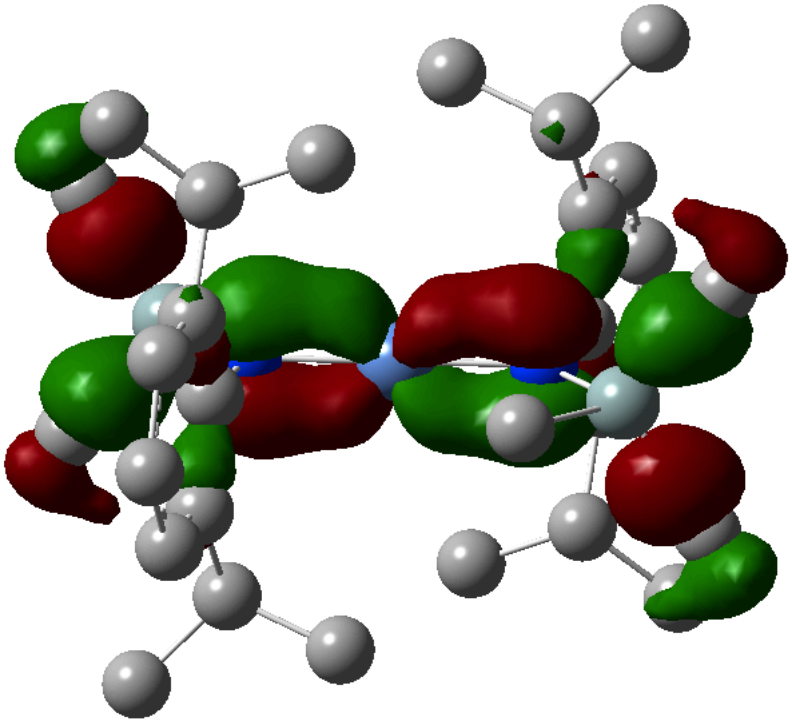

Calculated π-bonding MO for **1** using hybrid functional.

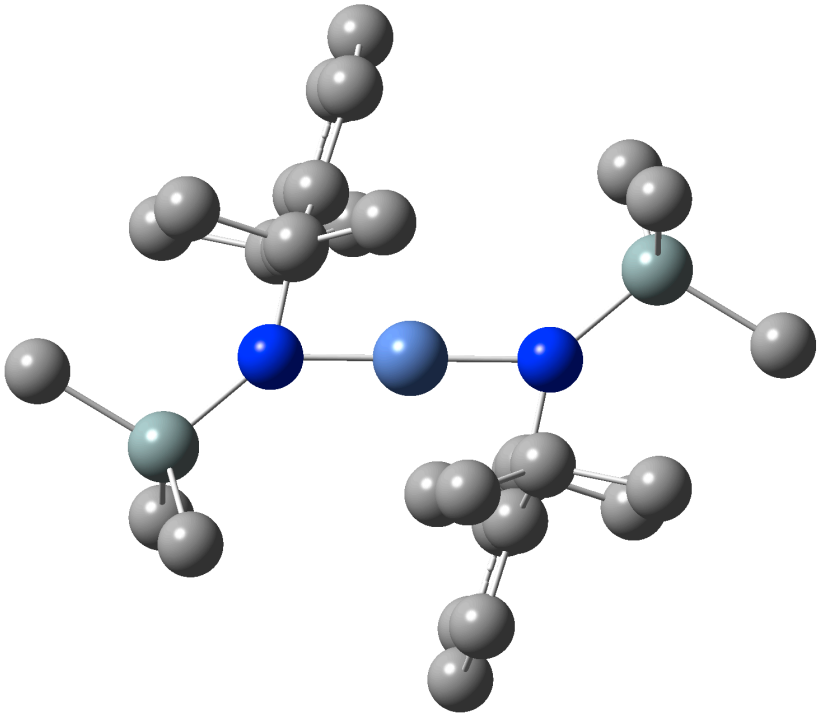

Optimized geometry of **5** using ωB97XD functional.

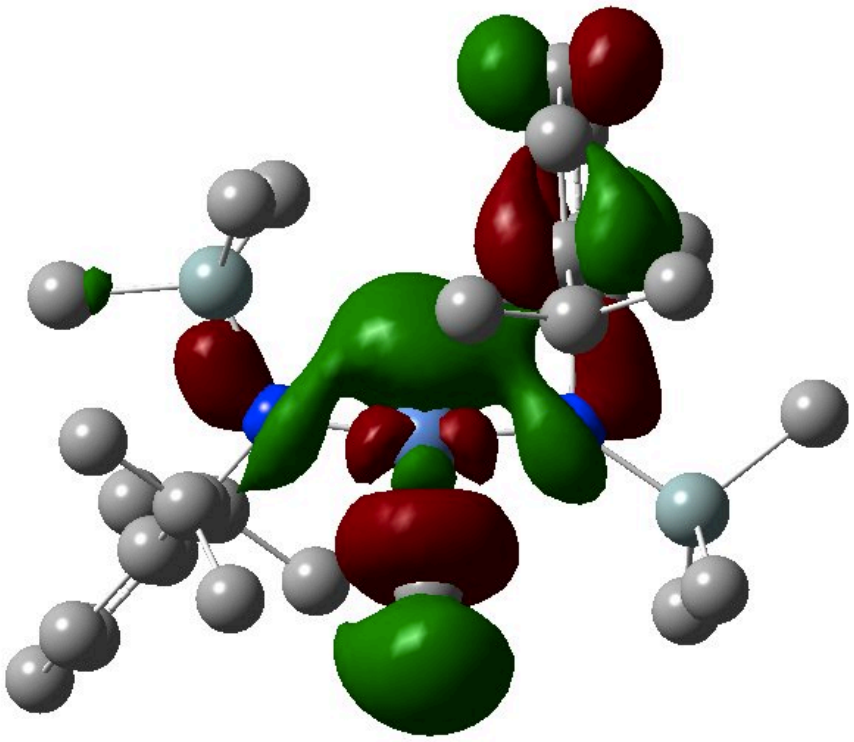

Calculated LUMO for **3** using revTPSS functional.

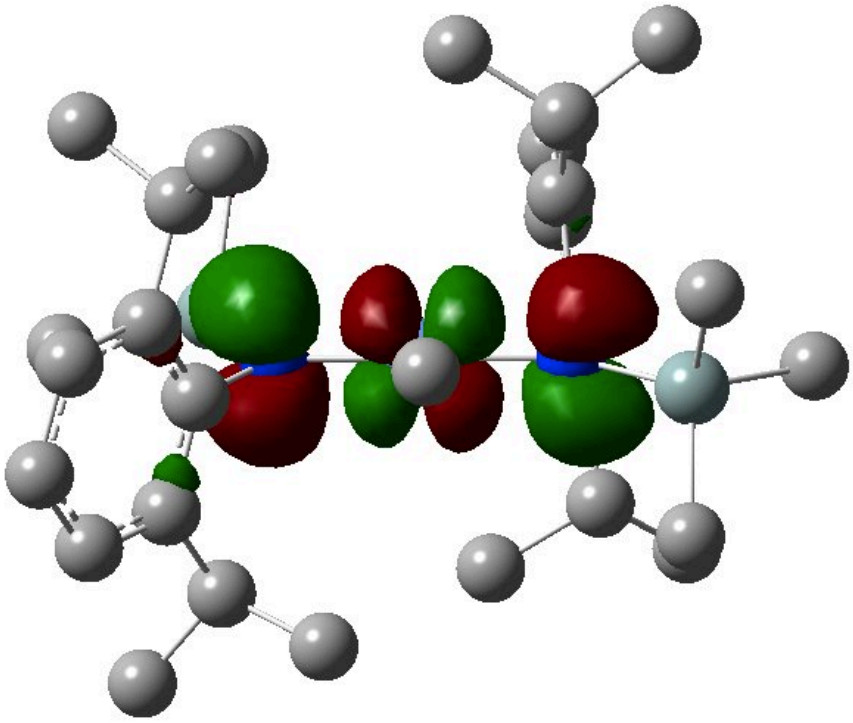

Calculated HOMO for **3** using revTPSS functional.

CYCLIC VOLTAMMOGRAMS

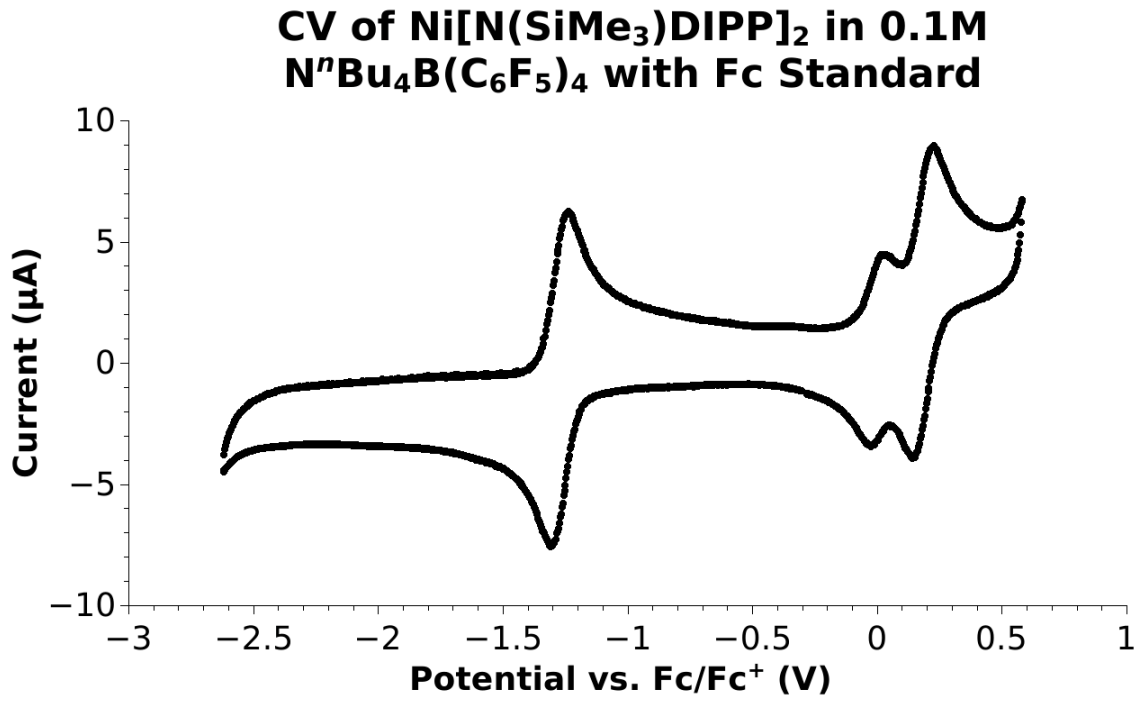

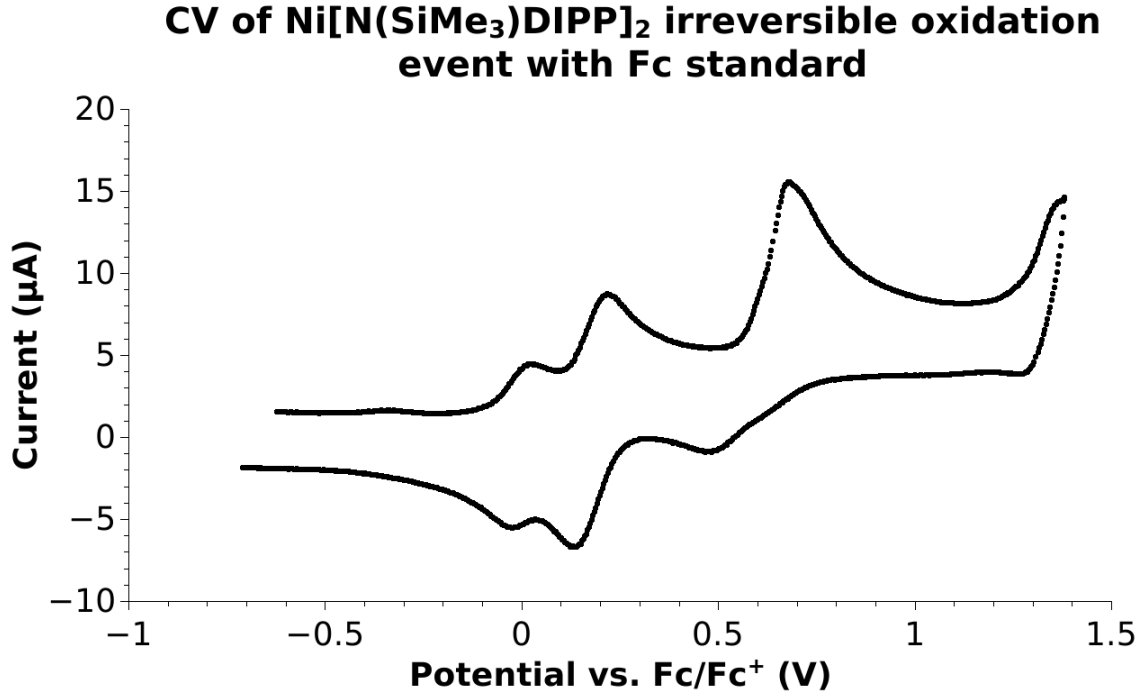

EPR SPECTRA

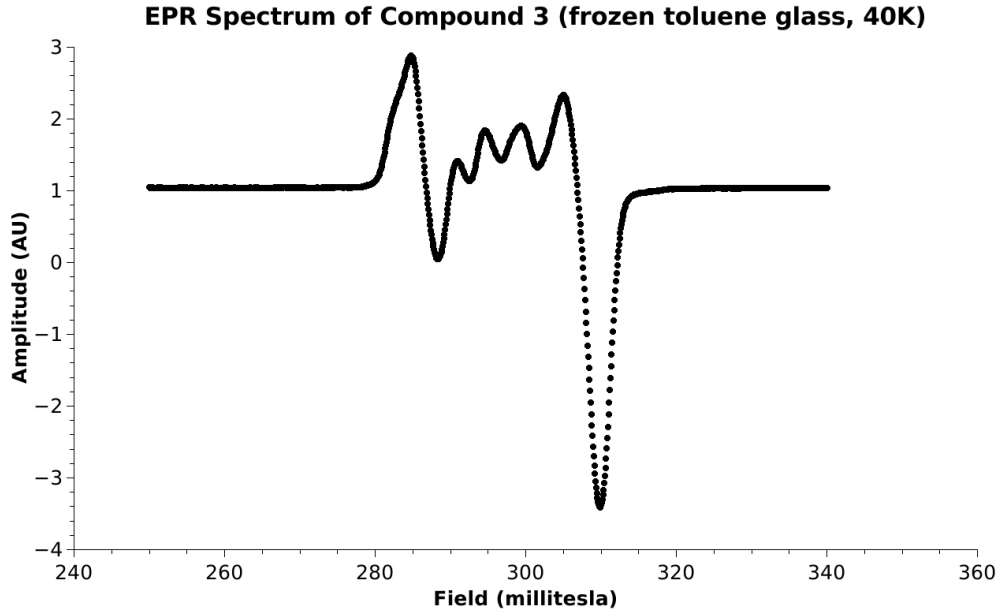

The EPR spectrum of **3** shows rhombic symmetry with g anisotropy values $g_{xx,}$ $g_{yy,}$ g_{zz} = (2.32, 2.15, 2.13). g-values are derived from simulation of the EPR spectrum (see Experimental Section for details). ^{14}N hyperfine coupling constants could not be simulated due to inhomogeneous broadening of the signal.

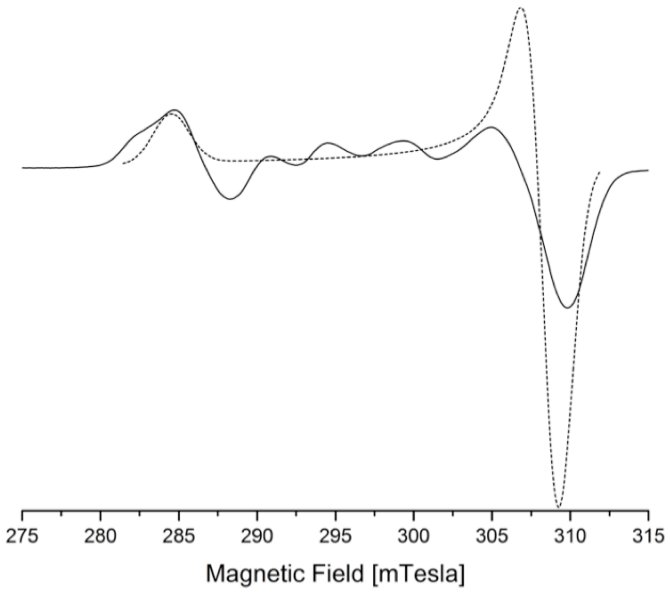

Simulated EPR spectrum of compound **3**.

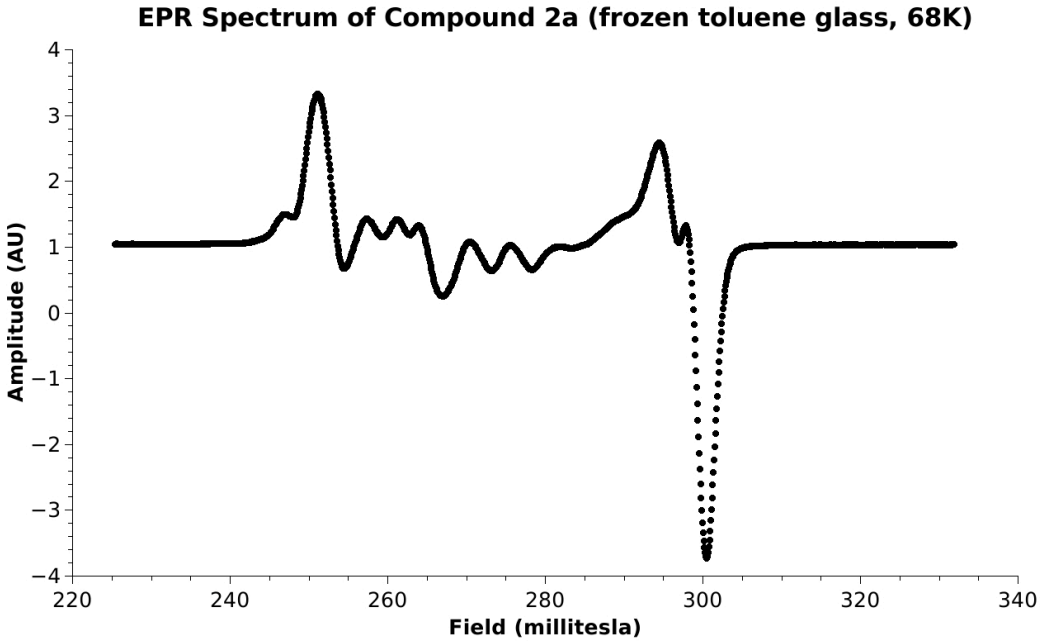

The EPR spectrum of **2a** shows rhombic symmetry with g anisotropy values g_{xx}, g_{yy}, g_{zz} = (2.63, 2.23, 2.20). g-values are derived from simulation of the EPR spectrum (see section 1 for details). ^{14}N hyperfine coupling constants could not be simulated due to inhomogeneous broadening of the signal.

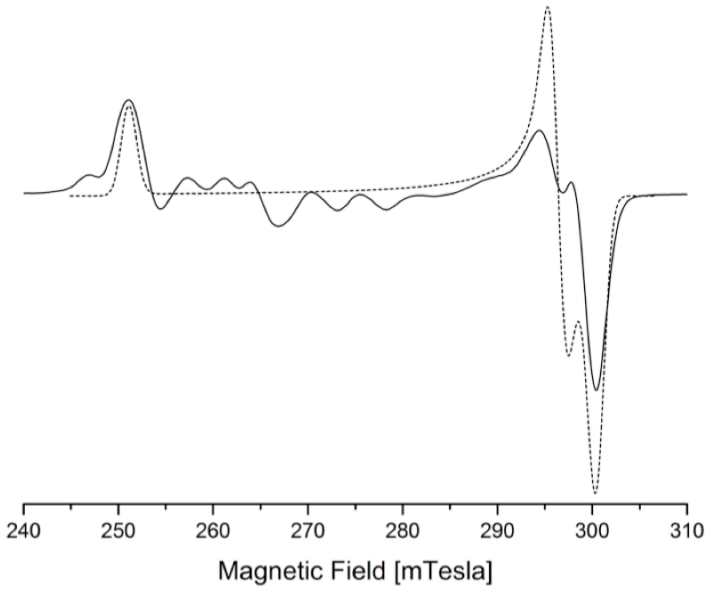

Simulated EPR spectrum of compound **2a**.

X-RAY DATA TABLES

Compound **2a**:

Empirical formula	C30 H52 K N2 Ni Si2
Formula weight	594.73
Temperature	100(2) K
Wavelength	0.71073 A
Crystal system, space group	Orthorhombic, Pccn
Unit cell dimensions	a = 13.3749(9) A alpha = 90 deg.
	b = 13.3774(9) A beta = 90 deg.
	c = 18.2349(12) A gamma = 90 deg.
Volume	3262.6(4) A^3
Z, Calculated density	4, 1.211 Mg/m^3
Absorption coefficient	0.816 mm^-1
F(000)	1284
Crystal size	0.12 x 0.12 x 0.11 mm
Theta range for data collection	2.15 to 25.38 deg.
Limiting indices	-16<=h<=16, -13<=k<=16, -20<=l<=21
Reflections collected / unique	40859 / 2999 [R(int) = 0.0557]
Completeness to theta = 25.00	100.0 %
Absorption correction	Multi-scan
Max. and min. transmission	0.9156 and 0.9084
Refinement method	Full-matrix least-squares on F^2
Data / restraints / parameters	2999 / 0 / 171
Goodness-of-fit on F^2	1.030
Final R indices [I>2sigma(I)]	R1 = 0.0284, wR2 = 0.0619
R indices (all data)	R1 = 0.0391, wR2 = 0.0676
Largest diff. peak and hole	0.336 and -0.256 e.A^-3

Compound **2b**:

Empirical formula	C46 H88 N3 Ni Si2
Formula weight	798.08
Temperature	100(2) K
Wavelength	0.71073 Å
Crystal system	Orthorhombic
Space group	P2(1)2(1)2(1)
Unit cell dimensions	a = 10.7683(6) Å a= 90°.
	b = 19.8450(12) Å b= 90°.
	c = 22.5472(12) Å g = 90°.
Volume	4818.3(5) Å3
Z	4
Density (calculated)	1.100 Mg/m3
Absorption coefficient	0.484 mm-1
F(000)	1764
Crystal size	0.08 x 0.08 x 0.03 mm3

Theta range for data collection	1.37 to 28.35°.
Index ranges	-8<=h<=12, -26<=k<=23, -28<=l<=23
Reflections collected	36187
Independent reflections	9409 [R(int) = 0.0379]
Completeness to theta = 25.00°	98.0 %
Absorption correction	Multi-scan
Max. and min. transmission	0.9856 and 0.9623
Refinement method	Full-matrix least-squares on F2
Data / restraints / parameters	9409 / 0 / 487
Goodness-of-fit on F2	1.037
Final R indices [I>2sigma(I)]	R1 = 0.0364, wR2 = 0.0625
R indices (all data)	R1 = 0.0526, wR2 = 0.0673
Absolute structure parameter	-0.002(8)
Largest diff. peak and hole	0.401 and -0.379 e.Å-3

Compound **3**:

Empirical formula	C31 H55 N2 Ni Si2
Formula weight	570.66
Temperature	100(2) K
Wavelength	0.71073 A
Crystal system, space group	Triclinic, P-1
Unit cell dimensions	a = 11.8649(13) A alpha = 82.230(5) deg. b = 17.206(2) A beta = 71.210(5) deg. c = 17.3304(19) A gamma = 88.850(5) deg.
Volume	3317.7(6) A^3
Z, Calculated density	4, 1.142 Mg/m^3
Absorption coefficient	0.678 mm^-1
F(000)	1244
Crystal size	0.08 x 0.03 x 0.01 mm
Theta range for data collection	1.19 to 25.52 deg.
Limiting indices	-14<=h<=14, -20<=k<=20, -20<=l<=20
Reflections collected / unique	40695 / 12267 [R(int) = 0.0408]
Completeness to theta = 25.00	99.9 %
Absorption correction	Multi-scan
Max. and min. transmission	0.9933 and 0.9478
Refinement method	Full-matrix least-squares on F^2
Data / restraints / parameters	12267 / 0 / 679
Goodness-of-fit on F^2	1.040
Final R indices [I>2sigma(I)]	R1 = 0.0390, wR2 = 0.0821
R indices (all data)	R1 = 0.0551, wR2 = 0.0895
Largest diff. peak and hole	1.186 and -0.677 e.A^-3

Compound **4**:

Empirical formula	C42 H62 N3 Ni Si
Formula weight	695.75

Temperature	100(2) K
Wavelength	0.71073 A
Crystal system, space group	Monoclinic, P2(1)/n
Unit cell dimensions	a = 10.4100(4) A alpha = 90 deg. b = 18.0926(7) A beta = 99.612(2) deg. c = 22.1319(8) A gamma = 90 deg.
Volume	4109.9(3) A^3
Z, Calculated density	4, 1.124 Mg/m^3
Absorption coefficient	0.531 mm^-1
F(000)	1508
Crystal size	0.19 x 0.15 x 0.07 mm
Theta range for data collection	1.46 to 27.55 deg.
Limiting indices	-13<=h<=13, -23<=k<=23, -28<=l<=28
Reflections collected / unique	62759 / 9320 [R(int) = 0.0439]
Completeness to theta = 25.00	100.0 %
Absorption correction	Multi-scan
Max. and min. transmission	0.9637 and 0.9058
Refinement method	Full-matrix least-squares on F^2
Data / restraints / parameters	9320 / 0 / 439
Goodness-of-fit on F^2	1.024
Final R indices [I>2sigma(I)]	R1 = 0.0374, wR2 = 0.0837
R indices (all data)	R1 = 0.0559, wR2 = 0.0922
Largest diff. peak and hole	0.363 and -0.314 e.A^-3

Compound **6**:

Empirical formula	C30 H52 Co N2 Si2
Formula weight	555.85
Temperature	100(2) K
Wavelength	0.71073 A
Crystal system, space group	Triclinic, P-1
Unit cell dimensions	a = 8.8146(8) A alpha = 102.530(4) deg. b = 9.1675(8) A beta = 92.358(4) deg. c = 11.1307(10) A gamma = 113.879(3) deg.
Volume	794.44(12) A^3
Z, Calculated density	1, 1.162 Mg/m^3
Absorption coefficient	0.635 mm^-1
F(000)	301
Crystal size	0.12 x 0.11 x 0.04 mm
Theta range for data collection	1.89 to 25.39 deg.
Limiting indices	-10<=h<=10, -11<=k<=11, -13<=l<=13
Reflections collected / unique	21145 / 2919 [R(int) = 0.0230]
Completeness to theta = 25.00	99.9 %
Absorption correction	Multi-scan
Max. and min. transmission	0.9750 and 0.9277

Refinement method	Full-matrix least-squares on F^2
Data / restraints / parameters	2919 / 0 / 167
Goodness-of-fit on F^2	1.076
Final R indices [I>2sigma(I)]	R1 = 0.0226, wR2 = 0.0605
R indices (all data)	R1 = 0.0240, wR2 = 0.0614
Largest diff. peak and hole	0.318 and -0.192 e.A^-3

Chapter 3. Carbon-carbon cross-coupling reactions catalyzed by a two-coordinate nickel(II) bis(amido) complex *via* observable Ni^{I}, Ni^{II} and Ni^{III} intermediates

INTRODUCTION

Transition-metal catalyzed cross-coupling reactions encompass highly versatile methods for the construction of complex molecules from simple building blocks.[1] Efficient catalytic systems for a wide range of substrates are utilized in both research laboratories and industry. The most efficient and commonly employed cross-coupling catalysts feature 2nd- and 3rd-row transition metals, most notably palladium, to achieve high turnover numbers.[1a,2] Despite the mature state of this synthetic methodology, cross-coupling catalysis continues to attract significant interest, especially with respect to development of more sustainable catalysts based on abundant 1st-row transition metals.[1a,j,k,3] Various cross-coupling catalysts with 1st-row metals have been reported, and those based on nickel are particularly promising.[1g,4]

While nickel catalysts are effective in many of the same transformations known for palladium, recent reports indicate that nickel also promotes couplings of more challenging substrates, including Grignard reagents and unactivated alkyl halides.[5] These catalysts are thought to employ mechanisms that are distinct from those of palladium, involving one-electron redox processes that feature Ni(III)-alkyl or -aryl species as key intermediates.[6] While a few Ni(III) species of this type have been isolated and characterized, none have been rigorously proven to be an intermediate in a catalytic cross-coupling.[7] Thus, a primary objective of research in this area is the acquisition of mechanistic information, and defining the role of nickel(III) species in an operative catalytic cycle. In this context, it was of interest to investigate the recently reported nickel(III) alkyl complex (Me)Ni[N(SiMe$_3$)DIPP]$_2$ (**1**)[7a] and explore its potential relevance as a catalytic intermediate. This investigation led to the discovery and mechanistic elaboration of C-C cross-couplings catalyzed by Ni[N(SiMe$_3$)DIPP]$_2$ (**2**). The latter complex appears to represent a new class of coupling catalysts, based on a two-coordinate bis(amido) ligand framework.

RESULTS AND DISCUSSION

Reaction of **1** with one equivalent of PhI or $C_{12}H_{25}I$ in THF did not lead to any observed products within the time that **1** decomposed to ethane and Ni[N(SiMe$_3$)DIPP]$_2$ (**2**, *ca.* 24 h). However, in light of a mechanism for nickel-catalyzed alkyl-alkyl cross-couplings recently proposed by Breitenfeld and Hu,[6a] in which the alkyl halide is initially activated by a nickel(II) alkyl complex, the reduction of **1** to a Ni(II) analogue was examined. Cyclic voltammetry revealed that **1** undergoes a reversible Ni(II/III) reduction at -1.30 V ($E_{1/2}$ vs. Fc/Fc$^+$, ip_a/ip_c = 0.98), suggesting that **1** might be readily reduced to the corresponding, anionic Ni(II) methyl complex. Indeed, reduction of **1** with KC_8 at -30ºC in toluene over 25 minutes, followed by precipitation from toluene/pentane, provided the blue, anionic nickel(II) methyl complex K{(Me)Ni[N(SiMe$_3$)DIPP]$_2$} (**3**) in 64% yield (Scheme 1).

Analysis of **3** by single-crystal X-ray diffraction revealed molecular units containing a T-shaped, three-coordinate nickel center, linked into a polymeric chain *via* coordination of the potassium ions to the aryl rings of adjacent units (Figure 1). Comparison of this structure to that of the nickel(III) species **1** reveals that the nickel(II) complex **3** possesses a longer average Ni-N bond length (av. 1.891(2) Å Ni(II); 1.813(2) Å Ni(III)), as expected based on a larger covalent radius for the more reduced nickel center. However, the Ni^{II}–C bond length in **3** (av. 1.891(2) Å) is unexpectedly shorter than the corresponding Ni^{III}–C distance in **1** (1.923(4) Å), presumably due to population of a Ni–σ* orbital in the latter (see Appendix). Despite being three-coordinate,

3 is low-spin and diamagnetic, with the methyl resonance appearing as a singlet in the ^{1}H NMR spectrum at -0.95 ppm. Like complex **1**, **3** is thermally unstable and decomposes over a period of 7 days in C_6D_6 *via* reductive homolysis to the previously reported anionic nickel(I) complex K{Ni[N(SiMe$_3$)DIPP]$_2$} (**4**),[7a] with elimination of ethane (^{1}H and ^{13}C NMR spectroscopy). Compound **3** exhibits no signs of decomposition after several months as a solid stored at -30ºC.

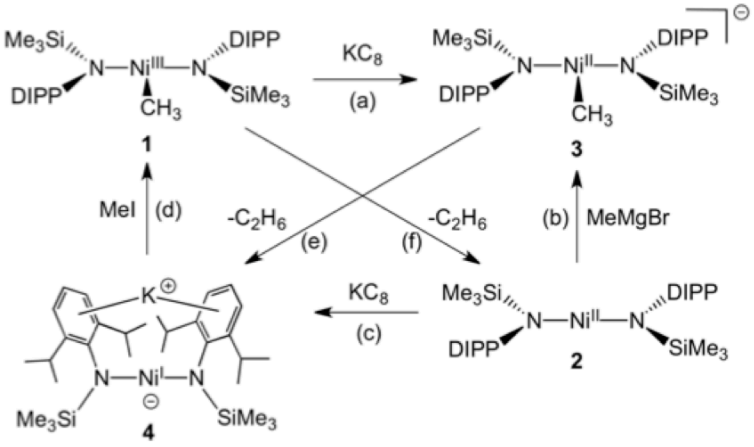

Scheme 1. Reactions of related Ni-bis(amido) species. Conditions: (a) toluene, 25 minutes. (b) THF, seconds (c) toluene, 15 minutes. (d) THF, 30 minutes. (e) benzene, 7 days. (f) benzene, 1 day.

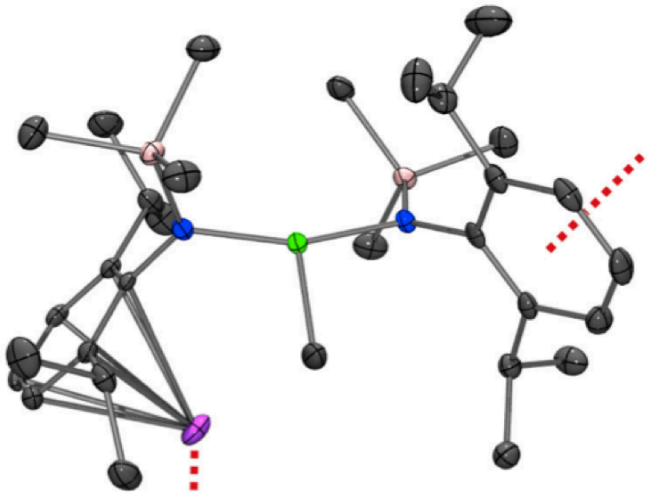

Figure 1. ORTEP diagram of **3**. Thermal ellipsoids shown at 50% probability. Dashed red lines indicate intermolecular connectivity in the solid state. Selected bond lengths and angles: Ni-C: 1.879(2) Å; Ni-N: 1.8914(2) Å (av.); N-Ni-N: 161.42(7)º.

The accessibility of analogous Ni(II) and Ni(III) alkyls in this system, and the possible roles for such species as intermediates in catalytic C-C cross-coupling reactions, prompted an examination of **2** as a catalyst for the cross-coupling of Grignard reagents with alkyl and aryl halides. As shown in Table 1, **2** is a competent catalyst for the cross coupling of aryl halides with both aryl and methyl Grignard reagents at ambient temperature. Electron-poor substrates appear

to be preferred (e.g., 8-bromoquinoline (93%) vs. 3-bromoanisole (<10%); entries 4 and 6 respectively), though electron rich aryl iodide substrates also performed well. This catalytic system is also effective for more challenging aryl chloride substrates as well as aryl bromides and iodides. Heterocyclic compounds, including coordinating pyridine units, are also well tolerated despite concern that strong coordination of pyridines to **2** could inhibit catalysis.[8] Attempts to couple aryl and alkyl Grignards with unactivated alkyl iodides resulted in only trace amounts of the cross-coupled product with the balance of products going to C12 alkene isomers and dodecane (entry 10).

Use of EtMgBr as the Grignard reagent resulted in a substantially reduced yield compared to MeMgBr (30% vs. 74% in the coupling with 1-iodonaphthalene; Table 1, entry 2). To evaluate the stability of the anionic Ni(II) ethyl complex, the stoichiometric reaction between **2** and EtMgBr in d_8-THF was monitored by ^{1}H NMR spectroscopy. Addition of EtMgBr resulted in an immediate color change and complete consumption of **2**. Stoichiometric quantities of ethylene were detected in solution, suggesting that ß-hydride elimination had occurred. Similar results have been observed for other Ni(II) alkyl complexes,[9] and ß-hydride elimination is thought to represent a significant hurdle for Ni-catalyzed carbon-carbon couplings involving alkyl groups.[10]

Analysis of the isolated, post-catalytic reaction mixture from catalytic coupling of MeMgBr with PhI revealed that the primary nickel-containing product was anionic **3** (presumably as the $BrMg^+$ salt), accounting for 89% of the initial catalyst loading (^{1}H NMR spectroscopy in d_8-THF *vs.* internal standard). Small quantities of **4** also present in the post-catalytic reaction mixture may result from slight thermal decomposition of **3**. The relatively large proportion of molecular Ni complexes present after catalysis suggests that these species may be directly involved in the catalytic cycle. Additionally, the yield and qualitative rate of the coupling reactions were found to be unaffected by the presence of mercury, further supporting the involvement of a homogeneous catalyst.

Given the efficiency of carbon-carbon coupling catalysis by **2**, the relatively broad substrate scope, and the isolation of potential intermediates, it was of interest to explore the catalytic mechanism. Mechanistic studies involved observation of stoichiometric transformations for candidate intermediates **1**-**4**, and led to the proposed mechanism illustrated in Scheme 2. Initial addition of the Grignard reagent to the neutral nickel(II) bis(amido) complex **2** occurs to form an anionic nickel(II) alkyl or aryl complex (**3'**) analogous to **3**. This anionic complex then reduces the organic halide, with formation of an organic radical species and a nickel(III) alkyl or aryl complex (**1'**). The nature of this radical is currently undefined, and especially given the complexity of the reaction mixture, such radical species may not be "free". The organic radical then combines with a second equivalent of **3'** to form the cross-coupled product. This step may involve an anionic nickel(III) complex **5'**, which rapidly undergoes C–C reductive elimination to give the anionic nickel(I) complex **4**; alternatively, the radical may directly attack the metal-bound alkyl group of **3'**. The nickel(I) anion then reduces the nickel(III) complex resulting from reduction of the alkyl or aryl halide, to reform one equivalent each of **2** and **3'**. Based on the measured reduction potentials of **1** (-1.30 V vs. Fc/Fc^+, *vide supra*) and **2** (-1.28 V vs. Fc/Fc^+),[7a] this final redox step is expected to result in an equilibrium mixture of reactants and products.

Table 1. Substrate table for Grignard/Ar-X cross-coupling reactions catalysed by 5 mol % Ni[N($SiMe_3$)DIPP]$_2$ (**2**) with 1.1 eq. R'MgBr.

Entry	R-X	R'MgBr	Time	Yield (Et_2O)	Yield (THF)
1		PhMgBr	30 m	98%	92%
2	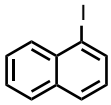	PhMgBr[a]	30 m	100%	67%
		MeMgBr	1.5 h	74%	87%
		EtMgBr	40 m	30%	-
3	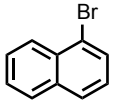	PhMgBr	1 h	68%	95%
4	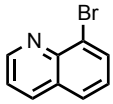	PhMgBr	1.5 h	93%	18%
5	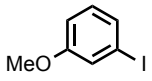	PhMgBr	1.5 h	99%	33%
		MeMgBr	3.5 h	93%[b]	-
6	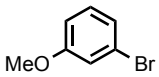	PhMgBr	5.5 h	<10%	56%
7	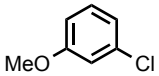	PhMgBr	66 h	<10%	59%
8	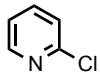	PhMgBr	2 h	78%	47%
9	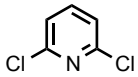	PhMgBr[c]	6 h	92%	-
10	$C_{12}H_{25}I$	MeMgBr	45 m	<1%	<10%
		PhMgBr	45 m	0%	0%
11		PhMgBr	40 m	-	79%[d]

[a] Catalysis performed using 0.5 mol % **2**. [b] Yield determined by calibrated GC/FID instead of NMR due to the volatility of the product. [c] 2.1 eq. of PhMgBr were used. [d] Yield is of the ring-opened product 4-phenyl-1-butene.

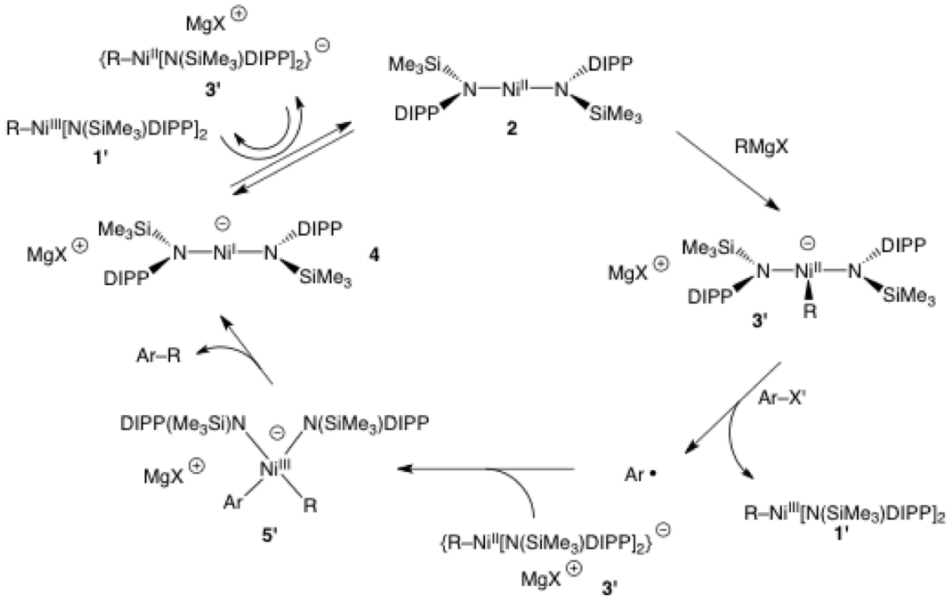

Scheme 2. Proposed mechanism of catalytic coupling of Grignard reagents with aryl halides by **2**. All species have been directly observed except **5'** and Ar•.

The feasibility of each step of the proposed catalytic cycle was tested by investigating relevant stoichiometric reactions of **1**-**4** and the catalytic substrates. The first step of this mechanism, the addition of a carbanion to **2**, was easily demonstrated by the reaction of **2** with 1.1 equivalents of MeMgBr at -30ºC in THF over 30 seconds, which resulted in formation of a solution having the characteristic blue color of **3**. Analysis of the products by ^{1}H NMR and UV-vis spectroscopies revealed the presence of a diamagnetic species with spectra indistinguishable from those of **3** (see Appendix). The methylation of **2** with MeMgBr to form **3**, the resting state of the catalysis, proceeds well within the timeframe of catalysis and in nearly quantitative yield (>98% by UV-vis).

The stoichiometric (1:1) reaction of **3** with 1-iodonaphthalene was observed to proceed sluggishly over 45 minutes to give the cross-coupled product 1-methylnaphthalene in only 13% yield. This reaction also produces significant quantities of the nickel(III) methyl complex **1**, along with 1,1'-binaphthalene (64%) and unreacted 1-iodonaphthalene (23%). Addition of one equivalent of **1** to the reaction mixture (**1**, **3** and 1-iodonaphthalene in a 1:1:1 ratio) did not result in improved yield of the cross-coupled product (10%), indicating that **1** is not an effective trap for the species produced by reduction of the aryl iodide. In fact, two equivalents of **3** are required for efficient conversion of the aryl halide to product, as indicated by reaction of 1-iodonaphthalene with two equivalents of **3** in THF, which proceeded to completion within minutes to cleanly produce 1-methylnaphthalene in 98% yield. Thus, the cross-coupling of aryl halide requires two equivalents of **3**, which appears to be the species that traps the radical rather than **1**. Analysis of the post-coupling reaction mixture indicated the presence of all four species **1**-**4**, as expected given the rapid equilibrium that converts **1** and **4** to **2** and **3** (*vide infra*).

The nature of the reduced aryl or alkyl halide was probed with use of the radical clock substrate (iodomethyl)cyclopropane. The cross-coupling of (iodomethyl)cyclopropane with 1.1 equivalents of PhMgBr catalyzed by 5 mol % of **2** resulted in a 79% yield of 4-phenyl-1-butene,

the product resulting from rearrangement of the (cyclopropyl)methyl radical (Table 1, entry 11). This suggests that a radical intermediate results from reduction of the alkyl halide, as shown in the proposed mechanism of Scheme 2. No unrearranged product was observed, and no coupling products of any kind were observed in the absence of **2**.

The last step in the catalytic cycle, the reduction of **1** by **4**, to form **2** and **3**, was demonstrated by addition of one equivalent of **1** to the $N^nBu_4^+$ salt of **4** (**4a**)[7a] in THF, resulting in an immediate color change from dark green to dark grey/black. Due to extensive paramagnetic broadening in d_8-THF solutions of paramagnetic species **1**, **2** and **4**, it was not possible to accurately measure the equilibrium constant by ^{1}H NMR. However, all four species **1**-**4** were detected and the $N^nBu_4^+$ salt of **3** was isolated from the other Ni-containing species in 29% yield (^{1}H NMR spectroscopy in d_8-THF *vs.* an internal standard, see Experimental Section), consistent with the equilibrium mixture predicted by the observed redox potentials.

This redox equilibrium step plays an important role in determining the efficiency of catalysis. This is indicated, for example, by stoichiometric reactions of **3** with 1-iodonaphthalene. This reaction produces a low yield of cross-coupled product (13%); however, addition of one equivalent of MeMgBr to the reaction mixture led to a substantially better yield (77%). This is attributed to the Grignard reagent's effect on the redox equilibrium step of the cycle (Scheme 2). Apparently, the rapid reaction of MeMgBr with **2** to form **3** pulls the redox equilibrium to the right (to **2** and **3** and ultimately, to only **3**). Consistently, addition of one equivalent of MeMgBr to an equilibrium mixture of **1**-**4** (produced by reaction of **4a** with **1**) resulted in an immediate color change from dark grey/black to the characteristic blue color of **3**. Analysis of the resulting products by ^{1}H NMR spectroscopy indicated that all Ni-containing species had been converted to **3**. By shifting the equilibrium in this way, the Grignard reagent ensures efficient recycling of **1** and **4** to **3**, such that every radical in the cycle has a coupling partner. In the absence of Grignard, **3** is consumed in the reduction of the aryl halide and because the redox reaction produces an equilibrium mixture, the Ni-byproducts are not efficiently recycled. Additionally, **4** was found to react with aryl halides to produce undesired homocoupling products: reaction of **4** with 1-iodonaphthalene in THF over 1 hour produced 1,1'-binaphthalene in 80% yield. This unproductive process is also prevented by the Grignard's effect on the equilibrium. Notably, this reaction of **4** with aryl halide is substantially slower than the oxidation of **4** by **1**, a result predicted by Breitenfeld and Hu for an analogous nickel(I) intermediate in their system.[6a]

The stoichiometric reaction chemistry described above provides compelling support for the proposed mechanism of Scheme 2. Significantly, this mechanism involves several intermediates (**1**-**4**) that have been isolated, completely characterized, and observed to participate in catalytically competent reaction steps. These results lend substantial support to proposed mechanisms for nickel-mediated cross-couplings that feature one-electron redox events for the nickel species,[4d] and especially corroborate the bimetallic oxidative addition mechanism (featuring comparable but inner sphere redox events) suggested by Breitenfeld and Hu.[6a] This study also provides experimental mechanistic evidence for the roles of nickel(I) and nickel(III) intermediates in this catalysis. Of particular interest is demonstration of a function for the nickel(III) alkyl complex (**1**), especially given previous speculation about such species in cross-coupling chemistry. In catalysis initiated by the bis(amido) complex **2**, the neutral nickel(III) alkyl species appear to participate only in redox reactions, and not directly in any of the key bond-forming or bond-breaking steps. This nickel(III) species is formed as a byproduct of the C–X bond activation, and plays a key role in oxidizing nickel(I) in the catalytic mixture back to nickel(II). The latter redox process not only provides nickel(II) species required for the coupling

steps, but removes nickel(I) which is active for the nonproductive homo-coupling of the halide substrate.

A somewhat more speculative aspect of this reaction mechanism concerns detail for reaction of the radical species with the anionic nickel(II) complex. This step may involve attack of the radical on the nickel center, to generate the nickel(III) complex **5'** (Scheme 2), from which the product is formed by reductive elimination. Alternatively, the organic radical might directly attack the alkyl or aryl ligand of **3'** to give **4** and the coupled product. The pathway involving **5'** is currently assumed, given spectroscopic observation of related intermediates by Vicic[11] as well as the observation of reductive elimination from Ni(III) alkyl species by Kochi[12] and Mirica.[7d] Also, the two-electron Ni(III/I) reductive elimination from **5'** seems reasonable given that the reverse process, a two-electron Ni(I/III) oxidative addition, has been experimentally demonstrated in the independent synthesis of **1** (Scheme 1).

This catalytic system is noteworthy as one of the only examples of an intact two-coordinate metal complex that competently catalyzes an organic transformation. Previously, $Fe[N(SiMe_3)_2]_2$ has been described as an active precatalyst for the hydrosilylation of organic carbonyls,[13] and **2** catalyzes the hydrosilylation of alkenes.[8] The catalytic mechanism of Scheme 2 is unusual in several respects that appear to leverage the very low coordination number of **2**. Direct alkylation of **2** by the Grignard without halogen displacement exploits the inherent electron deficiency of two-coordination, to stabilize a strongly reducing, anionic intermediate (**3**). The various redox processes of the mechanism proceed without ligand exchange, which is facilitated by the ability of this stable two-coordinate framework to support multiple oxidation states. These results suggest that two-coordinate complexes are a promising new class of potential catalysts whose unique chemical properties enable novel metal-mediated transformations.

CONCLUSION

In conclusion, a well-defined catalytic system for C-C coupling of aryl halides with Grignard reagents catalyzed by a two-coordinate nickel complex has been identified and mechanistically evaluated. Isolation and identification of the catalytic intermediates and stoichiometric reactions among those intermediates provides strong support for activation of the aryl halide by two metal centers and implicates a nickel(II) alkyl species as the coupling partner of the generated aryl radical rather than a nickel(III) alkyl species.

EXPERIMENTAL

General Considerations. Unless otherwise stated, all reactions and manipulations were carried out in a MBraun Lab Master DP glovebox or using standard Schlenk techniques under a nitrogen atmosphere. Pentane, hexanes, benzene, toluene, and 1,2-difluorobenzene were purchased from Sigma Aldrich. Diethyl ether was purchased from Honeywell and tetrahydrofuran was purchased from Macron Chemicals. Pentane, toluene, tetrahydrofuran, diethyl ether and 1,2-difluorobenzene were dried using a JC Meyers Phoenix SDS solvent purification system. Benzene and hexane were dried and degassed using a Vacuum Atmosphere solvent purifier system. Prior to drying, benzene was dethiophenated using standard techniques.[14] C_6D_6 was purchased from Cambridge Isotope Laboratories, dried over Na/K alloy and then degassed by four freeze-pump-thaw cycles. Potassium graphite[15] was prepared by standard

literature procedure. Compounds **1**[7a], **2**[8] and **4**[7a] were prepared by previously reported methods. All NMR spectra were collected at ambient temperature (ca. 22°C) on Bruker AVB-400, AV-500, AV-600 or AVQ-400 NMR spectrometers, each equipped with a 5 mm BB probe, and referenced to the residual proteo solvent signals. UV-Vis spectra were acquired in quartz cuvettes fitted with Chemglass Air-Free Teflon stoppered valves using a Varian Cary 50 UV-Vis spectrometer. Solution magnetic susceptibilities were determined by ^{1}H NMR spectroscopy using Evans's method.[16] Elemental analyses were performed by the UC Berkeley College of Chemistry Microanalytical facility. The abbreviation "DIPP" refers to a 2,6-diisopropylphenyl moiety.

Cyclic Voltammetry Experiments. Cyclic voltammetry experiments were conducted at ambient temperature in a Vacuum Atmospheres glovebox. Measurements employed a Bio-Logic SP-200 potentiostat with a standard three electrode configuration. The working electrode was a 3mm diameter glassy carbon electrode purchased from ALS. Silver wire was used as a quasi-reference electrode and sublimed ferrocene was used as an internal potential reference. The counter electrode was a 1/8 inch diameter graphite rod purchased from Electron Microscopy Sciences. The glassy carbon electrode was polished with 1 μm alumina prior to each use. The graphite rod was cleaned with acetone and dried prior to each use. Analyses of **1** were performed in a 0.1 M solution of tetrabutylammonium hexafluorophosphate in 1,2-difluorobenzene with an analyte concentration of 1 mM at a scan rate of 100 mV/s. No solution resistance correction was applied. All potential values are reported as $E_{1/2}$ for reversible events and E_p for irreversible events.

DFT Calculations. Calculations on **1** and **2** were reported in a prior publication[7a] and Chapter 2. Calculations on **3** were performed using the Gaussian 09 program[17] using the revTPSS[18] functional. The basis set used for all atoms was 6-31+G(d), using polarization and diffuse orbitals for all atoms except hydrogen. In all cases, frequency calculations confirm that the optimized structure resides at an energetic minimum. All geometries were optimized in the gas phase starting from the geometry indicated by X-ray diffraction.

X-ray Diffraction Experiments. Single crystal X-ray diffraction experiments were carried out at UC Berkeley CHEXRAY crystallographic facility. Measurements of compound **3** were performed on a Bruker APEX-II CCD area detector using Mo Kα radiation (λ = 0.71073 Å) monochromated using QUAZAR multilayer mirrors. Specific details of the experiment can be found below, and in the Appendix.

Experimental Details:

	Detector Distance	Image Width	Exposure Time
Compound **3**	50mm	0.5°	30 s

Coupling Experiments. Coupling reactions were performed in dry and degassed solvent under an inert atmosphere, as described above. The progress of the reaction was monitored by GC/MS and yields were determined by ^{1}H NMR by integration against the hexamethylbenzene internal standard. Products were identified by GC/MS and by comparison of their NMR spectra to those previously reported in the literature: biphenyl[19], 1-phenylnaphthalene[20], 1-

methylnaphthalene[21], 1-ethylnaphthalene[21], 8-phenylquinoline[22], 3-methoxy-1,1'-biphenyl[19], 3-methylanisole[23], 2-phenylpyridine[24], 2,6-diphenylpyridine[24], 4-phenyl-1-butene.[25]

General Procedure for C-C Coupling Reactions: To a 20 mL scintillation vial was added ArX (approx. 0.720 mmol), hexamethylbenzene (approx. 0.065 mmol), compound **2** (0.072 or 0.007 mmol for 5% and 0.5% loading, respectively) and 6 mL of diethyl ether. The vial was equipped with a Teflon coated magnetic stirbar and placed in a -35ºC freezer for approx. 20 min. The vial was then removed, the solution was stirred vigorously, and 1.1 equiv. of 3.0 M RMgBr solution in diethyl ether was added via syringe. The solution was then allowed to warm to room temperature while stirring. Yields were determined by quenching an aliquot of the reaction mixture with water and using ^{1}H NMR to integrate the product signals against the hexamethylbenzene internal standard.

Modified C-C Coupling Procedure for (iodomethyl)cyclopropane: To a 20 mL scintillation vial was added **2** (0.016 g, 0.029 mmol), hexamethylbenzene (0.0108 g, 0.067 mmol) and 4 mL of THF, forming a dark purple solution. The vial was equipped with a Teflon-coated magnetic stirbar and the solution was stirred vigorously. To the stirring solution was added 0.22 mL of a 3.0 M solution of PhMgBr (0.66 mmol) in Et_2O, dropwise, via syringe, causing a color change from purple to blue. To this stirring solution was added a solution of (iodomethyl)cyclopropane (0.108 g, 0.593 mmol) dissolved in 2 mL of THF, dropwise, over a period of 5 min. After 40 min, the reaction was quenched with water and the volatile components of an aliquot of the reaction mixture were removed under reduced pressure. Yield was determined by using ^{1}H NMR to integrate the product signals against the hexamethylbenzene internal standard (79% yield relative to alkyl iodide).

Reaction of 2 with EtMgBr. To a solution of **2** (0.010 g, 0.018 mmol) and hexamethylbenzene (0.004 g, 0.025 mmol) in 0.7 mL d_8-THF in an NMR tube was added 1 drop of a solution of EtMgBr in Et_2O. The mixture was sealed and shaken, causing an immediate color change from dark purple to a turquoise color. The solution was then analyzed by ^{1}H NMR. Stoichiometric quantities of ethylene were detected. The yield determined from integration against the internal standard corresponded to approximately 55%, but this does not account for ethylene in the headspace of the NMR tube. Ethane was also detected along with **4**, probably formed due to the instability of the resulting anionic Ni(II) hydride.

Coupling of PhI and MeMgBr and Analysis of Post-Catalytic Reaction Mixture. The general procedure for catalytic coupling reactions described above was followed. After 1 h of stirring, an aliquot was taken and the solvent and C-C coupling product were removed under vacuum. The Ni-containing components of the reaction mixture were then analyzed by ^{1}H NMR in d_8-THF whereupon both **3** and **4** were detected. Integration of the signals from **3** against the hexamethylbenzene standard indicated that 89% of the original catalytic loading was accounted for as **3**.

Mercury Drop Test. The effect of mercury on the rate of the reaction was analyzed by preparing a catalytic cross-coupling between MeMgBr and 1-iodonaphthalene under the standard conditions described above. After addition of the MeMgBr, the reaction mixture was immediately divided into two portions and 300 equiv. of mercury (relative to the catalyst) was added to one portion. The parallel reactions were monitored by GC/MS and found to reach completion at the time.

Methylation of 2 by MeMgBr and Analysis of Product. To a stirred, purple solution of **2** (0.100 g, 0.180 mmol) in 6 mL of THF chilled to -30ºC was added 0.66 mL of a 0.30 M solution of MeMgBr (0.198 mmol), dropwise, via syringe over 30 s. Upon completion of the addition, the color had changed from dark purple to the characteristic blue color of **3**.

Spectroscopic Analysis and Yield Determination of the Product: An aliquot of the above solution was diluted to a concentration appropriate for analysis by UV-vis spectroscopy and its spectrum was compared to that of **3** prepared independently *via* reduction of **1** with KC_8 and found to match (see Appendix). The yield of the reaction was determined from the UV-vis spectra using the molar absorption coefficient determined from the spectrum of independently prepared **3**. The solvent from a second aliquot of the original reaction mixture was removed under vacuum and the resulting residue was analyzed by ^{1}H NMR spectroscopy d_8-THF and the spectrum was found to match that of independently prepared **3**. Addition of independently prepared **3** to the NMR sample did not result in additional shifts in the ^{1}H NMR spectrum, confirming that the product of the reaction of **2** and MeMgBr is **3**.

Stoichiometric Reactions Between 1, 3 and 1-Iodonaphthalene.

1-Iodonaphthalene and **3** (1 to 1): A solution of **3** (0.180 mmol) in 6 mL of THF was prepared from **2** (0.100 g, 0.180 mmol) and MeMgBr (0.198 mmol) in the manner described above. The solution was allowed to warm to room temperature. To this stirring solution was added a solution of 1-iodonaphthalene (0.046 g, 0.181 mmol) and hexamethylbenzene (0.011 g, 0.068 mmol) in 2 mL of THF. The reaction was stirred for 45 min, during which it was monitored by GC/MS and found to no longer be progressing. An aliquot of the reaction mixture was then taken, the solvent removed under vacuum, and the organic products were analyzed by ^{1}H NMR in $CDCl_3$. The yield of 1-methylnaphthalene (16%) was determined by integration of the product signal against those of hexamethylbenzene.

1-Iodonaphthalene, **1** and **3** (1 to 1 to 1): A solution of **3** (0.180 mmol) in 6 mL of THF was prepared from **2** (0.100 g, 0.180 mmol) and MeMgBr (0.198 mmol) in the manner described above. To this solution was added **1** (0.103 g, 0.180 mmol), followed immediately by a solution of 1-iodonaphthalene (0.046 g, 0.181 mmol) and hexamethylbenzene (0.011 g, 0.068 mmol) in 2 mL of THF. The reaction was analyzed after 45 min in the same manner as described above and the yield of 1-methylnaphthalene was found to be 10%.

1-Iodonaphthalene and **3** (1 to 2): A solution of **3** (0.360 mmol) in 6 mL of THF was prepared from **2** (0.100 g, 0.360 mmol) and MeMgBr (0.378 mmol) in a manner analogous to that described above. The solution was allowed to warm to room temperature. To this stirring solution was added a solution of 1-iodonaphthalene (0.046 g, 0.181 mmol) and hexamethylbenzene (0.011 g, 0.068 mmol) in 2 mL of THF. After 10 min, the solution became dark and an aliquot was analyzed in the same manner as described above. The yield of 1-methylnaphthalene was found to be 98%. A separate aliquot was taken, the solvent was removed under vacuum, and the resulting residue was washed with three aliquots of 2 mL of pentane, leaving behind a blue/green residue. The solvent from the pentane washings was removed under vacuum leaving behind a dark residue. The pentane-insoluble and pentane-soluble residues were analyzed by ^{1}H NMR in d_8-THF and d_6-benzene, respectively. The pentane-insoluble components were found to contain **3** and **4** and the pentane-soluble components were found to contain **1** and **2**. Quantification of **3** was not possible due to the solubility of hexamethylbenzene in pentane.

Redox Equilibrium Experiments

Determination of Conversion of **4a** and **1** to **2** and **3**: To a yellow solution of **4a** (0.0120 g, 0.015 mmol) in 1 mL of THF was added a dark green solution of **1** (0.0085 g, 0.015 mmol) in 1 mL of THF, resulting in an immediate color change to black. The volatile components were then removed under vacuum and the resulting residue was washed with three aliquots of 2 mL of pentane, leaving behind a blue residue. To this residue was added hexamethylbenzene (0.0036 g, 0.022 mmol) and *ca.* 0.5 mL d_8-THF. Integration against the hexamethylbenzene internal standard indicated a 29% yield of **3**.

Effect of MeMgBr on Redox Equilibrium: To a yellow solution of **4a** (0.120 g, 0.15 mmol) and hexamethylbenzene (0.0115 g, 0.07 mmol) in 3 mL of THF was added a dark green solution of **1** (0.085 g, 0.15 mmol) in 3 mL of THF, resulting in an immediate color change to black. The solution was stirred and 0.5 mL of a 0.30 M solution of MeMgBr in Et_2O (0.15 mmol) was added dropwise. Upon completion of the addition, the color had changed to characteristic blue color of **3**. An aliquot was removed and the volatile components were removed under vacuum. The resulting residue was dissolved in *ca.* 0.7 mL d_8-THF. Integration against the hexamethylbenzene internal standard indicated complete conversion of all Ni-containing compounds to **3** (>98%).

Homocoupling of 1-Iodonaphthalene to 1,1'-Binaphthalene by 4. To a stirring, yellow solution of **4** (0.100 g, 0.168 mmol) in 4 mL of THF was added a solution of 1-iodonaphthalene (0.043 g, 0.169 mmol) and hexamethylbenzene (0.010 g, 0.062 mmol) in 2 mL of THF. The reaction mixture slowly darkened over the course of 1 h, at which point the reaction mixture was dark purple. An aliquot was taken and analyzed by ^{1}H NMR in $CDCl_3$, which indicated that the yield of 1,1'-binaphthalene was 80%.

Investigation of Carbanion Transfer from [Ni(II)-R]$^-$ to Ni(III)-R. To a stirring solution of **3** (0.090 mmol) in 2 mL of THF prepared from **2** and MeMgBr as described above, was added **1** (0.051 g, 0.090 mmol) dissolved in 2 mL of THF. The reaction mixture was stirred at ambient temperature for three h and then analyzed by ^{1}H NMR spectroscopy. Large quantities of both **1** and **3** remained along with trace amounts of **2**, likely from the thermal decomposition of **1**. From these results, we conclude that a transfer of a hydrocarbyl group from an anionic nickel(II) alkyl species such as **3** to a neutral Ni(III) alkyl species such as **1** is too slow to be catalytically relevant.

(Me)Ni[N(SiMe$_3$)DIPP]$_2$ (1). Full preparation and characterization data for **1** is available in a prior publication[7a] and Chapter 2. Cyclic voltammetry (1,2-difluorobenzene, NBu_4PF_6, 100 mV/s): –1.30 V (ip_a/ip_c = 0.98).

Ni[N(SiMe$_3$)DIPP]$_2$ (2). Full preparation and characterization data for **1** is available in a prior publication[8] and Chapter 1. Cyclic voltammetry data is available in Chapter 2 and in a prior publication.[7a]

K{(Me)Ni[N(SiMe$_3$)DIPP]$_2$} (3). To a 20 mL scintillation vial was added **1** (0.100 g, 0.175 mmol) and 8 mL of toluene, forming a dark green solution. The mixture was stirred vigorously for approximately 5 min to ensure complete dissolution of **1**. The solution was then

placed in a freezer at -30 °C where it was allowed to cool for 20 min. The vial containing the solution was then removed and the solution was stirred. To the stirring solution of **1** was added potassium graphite (0.026 g, 0.192 mmol) as a solid. The mixture was allowed to warm to room temperature and stirring was continued for 25 min at which point the color of the solution had changed from dark green to blue. The mixture was then filtered and the volatile components of the filtrate were removed under reduced pressure. The resulting residue was dissolved in 6 mL of toluene, forming a blue solution, upon which was layered 8 mL of pentane. The vial was placed in the freezer at -30 °C for two days, yielding 0.068 g (64%) of **3** as a blue powder which was isolated by decantation and dried in vacuo. ^{1}H NMR (600 MHz, C_6D_6, 22°C) δ 6.87 (d, 7.5Hz, 4H, Ar-meta-*H*), 6.74 (t, 7.4Hz, 2H, Ar-para-*H*), 3.36 (m, 4H, Me_2C-*H*), 1.12 (d, 6.7Hz, 12H, $H(CH_3)_2$), 1.08 (d, 6.8Hz, 12H, $H(CH_3)_2$), 0.67 (s, 9H, $Si(CH_3)_3$), -0.95 (s, 3H, Ni-CH_3). ^{13}C NMR (151 MHz, C_6D_6, 22 °C) δ 154.71, 148.44, 123.78, 118.61, 34.45, 27.43, 25.76, 24.89, 22.73, 14.27, 5.17, -46.5. The shift at -46.5 is not observable in the 1D ^{13}C NMR and is only visible in a 2D ^{1}H-^{13}C HSQC experiment. As such, its precise chemical shift is necessarily less accurate. Anal. Calcd. for $C_{31}H_{55}KN_2NiSi_2$: C, 61.06%; H, 9.09%; N, 4.59%. Found: C, 60.68%; H, 9.00%; N, 4.84%. UV-vis (THF) λ_{max}, ε (L mol^{-1} cm^{-1}) 630 nm, 456; 870 nm, 325. Crystals suitable for single crystal X-ray diffraction studies were grown from a saturated solution of **3** in toluene cooled to -30ºC for three days.

K{Ni[N(SiMe$_3$)DIPP]$_2$} (4). Full preparation and characterization data for **1** is available in a prior publication[7a] and Chapter 2.

REFERENCES

(1) (a) Jana, R.; Pathak, T.P.; Sigman, M. S. *Chem. Rev.* **2011**, *111*, 1417. (b) Cahiez, G.; Moyeux, A. *Chem. Rev.* **2010**, *110*, 1435. (c) Miyaura, N.; Suzuki, A. *Chem. Rev.* **1995**, *95*, 2457. (d) Liu, C.; Zhang, H.; Shi, W.; Lei, A. *Chem. Rev.* **2011**, *111*, 1780. (e) Beletskaya, I. P.; Ananikov, V. P. *Chem. Rev.* **2011**, *111*, 1596. (f) Roglans, A.; Pla-Quintana, A.; Moreno-Mañas, M. *Chem. Rev.* **2006**, *106*, 4622. (g) Rosen, B. M.; Quasdorf, K. W.; Wilson, D. A.; Zhang, N.; Resmerita, A.-M.; Garg, N. K.; Percec, V. *Chem. Rev.* **2011**, *111*, 1346. (h) Suzuki, A. *J. Organomet. Chem.* **1999**, *576*, 147. (i) Chinchilla, R.; Nájera, C. *Chem. Rev.* **2007**, *107*, 874. (j) Bolm, C.; Legros, J.; Paih, J. L.; Zani, L. *Chem. Rev.* **2004**, *104*, 6217. (k) Sherry, B. D.; Fürstner, A. *Acc. Chem. Res.* **2008**, *41*, 1500.

(2) Seechurn, C. C. C. J.; Kitching, M. O.; Colacot, T. J.; Snieckus, V. *Angew. Chem. Int. Ed.* **2001**, *51*, 5062.

(3) (a) Vechorkin, O.; Hu, X. *Angew. Chem. Int. Ed.* **2009**, *48*, 2937. (b) Steib, A. K.; Kuzmina, O. M.; Fernandez, S.; Flubacher, D.; Knochel, P. *J. Am. Chem. Soc.* **2013**, *135*, 15346. (c) Ge, S.; Green, R. A.; Hartwig, J. F. *J. Am. Chem. Soc.* **2014**, *136*, 1617; (d) Bullock, R. M. *Catalysts Without Precious Metals*; (Wiley VCH, Weinheim, 2010).

(4) (a) Csok, Z.; Vechorkin, O.; Harkins, S. B.; Scopelliti, R.; Hu, X. *J. Am. Chem. Soc.* **2008**, *130*, 8156. (b) Jones, G. D.; Martin, J. L.; McFarland, C.; Allen, O. R.; Hall, R. E.; Haley, A. D.; Brandon, R. J.; Konovalova, T.; Desrochers, P. J.; Pulay, P.; Vicic, D. A. *J. Am. Chem. Soc.* **2006**, *128*, 13175. (c) Breitenfeld, J.; Scopelliti, R.; Hu, X. *Organometallics* **2012**, *31*, 2128. (d) Hu, X. *Chem. Sci.* **2011**, *2*, 1867.

(5) (a) Böhm, V. P. W.; Weskamp, T.; Gstöttmayr, C. W. K.; Herrmann, W. A. *Angew. Chem. Int. Ed.* **2000**, *39*, 1602. (b) Xi, Z.; Liu, B.; Chen, W. *J. Org. Chem.* **2008**, *73*, 3954. (c) Xu, Y.-C.; Zhang, J.; Sun, H.-M.; Shen, Q.; Zhang, Y. *Dalton Trans.* **2013**, *42*, 8437.
(6) (a) Breitenfeld, J.; Ruiz, J.; Wodrich, M. D.; Hu, X. *J. Am. Chem. Soc.* **2013**, *135*, 12004. (b) Tsou, T. T.; Kochi, J. K. *J. Am. Chem. Soc.* **1979**, *101*, 7547. (c) Biswas, S.; Weix, D. J. *J. Am. Chem. Soc.* **2013**, *135*, 16192.
(7) (a) Lipschutz, M. I.; Yang, X.; Chatterjee, R.; Tilley, T. D. *J. Am. Chem. Soc.* **2013**, *135*, 15298. (b) Lee, C.-M.; Chen, C.-H.; Liao, F.-X.; Hu, C.-H.; Lee, G.-H. *J. Am. Chem. Soc.* **2010**, *132*, 9256. (c) Grove, D. M.; van Koten, G.; Zoet, R.; Murrall, N. W.; Welch, A. *J. Am. Chem. Soc.* **1983**, *105*, 1379. (d) Zhang, B.; Tang, F.; Luo, J.; Schultz, J. W.; Rath, N. P.; Mirica, L. M. *J. Am. Chem. Soc.* **2014**, *136*, 6499.
(8) Lipschutz, M. I.; Tilley, T. D. *Chem. Commun.* **2012**, *48*, 7146.
(9) Liang, L.-C.; Chien, P.-S.; Lin, J.-M.; Huang, M.-H.; Huang, Y. L.; Liao, J.-H. *Organometallics* **2006**, *25*, 1399.
(10) Breitenfeld, J.; Vechorkin, O.; Corminboeuf, C.; Scopelliti, R.; Hu, X. *Organometallics* **2010**, *29*, 3686.
(11) Zhang, C. P.; Wang, H.; Klein, A.; Biewer, C.; Stirnat, K.; Yamaguchi, Y.; Xu, L.; Gomez-Benitez, V.; Vicic, D. A. *J. Am. Chem. Soc.* **2013**, *135*, 8141.
(12) Tsou, T. T.; Kochi, J. K. *J. Am. Chem. Soc.* **1978**, *100*, 1634.
(13) Yang, J.; Tilley, T. D. *Angew. Chem. Int. Ed.* **2010**, *49*, 10186.
(14) Armarego, W. L. F.; Chai, C. L. L. Purification of Organic Chemicals. *Purification of Laboratory Chemicals,* 6th Edition; Butterworth-Heinemann; Oxford, UK; 2009; p. 236.
(15) Bergbreiter, D. E.; Killough, J. M. *J. Am. Chem. Soc.,* **1978**, *100*, 2126.
(16) Evans, D. F. *J. Chem. Soc.*, **1959**, 2003.
(17) Frisch, M. J. *Gaussian 09, Revision C.01*, Gaussian, Inc.: Wallingford CT, 2009.
(18) Perdew, J. P.; Ruzsinszky, A.; Csonka, G. I.; Constantin, L. A.; Sun, J. *Phys. Rev. Lett.,* **2011**, *106*, 179902.
(19) Zhang, Q.; Su, H.; Luo, J.; Wei, Y. *Catal. Sci. Technol.* **2013**, *3*, 235.
(20) Zhou, F.; Simon, M.-O.; Li, C.-J. *Chem. Eur. J.* **2013**, *19*, 7151.
(21) Krüger, T.; Vorndran, K.; Linker, T. *Chem. Eur. J.* **2009**, *15*, 12082.
(22) Zhang, Y.; Gao, J.; Li, W.; Lee, H.; Lu, B. Z.; Senanayake, C. H. *J. Org. Chem.* **2011**, *76*, 6394.
(23) Huang, J.-L.; Dai, X.-J.; Li, C.-J. *Eur. J. Org. Chem.* **2013**, *29*, 6496.
(24) Moreno-Mañas, M.; Pleixats, R.; Serra-Muns, A. *Synlett* **2006**, *18*, 3001.
(25) Maity, S.; Manna, S.; Rana, S.; Naveen, T.; Mallick, A.; Maiti, D. *J. Am. Chem. Soc.* **2013**, *135*, 3355.

Chapter 3 Appendix

ENLARGED ORTEP DIAGRAMS

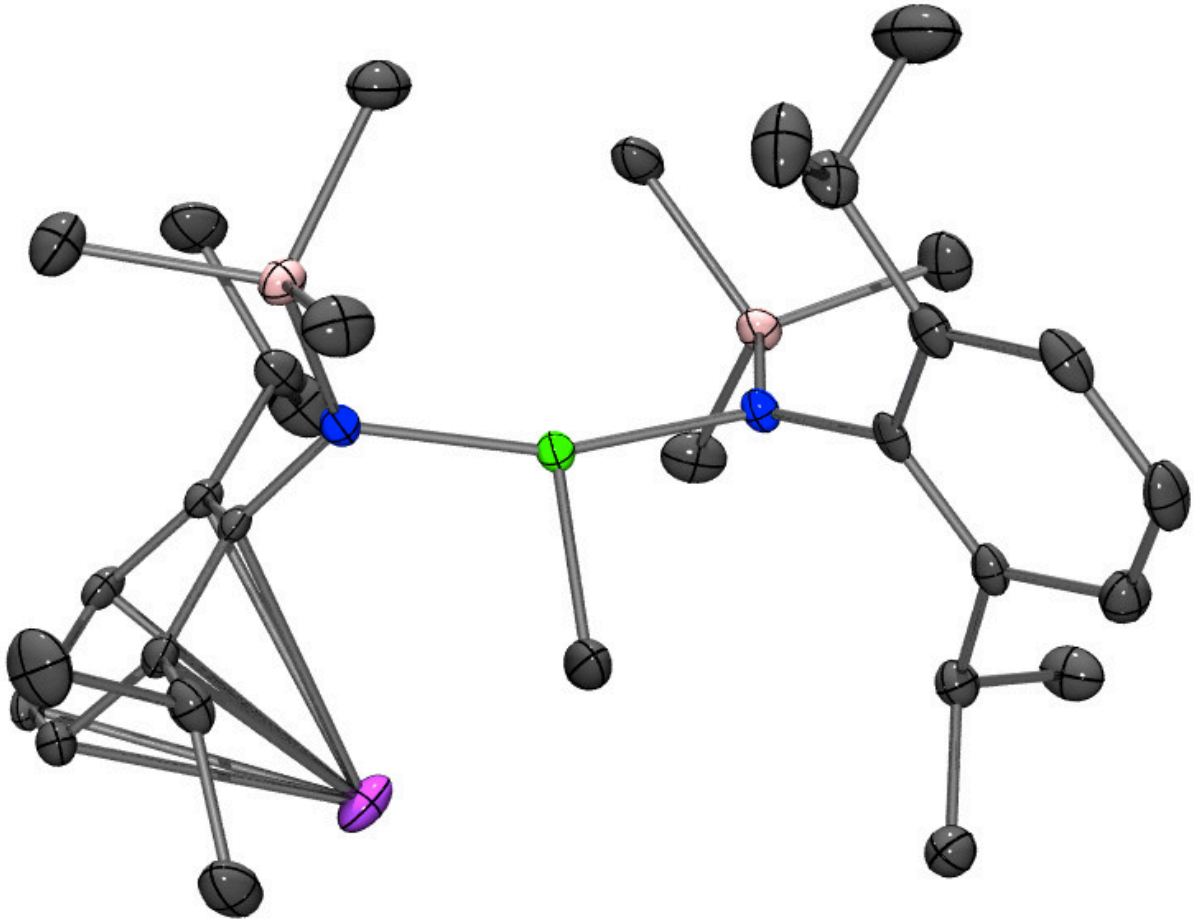

ORTEP diagram for compound **3** (thermal ellipsoids shown at 50% probability). Ni atom is shown in green, K atom in purple, N atoms in blue, Si atoms in pink and C atoms in dark grey.

UV-VIS SPECTRA

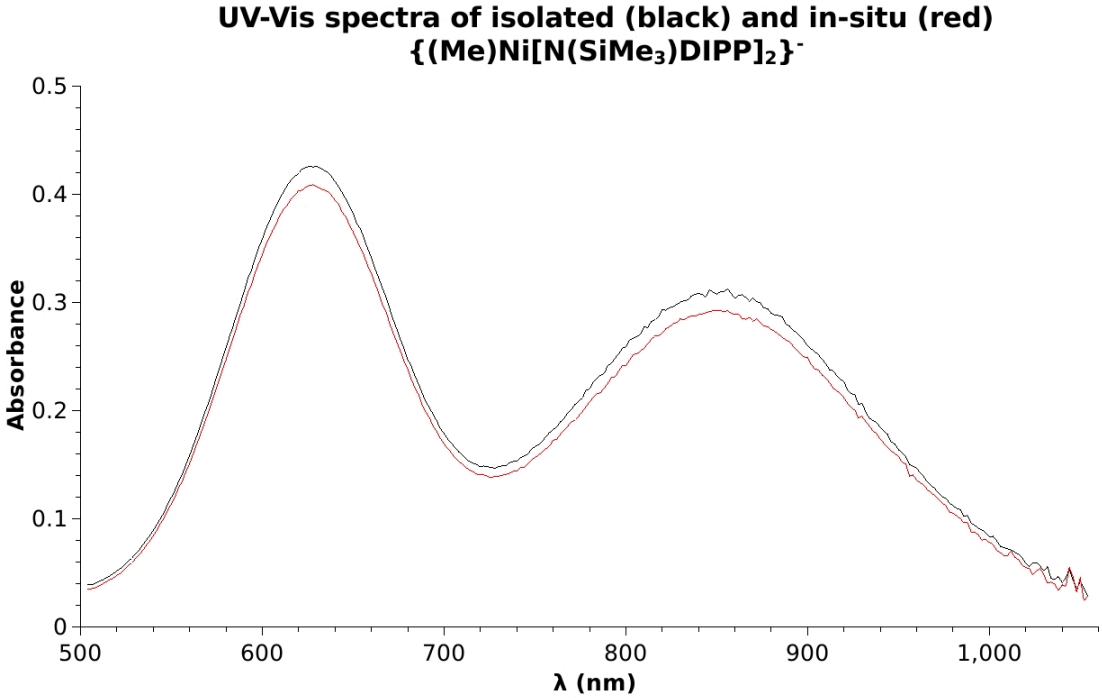

CYCLIC VOLTAMMOGRAM

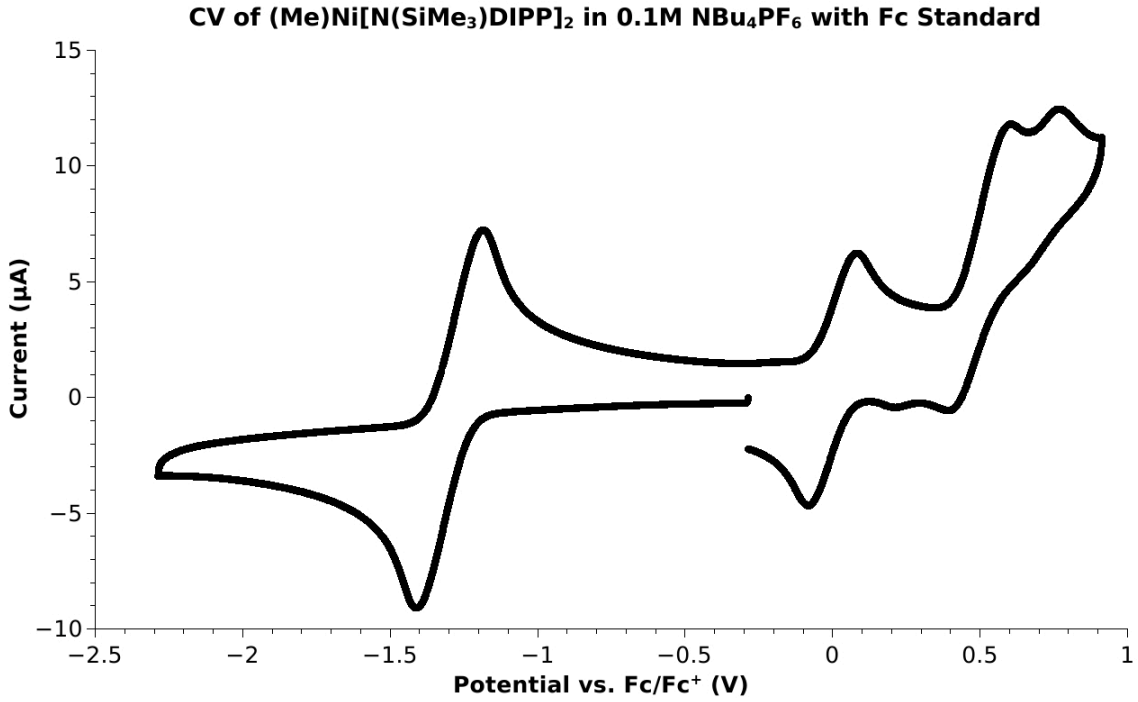

ELECTRONIC STRUCTURE COMPARISON: [Ni(II)Me]$^-$ (3) AND Ni(III)Me (1)

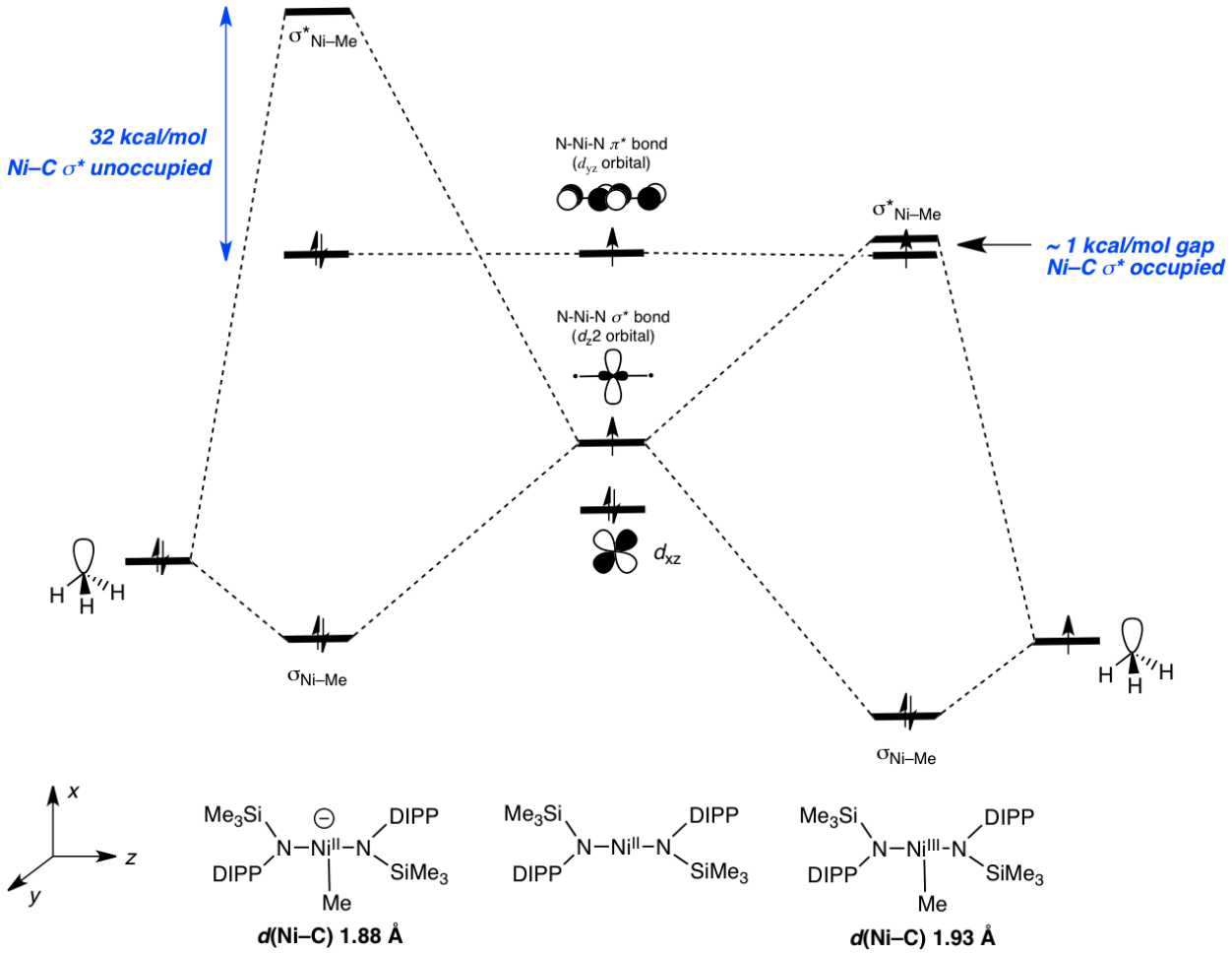

The above figure is a partial MO diagram depicting the interaction of a CH_3^- fragment (left) and a CH_3• fragment (right) with the neutral, Ni(II) bis(amido) complex **2** to depict the Ni-CH_3 interactions for the [Ni(II)Me]$^-$ species **3** and Ni(III)Me species **1**, respectively. The full computation treatment for **1** and **2** as well as the full MO diagram for **2** can be found in a prior publication.[7a] The computations for **3** were performed according to the description found in the Experimental section.

We attribute the unexpected shortening of the Ni-C bond upon reduction from a neutral Ni(III) complex to an anionic Ni(II) complex to partial occupancy of the Ni-C σ* orbital in the Ni(III) species, but not the Ni(II) species. As shown in the diagram above, the calculated frontier molecular orbitals of both species are the same, with a HOMO that has significant ,formal π* character for the N-Ni-N core and a LUMO corresponding to the Ni-C σ* orbital**.** In the Ni(III) species, the HOMO/LUMO gap is calculated to be very small (~1 kcal/mole) while in the Ni(II) species, it is substantially larger (~32 kcal/mole). The very small HOMO/LUMO gap in compound **1** suggests that the Ni-C σ* orbital may be thermally occupied, reducing the bond order of the Ni-C bond and resulting in a longer bond.

X-RAY DATA TABLES

Compound 3:

Empirical formula	C31 H55 K N2 Ni Si2	
Formula weight	609.76	
Temperature	100(2) K	
Wavelength	0.71073 Å	
Crystal system	Orthorhombic	
Space group	Pbca	
Unit cell dimensions	a = 16.7953(4) Å	a = 90º.
	b = 17.1335(4) Å	b = 90º.
	c = 23.8238(6) Å	g = 90º.
Volume	6855.6(3) Å ^{3}	
Z	8	
Density (calculated)	1.182 Mg/m^3	
Absorption coefficient	0.778 mm^{-1}	
F(000)	2640	
Crystal size	0.13 x 0.04 x 0.01 mm^3	
Theta range for data collection	1.71 to 25.37∞.	
Index ranges	-17<=h<=20, -20<=k<=20, -28<=l<=28	
Reflections collected	85599	
Independent reflections	6295 [R(int) = 0.0628]	
Completeness to theta = 25.00º	100.0 %	
Absorption correction	Semi-empirical from equivalents	
Max. and min. transmission	0.9923 and 0.9056	
Refinement method	Full-matrix least-squares on F^2	
Data / restraints / parameters	6295 / 0 / 349	
Goodness-of-fit on F^2	1.033	
Final R indices [I>2sigma(I)]	R1 = 0.0318, wR2 = 0.0650	
R indices (all data)	R1 = 0.0518, wR2 = 0.0722	
Largest diff. peak and hole	0.358 and -0.349 e. Å $^{-3}$	

Chapter 4. A Useful Method for the Preparation of Low-coordinate Ni(I) Complexes *via* Transformations of the Ni(I) Bis(amido) Complex K{Ni[N(SiMe$_3$)(2,6-^{i}Pr$_2$-C$_6$H$_3$)]$_2$}

INTRODUCTION

Two-coordinate transition metal complexes are a unique class of compounds that possess interesting chemical,[1] magnetic,[2] and redox[3] properties. Recent reports from this laboratory describe the catalytic C-C cross-coupling and hydrosilation activities of the two-coordinate nickel bis(amido) complex Ni[N(SiMe$_3$)DIPP]$_2$ (**1**), and suggest that two-coordinate first-row metal complexes hold significant promise as cheap, earth-abundant catalysts.[4,5] Analysis of the mechanism of the nickel-mediated cross-coupling revealed several key transformations that leverage the unusual coordination environment and redox properties of the two-coordinate structure. Related results from Hillhouse and coworkers demonstrate novel stoichiometric chemistry for several two- and three-coordinate nickel(I) complexes.[6] Other nickel(I) complexes have been shown to catalyze C-C and C-N cross-coupling reactions, or to serve as precursors to interesting Ni-E multiply bonded species.[7,8] Despite their high reactivity,[6] usefulness as synthetic precursors,[7,8] and potential as cheap, earth-abundant catalysts,[4,5] low-coordinate nickel(I) complexes have received little attention due to the lack of general synthetic methods for their preparation, and the limited number of conveniently prepared nickel(I) starting materials.

Nickel(I) complexes of the type L–Ni–X (L = 1,3-bis(2,6-diisopropylphenyl)imidazol-2-ylidene (**IPr**) and 1,2-bis(di-tert-butylphosphino)ethane (**dtbpe**)) represent the most well-studied set of nickel(I) complexes. These complexes have been obtained from Sigman's dimer[9] [(IPr)NiCl]$_2$, or from a related dimer reported by Hillhouse and coworkers, [(dtbpe)NiCl]$_2$.[8a] These sterically demanding ligand platforms can accommodate a variety of X-type ligands in the nickel(I) oxidation state, including alkyls,[6b,10-12] amides,[6a,8a,13] phosphides,[8b] hydrides[14] and silyls.[15] However, the incorporation of additional L-type ligands is limited by the lack of appropriate L$_n$Ni^{I}–X starting materials. These Ni(I) halide complexes are typically prepared and isolated from one-electron reduction of the parent Ni(II) halide, L$_n$Ni^{II}X$_2$,[8a,16] or via comproportionation between appropriate Ni(II) and Ni(0) sources.[9] Both of these approaches are limited to a few examples and often result in over-reduction to Ni(0) and complex mixtures of products. This chapter describes a convenient method for the preparation of two- and three-coordinate nickel(I) compounds from the recently reported complex K{Ni[N(SiMe$_3$)DIPP]$_2$} (**2**).[3] This method allows access to nickel(I) complexes of the form L–Ni–X, where both the L and X ligands can be varied.

RESULTS AND DISCUSSION

Reactions of Ni[N(SiMe$_3$)DIPP]$_2$ (1) with Sterically Hindered Donors. Initial investigations of the coordination chemistry of **1** demonstrated that small L-type donors such as MeCN and DMAP (*p*-dimethylaminopyridine) simply add to the nickel center to form T-shaped, three-coordinate Ni(II) complexes.[5] Attempts to extend this chemistry to larger L-donors, such as bulky N-heterocyclic carbenes (NHCs), resulted in no reaction at room temperature. For example, IPr and **1** did not react in benzene-d_6 over the course of 24 hours at 23 °C. However, at 80 °C one equiv of IPr reacted with **1** in benzene to form the two-coordinate Ni(I) species (IPr)Ni[N(SiMe$_3$)DIPP] (**3**; 61% isolated yield), rather than a three-coordinate Ni(II) adduct (eq 1).[5] This interesting process, in which the metal is reduced and the IPr formally displaces an equivalent of •N(SiMe$_3$)DIPP from **1**, is similar to the early preparation of (Ph$_3$P)$_2$Ni^{I}[N(SiMe$_3$)$_2$] from (Ph$_3$P)$_2$Ni^{II}Cl$_2$ and LiN(SiMe$_3$)$_2$ by Bradley and Welch, where the Ni is reduced and an equivalent of •N(SiMe$_3$)$_2$ is lost.[17] Given these results, the reaction of **1** with sterically hindered

donors appeared to represent a promising and general synthetic route to two-coordinate Ni(I) compounds.

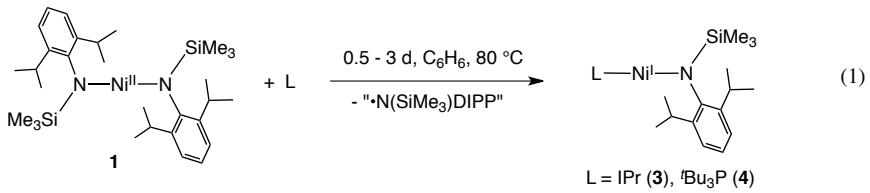

(1)

In an attempt to evaluate the generality of this ligand-induced reduction, complex **1** was treated with the sterically demanding phosphine $^{t}Bu_3P$ (1 equiv), in benzene at 80 °C over 3 days. Workup of the reaction mixture provided a low isolated yield (18%) of the new nickel(I) complex ($^{t}Bu_3P$)Ni[N(SiMe$_3$)DIPP] (**4**), isolated as orange crystals from hexanes. Other sterically-demanding ligands such as $^{i}Pr_3P$, Mes_3P, 1,2-diphenylphosphinoethane (**DPPE**) and 1,3-bis(2,4,6-trimethylphenyl)imidazol-2-ylidene (**IMes**) only resulted in the formation of HN(SiMe$_3$)DIPP upon reaction with **1**. No Ni(I) species could be isolated from these reactions, and no such species were observable by ^{1}H NMR spectroscopy. Thus, this simple synthetic route to two-coordinate Ni(I) complexes, based on the direct reaction of **1** with a two-electron donor, appears to be limited in scope. For this reason, an alternative approach to the synthesis of two-coordinate nickel(I) complexes, based on the stepwise combination of reduction and ligand-exchange reactions, was pursued.

Synthetic Route to Neutral, Two- and Three-Coordinate Ni(I) complexes. Homolytic metal-ligand bond cleavages related to that shown in eq 1 are potentially interesting in the context of synthesis, catalysis, and biochemistry, and exhibit a diverse range of mechanistic pathways.[18] Given the low to moderate yields associated with the conversions of eq 1, it has proven difficult to probe the mechanism of this interesting, ligand-induced homolytic cleavage. However, it seemed that this process might involve separate reduction and ligand displacement steps. The formal reduction of Ni(II) to Ni(I) is consistent with the previously reported redox properties of **1**. As reported elsewhere,[3] **1** undergoes a reversible reduction in 1,2-difluorobenzene at -1.28 V vs. Fc/Fc^+, and is readily reduced in high yield (89%) by KC_8 to the anionic Ni(I) complex K{Ni[N(SiMe$_3$)DIPP]$_2$} (**2**). Thus, it was of interest to investigate reactions of **2** with mild acids HX, which were anticipated to result in loss of HN(SiMe$_3$)DIPP and KX to produce a neutral Ni(I) fragment that might be subsequently trapped by an L-type donor. Indeed, such transformations were found to provide convenient access to the two- and three-coordinate Ni(I) complexes **3**-**6**.

Compounds **3**-**6** were prepared from **2** *via* the same method. This procedure involves treatment of a cold (-30 °C) diethyl ether solution of **2** and the donor ligand L (L = IPr, $^{t}Bu_3P$, $^{i}Pr_3P$, DPPE) with 1 equiv of NEt_3•HCl, followed by warming to room temperature over 0.5-3 hours (eq 2). The reactions result in elimination of KCl and HN(SiMe$_3$)DIPP and trapping of the resulting neutral Ni^{I}[N(SiMe$_3$)DIPP] fragment by L to provide the nickel(I) amido complexes **3**-**6** in 69-91% yield after recrystallization. While compound **3** is indefinitely stable at room temperature, compounds **4**-**6** are thermally unstable and decompose over weeks (**4** and **5**) or days (**6**) at ambient temperature. All compounds show no signs of decomposition after 3 months at -30 °C.

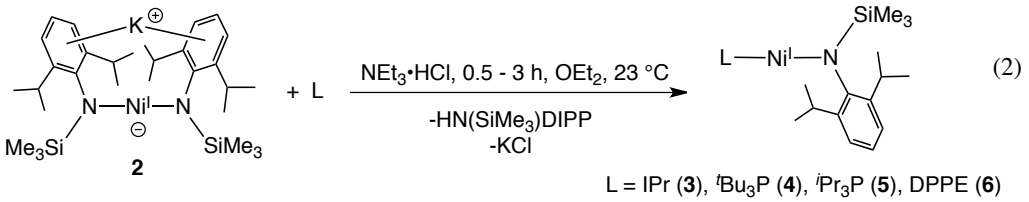

(2)

This synthetic method for the preparation of nickel(I) amido complexes of the form L–Ni^{I}–N($SiMe_3$)DIPP appears to be limited only by the ability of the L-donor to support the resulting two- or three-coordinate nickel(I) complex. Strong σ-donors, such as phosphines and N-heterocyclic carbenes, are effective in this regard whereas weaker, but similarly bulky σ-donors such as the aniline 2,6-$Mes_2C_6H_2NH_2$ result in reduction of NEt_3•HCl to hydrogen, with formation of **1** and no reaction of the donor (e.g., the aniline). The low oxidation state of the nickel center and the π-donating amido ligand suggest that the Ni^{I}–N($SiMe_3$)DIPP fragment might be stabilized by good π-accepting ligands. However, use of 1,4-cyclooctadiene, 1,2-bistrimethylsilylacetylene and 2-butyne in the procedure of eq 2 resulted only in the formation of hydrogen and **1** (by ^{1}H NMR spectroscopy). Presumably, these π-accepting ligands are not efficient at trapping or stabilizing the Ni^{I} fragment which may result from protonation of **2**.

The utility of the nickel(I) anionic complex **2** in providing access to neutral, two-coordinate complexes prompted an examination of further transformations of **3**-**6** involving simple ligand substitutions. In principle, it should be possible to substitute the basic amido ligand in these complexes with a variety of suitably bulky ligands, to produce a range of new L–Ni(I)–X complexes *via* proton-transfer reactions. Initial attempts to demonstrate this synthetic method involved the preparation of new aryloxide complexes **7** and **8** (Scheme 1). Treatment of **3** and **4** with one equiv of 2,6-di-*tert*-butyl-4-methylphenol (**dtbmp**) in THF at ambient temperature resulted in the loss of HN($SiMe_3$)DIPP and incorporation of the –O(2,6-^{t}Bu$_2$-4-Me-C_6H_2) ligand to give complexes **7** and **8** in 80 and 72% yields, respectively, after recrystallization.

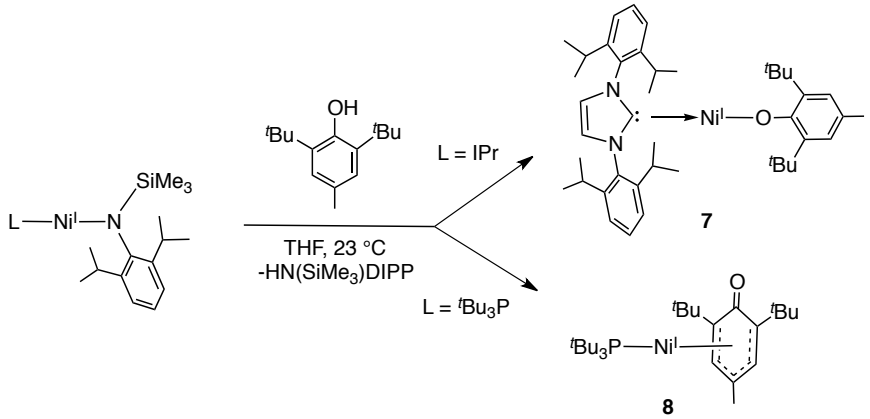

Scheme 1. Synthesis of **7** and **8** from **3** and **4**.

Structural Properties. The X-ray crystal structures of compounds **3-6** are shown in Figure 1. All four compounds feature similar Ni–N bond lengths (1.8250(2)-1.875(2) Å) that are consistent with comparable values previously reported for nickel(I) amido complexes.[6a,8a,13] The diphosphine compound **6** displays a distorted trigonal planar geometry with the Ni, N and P atoms all occupying the same plane (sum of angles around Ni is 360°). Compounds **3-5** are two-coordinate and linear with slight bending of the primary bond axis. The N-Ni-C bond angle of **3** is 173.01(7), ° while the N-Ni-P angles of **4** and **5** are 167.6(2) ° and 164.09(6) °, respectively. While there is some variation in specific bond distances and angles between these compounds, previous reports of two-coordinate Ni(I) complexes show that both electronic factors[12] and crystal-packing forces[6a] can have a significant effect on these parameters.

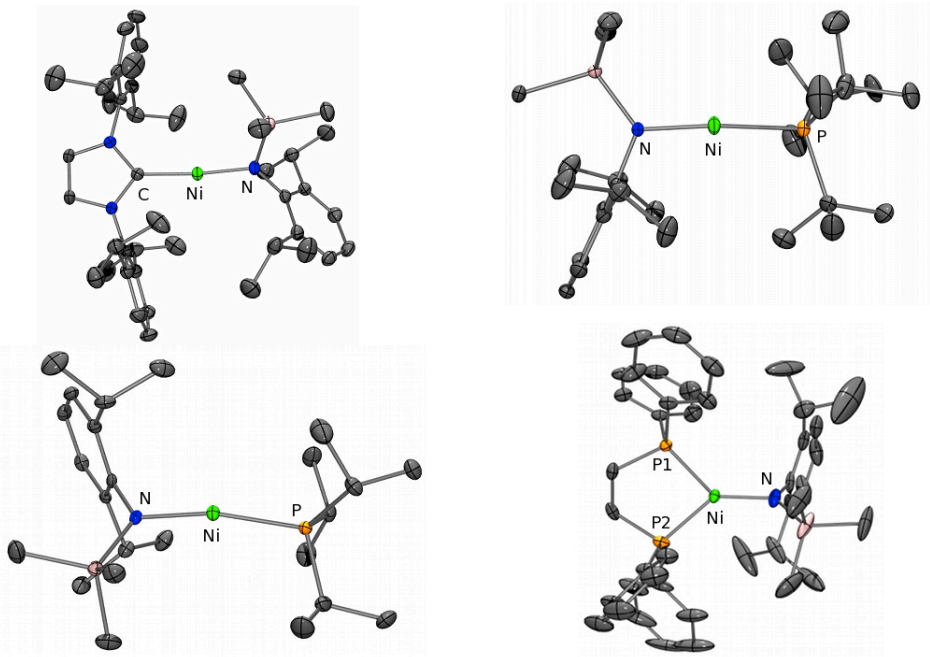

Figure 1. ORTEP diagrams of compounds **3** (top left), **4** (top right), **5** (bottom left) and **6** (bottom right) with all thermal ellipsoids shown at 50% probability. Selected bond lengths (Å) and angles (deg): **3**: Ni-N, 1.8271(2); Ni-C, 1.9123(2); N-Ni-C, 173.01(7). **4**: Ni-N, 1.8250(2); Ni-P, 2.2006(1); N-Ni-P, 165.6(1). **5**: Ni-N, 1.8407(2); Ni-P: 2.1992(7); N-Ni-P: 164.09(6). **6**: Ni-N, 1.875(2); Ni-P1, 2.1978(8); Ni-P2, 2.1922(8); P1-Ni-P2, 87.68(3).

Like compounds **3-5**, compound **7** possesses a linear, two-coordinate geometry with some bending along the primary bond axis. The solid-state structure of **7** (Figure 2) reveals three crystallographically independent molecules that display substantial variations in metrical parameters. The O-Ni-C bond angles vary from 162.19(9) to 173.3(1)° and the Ni-O bond distances vary from 1.7612(2) to 1.8374(2) Å. An area of particularly significant structural variation between the three molecules is found in the geometry about the O atom. The C_{Ar}-O-Ni bond angle varies from nearly linear (168.2(2)°), as would be expected for an *sp*-hybridized oxygen, to highly bent (131.82(2)°) and more consistent with sp^2-hybridization. Thus, compound **7** appears to be a particularly illustrative example of the effects that crystal-packing forces can have on the solid state geometry of a compound, and underscores the care that must be taken in the interpretation of such structures in terms of electronic structure and other chemical properties.

Attempted preparation of the $^{t}Bu_3P$ analog of **7** from **4** unexpectedly resulted in compound **8**, with dearomatization and η^5-coordination of the dtbmp ligand to the Ni center (Figure 2). This complex is best characterized as possessing a pentadienyl ligand that is part of a 6-membered ring also containing a ketonic carbonyl group. This type of bonding mode for a 2,6-substituted aryl oxide ligand is relatively rare, but a few examples of rhodium, ruthenium, iron and nickel complexes are known.[19] The five carbons comprising the pentadienyl fragment all lie between 2.1701(1) and 2.2534(1) Å from the Ni atom, while the carbon directly bound to the oxygen clearly lies out of the plane of the other five carbon atoms and is farther away from the Ni center (2.4648(1) Å). The intraligand bond distances further support this characterization of the bonding, as the C-C distances within the pentadienyl fragment fall between 1.4037(2) and 1.410(2) Å and are therefore consistent with a delocalized π-system. Furthermore, the C-C distances to the ketonic carbon are much longer at 1.4707(2) and 1.4721(2) Å, and consistent with a C-C single bond. Finally, the C-O bond distance of 1.2570(2) Å reflects double bond character.

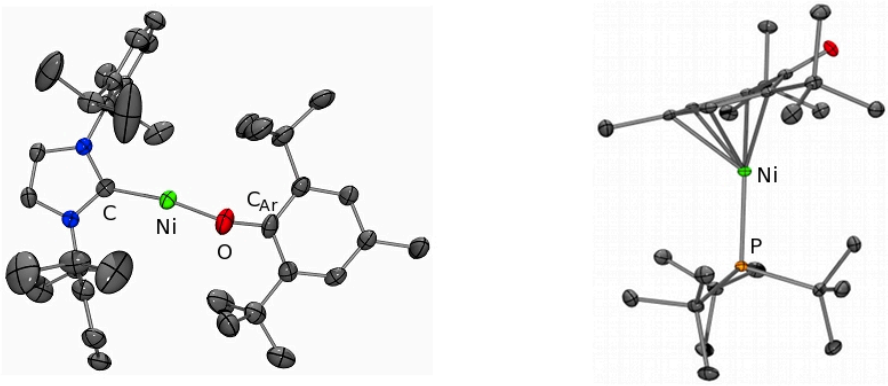

Figure 2. ORTEP diagrams of compounds **7** (left) and **8** (right) with thermal ellipsoids shown at 50% probability. For compound **7**, bond lengths and angles vary drastically among the crystallographically inequivalent molecules in the unit cell (see Appendix). Selected bond length (Å) for compound **7**: Ni-P, 2.2333(4) Å.

The difference in binding modes for the dtbmp ligands in compounds **7** and **8** seems somewhat surprising, since it appears to be associated with the L donors in these complexes (IPr and $^{t}Bu_3P$, respectively), which are both strong, bulky σ-donors. This difference in hapticity might be attributed to the differing abilities of IPr and $^{t}Bu_3P$ to participate in π-backbonding. When bound to a metal center through the oxygen atom in an η^1 fashion, the dtbmp ligand is a π-donor through the lone pairs on the oxygen, whereas when bound η^5 through the π-system, it may serve as a π-acceptor. The bonding mode of the dtbmp ligand changes to complement the nature of the L donor, acting as a π-donor when L is a competent π-acceptor (IPr) and as a π-acceptor when L is not ($^{t}Bu_3P$).

While phosphines are capable of acting as π-acceptor ligands through a σ* orbital, trialkylphosphines such as $^{t}Bu_3P$ have been shown through a variety of experimental and computational methods to be very poor π-acceptors.[20] On the other hand, the π-acidity of N-heterocyclic carbenes, which formally have a vacant carbon p-orbital capable of accepting electron density, can vary greatly depending upon the substitution pattern and conjugation of the imidazole ring.[21] In the case of IPr, structural comparison of the isosteric amido and alkyl compounds (IPr)Ni–$N(SiMe_3)_2$[6a] and (IPr)Ni–$CH(SiMe_3)_2$[6b] provides insight into the

significance of π-backbonding in these types of complexes. In the amido complex, where π-donation from the nitrogen lone pair would be expected to increase the degree of backbonding, the Ni-C_{NHC} bond length is 1.879(2) Å. This is somewhat shorter than the Ni-C_{NHC} bond distance in the alkyl complex, 1.910(2) Å, suggesting that IPr can participate in π-backbonding interactions with Ni(I). In the case of compound **7**, the Ni-C_{NHC} bond lengths of the three crystallographically independent units range from 1.880(2) to 1.863(3) Å, and suggest stabilization from π-backbonding to favor the η^1 conformation of the dtbmp ligand. The poorer π-acidity of ^{t}Bu$_3$P (relative to IPr) appears to favor participation of the dtbmp ligand as a π-acceptor in the η^5 bonding mode.

Magnetic Properties. The magnetic moments of compounds **2**-**8** were measured using Evans's method[22] and are given in Table 1. All seven compounds have moments consistent with the presence of one unpaired electron. However, there are substantial deviations from the expected spin-only value of 1.73 μ_B for the magnetic moment, with some moments falling substantially above or below that value. Compounds **3**, **4**, **5**, and **8** have higher than expected values, ranging from 2.12 μ_B (**3**) to 2.55 μ_B (**4**), while **6** exhibits a low value of 1.53 μ_B. Compounds **2** and **7** exhibit magnetic moments very close to the expected values (1.66 and 1.80 μ_B, respectively). The magnetic moments of two-coordinate transition metal complexes are known to deviate substantially from the spin-only value, due to contributions from unquenched spin-orbit coupling. Examples of both higher-[2a,b] and lower-than-expected[2c] magnetic moments due to the contribution from spin-orbit coupling have been observed and such effects are likely responsible for deviations from the spin-only values observed in complexes **2**-**8**.

Table 2. Magnetic moments of compounds **2**-**8** as measured by Evans's method.

Compound	**μ_{eff} (μ_B)**
K{Ni[N(SiMe$_3$)DIPP]$_2$} (**2**)	**1.66**
(IPr)Ni[N(SiMe$_3$)DIPP] (**3**)	**2.12**
(^{t}Bu$_3$P)Ni[N(SiMe$_3$)DIPP] (**4**)	**2.35**
(^{i}Pr$_3$P)Ni[N(SiMe$_3$)DIPP] (**5**)	**2.55**
(DPPE)Ni[N(SiMe$_3$)DIPP] (**6**)	**1.53**
(IPr)Ni[OAr] (**7**)	**1.80**
(^{t}Bu$_3$P)Ni[η^5-OAr] (**8**)	**2.29**

CONCLUSION

The easily prepared nickel(I) anion K{Ni[N(SiMe$_3$)DIPP]$_2$} has been shown to be a convenient and versatile starting material for the synthesis of two- and three-coordinate nickel(I) compounds. This method allows for the sequential substitution of both amido ligands, to give unsymmetrical L–Ni(I)–X type complexes in a modular fashion. The ability to prepare these previously inaccessible nickel(I) complexes will allow the further exploration of their chemical, structural, and electronic properties.

EXPERIMENTAL

General Considerations. Unless otherwise stated, all reactions and manipulations were carried out in a MBraun Lab Master DP glovebox or using standard Schlenk techniques under a nitrogen atmosphere. Pentane, toluene, dimethoxethane and 1,2-difluorobenzene were purchased from Sigma Aldrich. Diethyl ether was purchased from Honeywell and tetrahydrofuran was purchased from Macron Chemicals. Pentane, toluene, tetrahydrofuran, diethyl ether and 1,2-difluorobenzene were dried and degassed using a JC Meyers Phoenix SDS solvent purification system. C_6D_6 was purchased from Cambridge Isotope Laboratories, dried over Na/K alloy and then degassed by four freeze-pump-thaw cycles. Dimethoxyethane was dried over Na/K alloy and then degassed by four freeze-pump-thaw cycles. All NMR spectra were collected at ambient temperature (ca. 22°C) on Bruker AVB-400, AV-500, AV-600 or AVQ-400 NMR spectrometers, each equipped with a 5 mm BB probe, and referenced to the residual proteo solvent signals. Solution magnetic susceptibilities were determined by ^{1}H NMR spectroscopy using Evans's method[22] and the values given are the average of 3 measurements for each compound. Elemental analyses were performed by the UC Berkeley College of Chemistry Microanalytical facility. The abbreviation "DIPP" refers to a 2,6-diisopropylphenyl moiety. The abbreviation "DPPE" refers to 1,2-(bisdiphenylphosphino)ethane. The abbreviation "IPr" refers to the N-heterocyclic carbene N,N'-1,3-bis(2,6-diisopropylphenyl)imidazol-2-ylidene. DPPE and P*t*Bu$_3$ were purchased from Sigma Aldrich and used as received. NEt$_3$•HCl was purchased from Sigma Aldrich and sublimed before use. P*i*Pr$_3$ was purchased from STREM chemical and used as received. 2,6-di-*tert*-butyl-4-methyl-phenol was purchased from Pfaltz and Bauer and used as received. IPr was prepared according to the standard literature procedure.[23]

X-ray Diffraction Experiments. Single crystal X-ray diffraction experiments were carried out at UC Berkeley CHEXRAY crystallographic facility. Measurements of compounds **3**, **4**, **5**, **6**, **7** and **8** were performed on a Bruker APEX-II CCD area detector using Mo Kα radiation (λ = 0.71073 Å) monochromated using QUAZAR multilayer mirrors. Specific details of each experiment can be found below and in the appendix.

Experimental Details:

	Detector Distance	Image Width	Exposure Time
Compound **3**	40mm	0.5°	5 s
Compound **4**	40mm	0.5°	5 s
Compound **5**	40mm	0.5°	5 s
Compound **6**	40mm	0.5°	10 s
Compound **7**	40mm	0.5°	10 s
Compound **8**	40mm	0.5°	5 s

K{Ni[N(SiMe$_3$)DIPP]$_2$} (2). Full preparation and characterization data for **2** is available in a prior publication[3] as well as Chapter 2.

(IPr)Ni-N(SiMe$_3$)DIPP (3). To a 20 mL scintillation vial was added **2** (0.100 g, 0.168 mmol), IPr (0.066 g, 0.170 mmol) and 6 mL Et$_2$O, forming a yellow solution. To a separate 20 mL scintillation vial was added NEt$_3$•HCl (0.023 g, 0.168 mmol) and a magnetic stir bar and

both vials were cooled to -30ºC. The chilled solution of **2** and IPr was then transferred to the vial containing the NEt_3•HCl and the resulting suspension was stirred while warming to room temperature for 1 h, during which the color of the mixture changed from yellow to dark orange/brown. The mixture was then filtered and the volatile components were removed under reduced pressure. The resulting residue was dissolved in 1.5 mL dimethoxyethane upon which was layered 6 mL of pentane. The layered solution was then placed in the -30ºC freezer overnight, yielding 0.106 g of **3** (91%) as yellow/orange plates which were isolated by decantation, washed with 4 aliquots of 2 mL of -30ºC pentane and dried in vacuo. Full characterization data for **3** is available in a prior publication and Chapter 2. For convenience, its spectroscopic properties are reproduced here.[3] ^{1}H NMR (400 MHz, C_6D_6, 21ºC) δ 22.20 (2H), 10.93 (4H), 9.37 (2H), 8.37 (p-Ar-*H*, 1H), 4.17 (4H), 3.99 (2H), 3.82 (-Si(*CH*$_3$)$_3$, 9H), 3.56 (Ar-CH(*CH*$_3$)$_2$, 12H), 1.88 (Ar-CH(*CH*$_3$)$_2$, 12H), -0.65 (Ar-CH(*CH*$_3$)$_2$, 6H), -6.27 (Ar-CH(*CH*$_3$)$_2$, 6H), -11.69 (2H). Assignment of shifts to particular protons is given where integration allows unambiguous assignment. μ_{eff} = 2.12 μ_B (C_6D_6, 21°C, Evans's method).

(*t*Bu$_3$P)Ni-N(SiMe$_3$)DIPP (4). To a 20 mL scintillation vial was added **2** (0.138 g, 0.232 mmol), P*t*Bu$_3$ (0.047 g, 0.232 mmol) and 8 mL Et_2O, forming a yellow solution. To a separate 20 mL scintillation vial was added NEt_3•HCl (0.032 g, 0.232 mmol) and a magnetic stir bar and both vials were cooled to -30ºC. The chilled solution of **2** and P*t*Bu$_3$ was then transferred to the vial containing the NEt_3•HCl, resulting in an immediate color change from yellow to dark yellow/orange. The resulting suspension was stirred while warming to room temperature for 1.5 h, at which point the color of the mixture was dark orange. The mixture was then filtered and the volatile components were removed under reduced pressure. The resulting residue was dissolved in 8 mL Et_2O upon which was layered 12 mL of pentane. The layered solution was placed in the -30ºC freezer overnight, yielding 0.081 g of **4** as orange blocks which were collected by decantation and dried in vacuo. The volatile components of the supernatant were removed under reduced pressure, the resulting residue was washed with 2 mL of -30ºC pentane, and a second crystallization was set up in an identical fashion to the first using 3 mL of Et_2O and 6 mL pentane, yielding an additional 0.020 g of **4**. Total yield: 0.101 g (85%). ^{1}H NMR (500 MHz, C_6D_6, 20ºC) δ 24.97 (2H, Ar-C*H*(CH$_3$)$_2$ or *m*-Ar-*H*), 10.94 (1H, *p*-Ar-*H*), 3.30 (27H, P(C(C*H*$_3$)$_3$)$_3$, overlaps with –SiMe$_3$ signal), 3.21 (9H, Si(C*H*$_3$)$_3$, overlaps with –P*t*Bu$_3$ signal), -0.51 (6H, Ar-CH(C*H*$_3$)$_2$), -6.14 (6H, Ar-CH(C*H*$_3$)$_2$), -20.73 (2H, Ar-C*H*(CH$_3$)$_2$ or *m*-Ar-*H*). μ_{eff} = 2.35 μ_B (C_6D_6, 20°C, Evans's method). Anal. Calcd. for $C_{27}H_{53}NNiPSi$: C, 63.65%; H, 10.49%; N, 2.75%. Found: C, 63.73%; H, 10.45%; N, 2.82%. Crystals suitable for single crystal X-ray diffraction studies were obtained from the workup described above.

(*i*Pr$_3$P)Ni-N(SiMe$_3$)DIPP (5). To a 20 mL scintillation vial was added **2** (0.150 g, 0.252 mmol), P*i*Pr$_3$ (0.041 g, 0.256 mmol) and 6 mL Et_2O, forming a yellow solution. To a separate 20 mL scintillation vial was added NEt_3•HCl (0.035 g, 0.255 mmol) and a magnetic stir bar and both vials were cooled to -30ºC. The chilled solution of **2** and P*i*Pr$_3$ was then transferred to the vial containing the NEt_3•HCl, resulting in an immediate color change from yellow to dark orange. The resulting suspension was stirred while warming to room temperature for 30 min. The mixture was then filtered and the volatile components were removed under reduced pressure. The resulting gooey residue was dissolved in 1.5 mL of pentane and placed in the -30ºC freezer. Over 3 days, large, light orange blocks crystallized out of solution. These were collected by decantation and dried in vacuo, yielding 0.079 g of **5** (69%). Analysis of the mother liquor by ^{1}H

NMR indicates that additional **5** is present in the mother liquor, but due to its extreme solubility, no further product could be crystallized. ^{1}H NMR (500 MHz, C_6D_6, 20ºC) δ 26.80 (2H, Ar-C*H*$(CH_3)_2$ or *m*-Ar-*H*), 15.28 (3H, P(C*H*$(CH_3)_2)_3$), 11.68 (1H, *p*-Ar-*H*), 1.94 (6H, Ar-CH(C*H*$_3)_2$, overlaps with P(CH(C*H*$_3)_2)_3$), 1.82 (18H, P(CH(C*H*$_3)_2)_3$, overlaps with Ar-CH(C*H*$_3)_2$), -0.61 (9H, Si(C*H*$_3)_3$), -10.62 (6H, Ar-CH(C*H*$_3)_2$), -11.97 (2H, Ar-C*H*$(CH_3)_2$ or *m*-Ar-*H*). μ_{eff} = 2.55 μ_B (C_6D_6, 20°C, Evans's method). Anal. Calcd. for $C_{24}H_{47}NNiPSi$: C, 61.67%; H, 10.14%; N, 3.00%. Found: C, 61.33%; H, 10.46%; N, 2.96%. Crystals suitable for single crystal X-ray diffraction studies were obtained from the workup described above.

(DPPE)Ni-N(SiMe$_3$)DIPP (6). To a 20 mL scintillation vial was added **2** (0.100 g, 0.168 mmol), 1,2-(diphenylphosphino)-ethane (DPPE) (0.068 g, 0.171 mmol) and 8 mL Et_2O which, after several min of swirling, formed an orange solution. To a separate 20 mL scintillation vial was added NEt_3•HCl (0.024 g, 0.174 mmol) and a magnetic stirbar and both vials were cooled to -30ºC. The chilled solution of **2** and DPPE was then transferred to the vial containing the NEt_3•HCl, resulting in an immediate darkening of the orange color. The resulting suspension was stirred while warming to room temperature for 3 h, at which point the color of the solution was red. The mixture was then filtered and the volatile components were removed under reduced pressure. The resulting reside was dissolved in 2.5 mL of toluene upon which was layered 8 mL of pentane. The layered solution was placed in the -30ºC freezer overnight, yielding 0.085 g of **6** (77%) as red plates, which were isolated by decantation, washed with 2 mL of -30ºC pentane and dried in vacuo. The ^{1}H NMR spectrum of **5** reveals only a wavy, uneven baseline with no characteristic peaks. We attribute this to the paramagnetism of **5**. μ_{eff} = 1.53 μ_B (C_6D_6, 21°C, Evans's method). Anal. Calcd. for $C_{41}H_{50}NNiP_2Si$: C, 69.79%; H, 7.14%; N, 1.99%. Found: C, 70.15%; H, 6.94%; N, 2.26%. Crystals suitable for single crystal X-ray diffraction studies were obtained from the workup described above.

(IPr)Ni[(2,6-di-*tert*-butyl-4-methyl)C$_6$H$_2$]O (7). To a 20 mL scintillation vial was added **3** (0.135 g, 0.194 mmol) and 6 mL of THF, forming a yellow/orange solution. To this stirring solution at ambient temperature was added a solution of 2,6-di-*tert*-butyl-4-methylphenol (0.043 g, 0.194 mmol) in 4 mL of THF resulting in an immediate color change from yellow/orange to red. Stirring was continued for 30 min, then the mixture was filtered and the volatile components removed under reduced pressure. The resulting residue was dissolved in 2.5 mL toluene upon which was layered 8 mL of pentane. The layered solution was placed in the -30ºC freezer overnight, yielding 0.107 g of **7** (80%) as large red blocks, which were isolated by decantation and dried in vacuo. After extensive drying in this manner (>8 h), approximately 0.25 eq. of toluene of crystallization remained in the sample (quantified by ^{1}H NMR spectroscopy using an internal standard). The yield listed above takes into account its presence. ^{1}H NMR (400 MHz, C_6D_6, 24ºC) δ 21.38 (12H), 18.82 (4H), 16.69 (2H), 11.18 (2H), 6.80 (3H), 2.84 (12H), -0.94 (4H), -3.49 (2H), -7.09 (18H). μ_{eff} = 1.80 μ_B (C_6D_6, 20°C, Evans's method). Anal. Calcd. for $C_{42}H_{59}N_2NiO$ + 0.25(C_7H_8): C, 76.19%; H, 8.92%; N, 4.06%. Found: C, 76.54%; H, 9.12%; N, 3.72%. Crystals suitable for single crystal X-ray diffraction studies were obtained from the workup described above.

(*t*Bu$_3$P)Ni[η^5-(2,6-di-*tert*-butyl-4-methyl)C$_6$H$_2$O] (8). To a 20 mL scintillation vial was added **4** (0.094 g, 0.185 mmol) and 5 mL of THF which, after several min of stirring, formed an orange solution which was cooled to -30ºC. To this chilled, stirring solution was added a -30ºC

solution of 2,6-di-*tert*-butyl-4-methylphenol (0.041 g, 0.186 mmol) in 2 mL of THF. The solution was allowed to warm to ambient temperature and stirred for 3 h, at which point the solution was green. The volatile components were then removed under reduced pressure, resulting in a royal blue residue. The residue was extracted with 2 aliquots of 2 mL of 1,2-difluorobenzene, the extracts were filtered and the volatile components removed under reduced pressure. The resulting residue was washed with 3 aliquots of 2 mL of -30ºC pentane, dried in vacuo, then redissolved in 3 mL of 1,2-difluorobenzene, upon which was layered 8 mL of pentane. The layered solution was then placed in the -30ºC freezer for 2 days, yielding 0.063 g of **8** (72%) as clusters of dark blue plates, which were isolated by decantation and dried in vacuo. The ^{1}H NMR spectrum of **7** reveals only a single, extremely broad peak. ^{1}H NMR (500 MHz, C_6D_6, 20ºC) δ 4.90. μ_{eff} = 2.29 μ_B (C_6D_6, 20°C, Evans's method). Anal. Calcd. for $C_{27}H_{50}NiOP$: C, 67.51%; H, 10.49%. Found: C, 67.49%; H, 10.46%. Crystals suitable for single crystal X-ray diffraction studies were obtained from the workup described above.

REFERENCES

(1) Power, P. P. *Chem. Rev.* **2012**, *112*, 3482-3507.
(2) (a) Reiff, W. M.; LaPointe, A. M.; Witten, E. H. *J. Am. Chem. Soc.* **2004**, *126*, 10206-10207. (b) Merrill, W. A.; Stitch, T. A.; Brynda, M.; Yeagle, G. J.; Fettinger, J. C.; De Hont, R.; Reiff, W. M.; Schulz, C. E.; Britt, R. D.; Power, P. P. *J. Am. Chem. Soc.* **2009**, *131*, 12693-12702. (c) Boynton, J. N.; Guo, J.-D.; Fettinger, J. C.; Melton, C. E.; Nagase, S.; Power, P. P. *J. Am. Chem. Soc.* **2013**, *135*, 10720-10728. (d) Zadrozny, J. M.; Xiao, D. J.; Atanasov, M.; Long, G. J.; Grandjean, F.; Neese, F.; Long, J. R. *Nat. Chem.* **2013**, *5*, 577-581. (e) Bryan, A. M.; Merrill, W. A.; Reiff, W. M.; Fettinger, J. C.; Power, P. P. *J. Am. Chem. Soc.* **2012**, *51*, 3366-3373. (f) Zadrozny, J. M.; Atanasov, M.; Bryan, A. M.; Lin, C.-Y.; Rekken, B. D.; Power, P. P.; Neese, F.; Long, J. R. *Chem. Sci.* **2013**, *4*, 125-138.
(3) Lipschutz, M. I.; Yang, X.; Chatterjee, R.; Tilley, T. D. *J. Am. Chem. Soc.* **2013**, *135*, 15298-15301.
(4) Lipschutz, M. I.; Tilley, T. D. *Angew. Chem. Int. Ed.* **2014**, *53*, 7290-7294.
(5) Lipschutz, M. I.; Tilley, T. D. *Chem. Commun.* **2012**, *48*, 7146-7148.
(6) (a) Laskowski, C. A.; Hillouse, G. L. *J. Am. Chem. Soc.* **2008**, *130*, 13846-13847. (b) Laskowski, C. A.; Bungum, D. J.; Baldwin, S. M.; Del Ciello, S. A.; Iluc, V. M.; Hillhouse, G. L. *J. Am. Chem. Soc.* **2013**, *135*, 18272-18275. (c) Anderson, J. S.; Iluc, V. M.; Hillhouse, G. L. *Inorg. Chem.* **2010**, *49*, 10203-10207.
(7) Cross coupling: (a) Miyzaki, S.; Koga, Y.; Matsumoto, T.; Matsubara, K. *Chem. Comm.* **2010**, *46*, 1932-1934. (b) Zhang, K.; Conda-Sheridan, M.; Cooke, S. R.; Louie, J. *Organometallics* **2011**, *30*, 2546-2552. (c) Nagao, S.; Matsumoto, T.; Koga, Y.; Matsubara, K. *Chem. Lett.* **2011**, *40*, 1036-1038.
(8) Ni-E multiple bonds: (a) Mindiola, D. J.; Hillhouse, G. L. *J. Am. Chem. Soc.* **2001**, *123*, 4623-4624. (b) Melenkivitz, R.; Mindiola, D. J.; Hillhouse, G. L. *J. Am. Chem. Soc.* **2002**, *124*, 3846-3847. (c) Iluc, V. M.; Miller, A. J. M.; Anderson, J. S.; Monreal M. J.; Mehn, M. P.; Hillhouse, G. L. *J. Am. Chem. Soc.* **2011**, *133*, 13055-13063. (d) Kogut, E.; Wiencko, H. L.; Zhang, L.; Cordeau, D. E.; Warren, T. H. *J. Am. Chem. Soc.* **2005**, *127*, 11248-11249.
(9) Dibble, B. R.; Sigman, M. S.; Arif, A. M. *Inorg. Chem.* **2005**, *44*, 3774-3776.
(10) Hruszkewycz, D. P.; Wu, J.; Green, J. C.; Hazari, N.; Schmeter, T. J. *Organometallics* **2012**, *31*, 470-485.

(11) Kitiachvili, K. D.; Mindiola, D. J.; Hillhouse, G. L. *J. Am. Chem. Soc.* **2004**, *126*, 10554-10555.
(12) Wu, J.; Nova, A.; Balcells, D.; Brudwig, G. W.; Dai, W.; Guard, L. M.; Hazari, N.; Lin, P.-H.; Pokhrel, R.; Takese, M. K. *Chem. Eur. J.* **2014**, *20*, 5327-5337.
(13) Laskowski, C. A.; Morello, G. R.; Saouma, C. T.; Cundari, T. R.; Hillhouse, G. L. *Chem. Sci.* **2013**, *4*, 170-174.
(14) Bach, I.; Goddard, R.; Kopiske, C.; Seevogel, K.; Pörschke, K.-R. *Organometallics* **1999**, *18*, 10-20.
(15) Iluc, V. M.; Hillhouse, G. L. *J. Am. Chem. Soc.* **2010**, *132*, 11890-11892.
(16) (a) Aresta, M.; Nobile, C. F.; Sacco, A. *Inorg. Chim. Acta.* **1975**, *12*, 167-178. (b) Dapporto, P; Fallani, G.; Sacconi, L. *Inorg. Chem.* **1974**, *13*, 2847-2850. (c) Krüger, C.; Betz, P. *J. Organomet. Chem.* **1990**, *387*, 113-121. (d) Bai , G.; Wei, P.; Stephan, D. W. *Organometallics* **2005**, *24*, 5901-5908. (e) Holland, P. L.; Cundari, T. L.; Perez, L. L.; Eckert, N. A.; Lachicotte, R. J. *J. Am. Chem. Soc.* **2002**, *124*, 14416-14424.
(17) Bradley, D.C.; Hursthouse, M. B.; Smallwood, R. J.; Welch, A. J. *J. Chem. Soc. Chem. Comm.* **1972**, *15*, 872-873.
(18) (a) Ke, M.; Rettig, S. J.; James, B. R.; Dolphin, D. *J. Chem. Soc., Chem. Commun.* **1987**, 1110-1112. (b) He, M.; Dowd, P. *J. Am. Chem. Soc.* **1998**, *120*, 1133-1137. (c) Randaccio, L. *Comments Inorg. Chem.* **1999**, *21*, 327-376. (d) Jensen, K. P.; Ryde, U. *J. Am. Chem. Soc.* **2005**, *127*, 9117-9128. (e) Finke, R. G.; Hay, B. P. *Inorg. Chem.* **1984**, *23*, 3041-3043. (f) Wayland, B. B.; Ba, S.; Sherry, A. E. *J. Am. Chem. Soc.* **1991**, *113*, 5305-5311.
(19) (a) Dahlenburg, L; Hock, N. *J. Organomet. Chem.* **1985**, *284*, 129-138. (b) Wallasch, M.; Wolmershäuser, G.; Sitzmann, H. *Angew. Chem. Int. Ed.* **2005**, *44*, 2597-2599. (c) Cámpora, J.; Reyes, M. L.; Hackl, T. *Organometallics* **2000**, *19*, 2950-2952. (d) Loren, S. D.; Campion, B. K.; Heyn, R. H.; Tilley, T. D.; Bursten, B. E.; Luth, K. W. *J. Am. Chem. Soc.* **1989**, *111*, 4712-4718.
(20) (a) Marynick, D. N. *J. Am. Chem. Soc.* **1984**, *106*, 4064-4065. (b) Pacchioni, G.; Bagus, P. S. *Inorg. Chem.* **1992**, *31*, 4391-4398. (c) Mitoraj, M. P.; Michalak, A. *Inorg. Chem.* **2010**, *49*, 578-582.
(21) Khramov, D. M.; Lynch, V. M.; Bielawaski, C. W. *Organometallics* **2007**, *26*, 6042-6049.
(22) Evans, D. F. *J. Chem. Soc.*, **1959**, 2003-2005.
(23) Jafarpour, L.; Stevens, E. D.; Nolan, S. P. *J. Organomet. Chem.,* **2000**, *606*, 49-54.

Chapter 4 Appendix

ENLARGED ORTEP DIAGRAMS

Caron atoms are shown in dark grey, Nickel in green, Silicon in pink, Nitrogen in blue, Phosphorous in orange and Oxygen in red in all of the following diagrams. All thermal ellipsoids are shown at 50% probability.

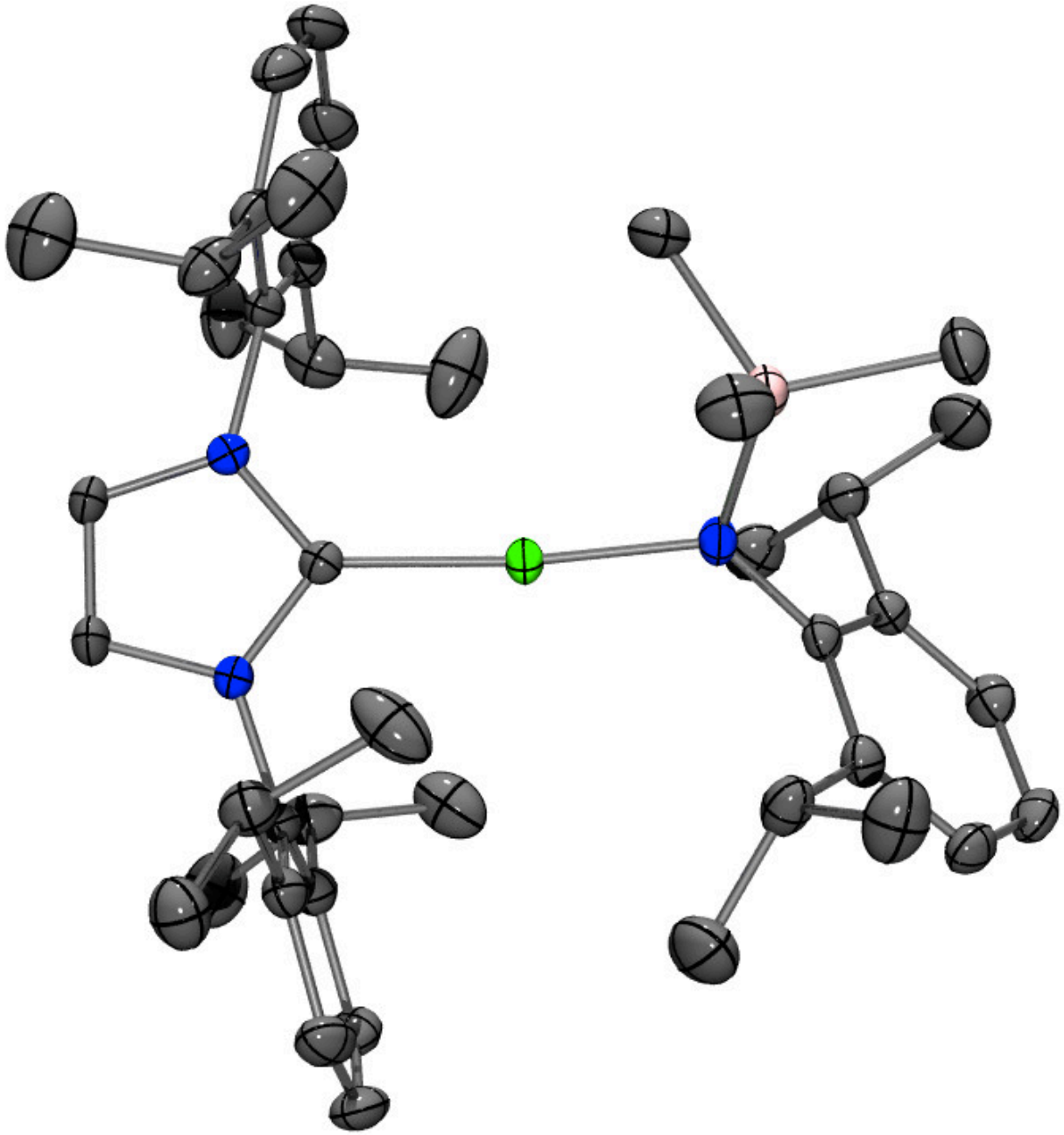

ORTEP diagram for compound **3**.

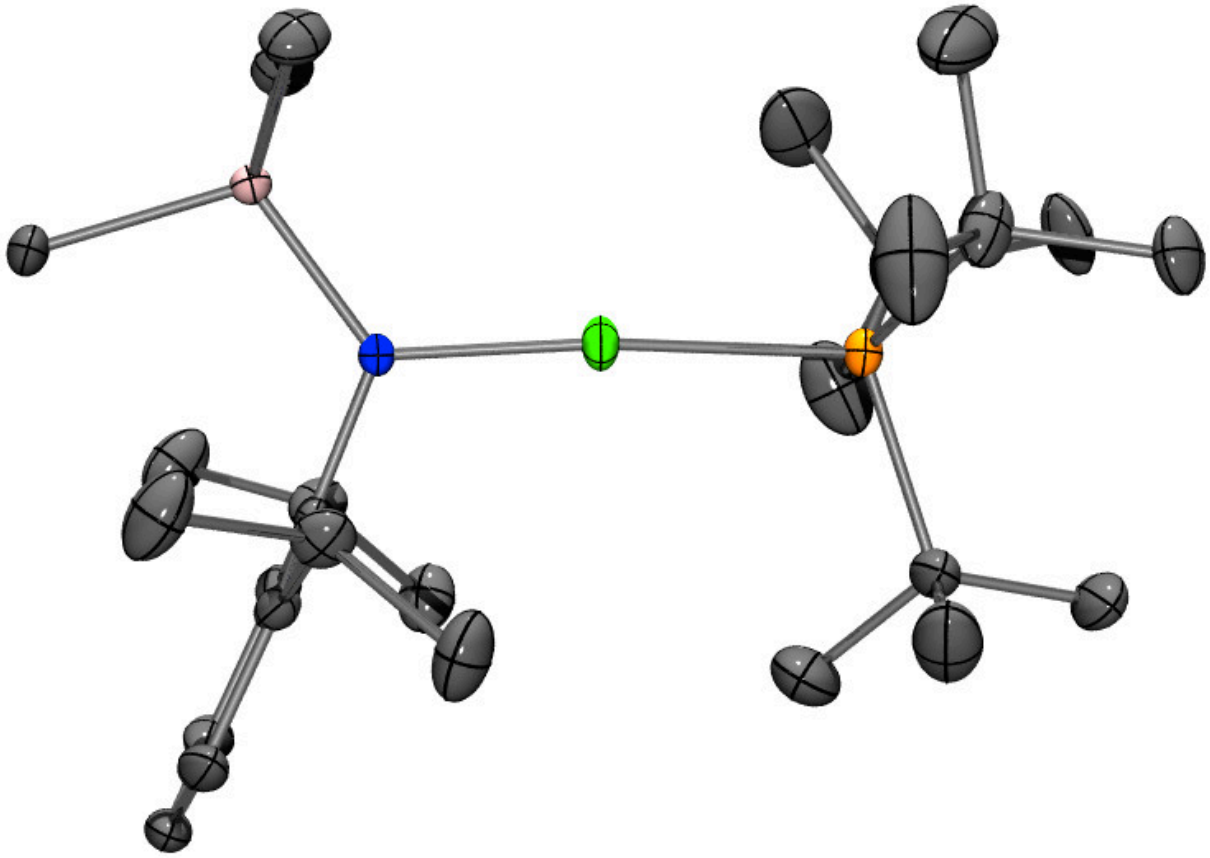

ORTEP diagram for compound **4**.

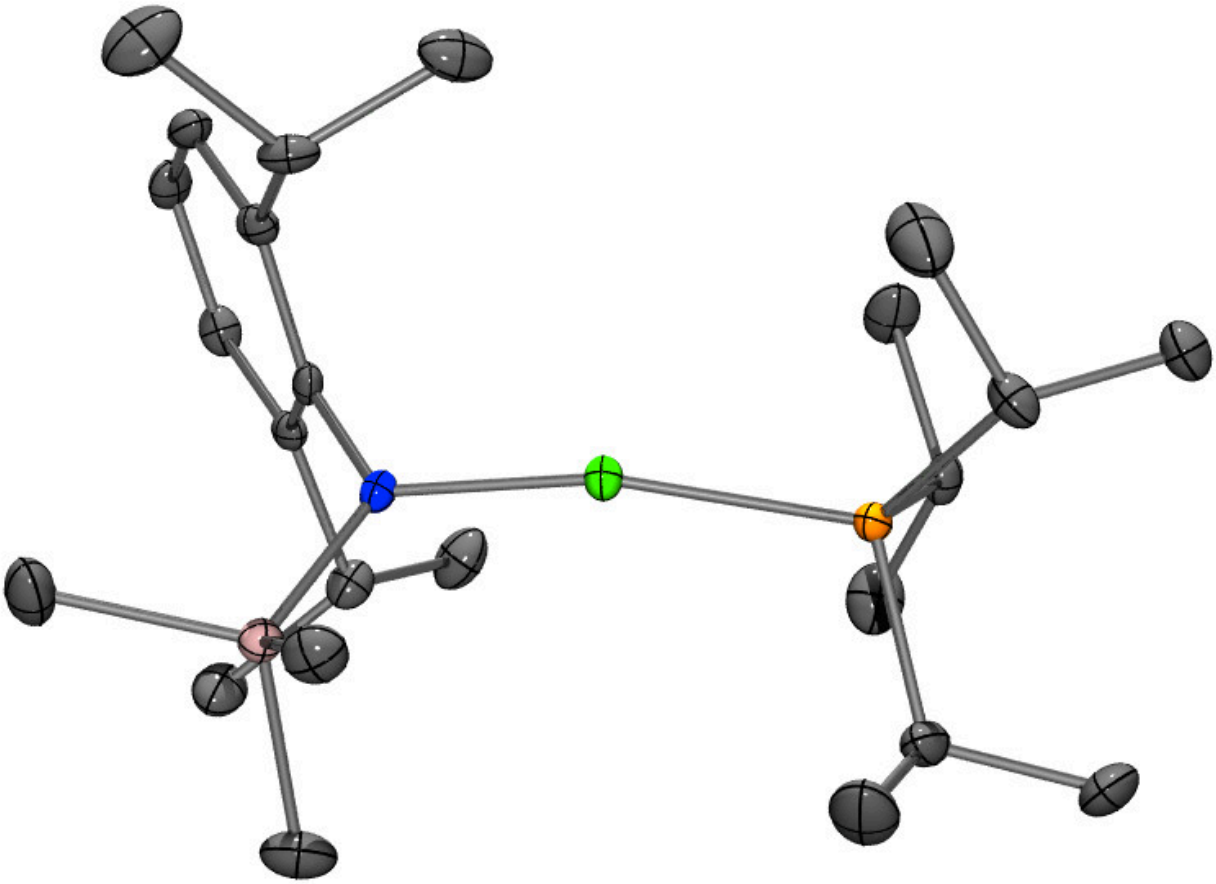

ORTEP diagram for compound **5**.

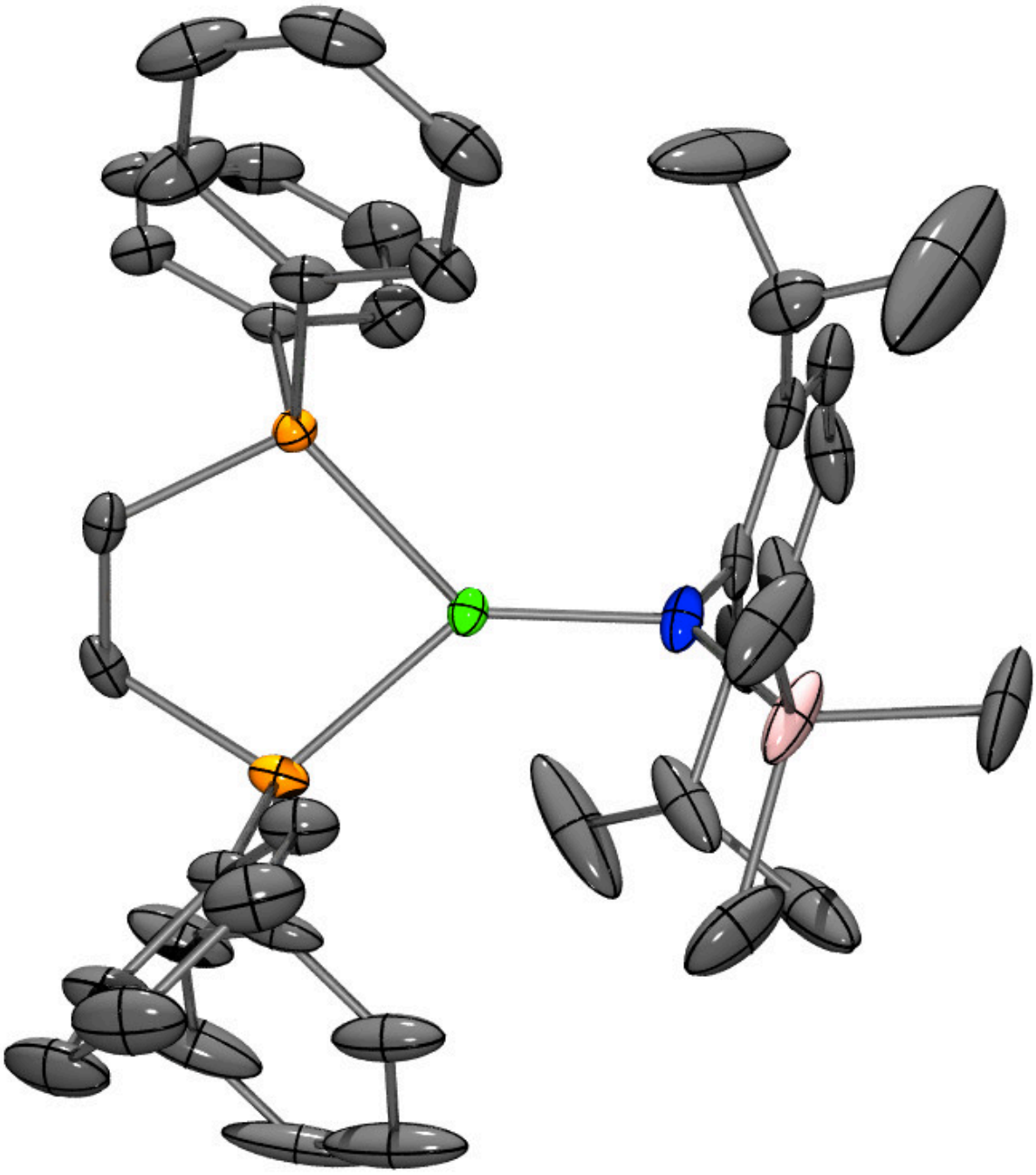

ORTEP diagram for compound **6**.

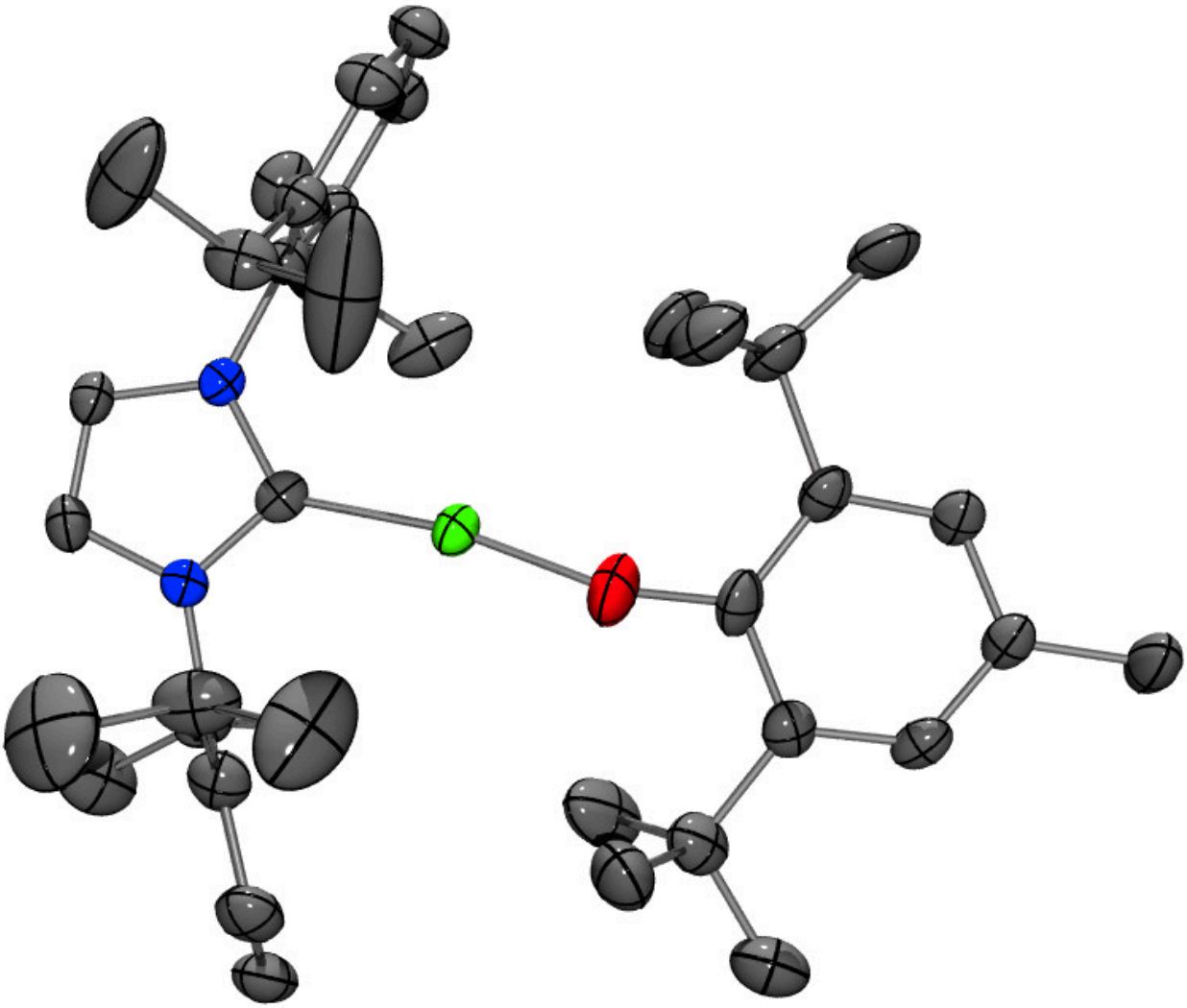

ORTEP diagram for compound **7**.

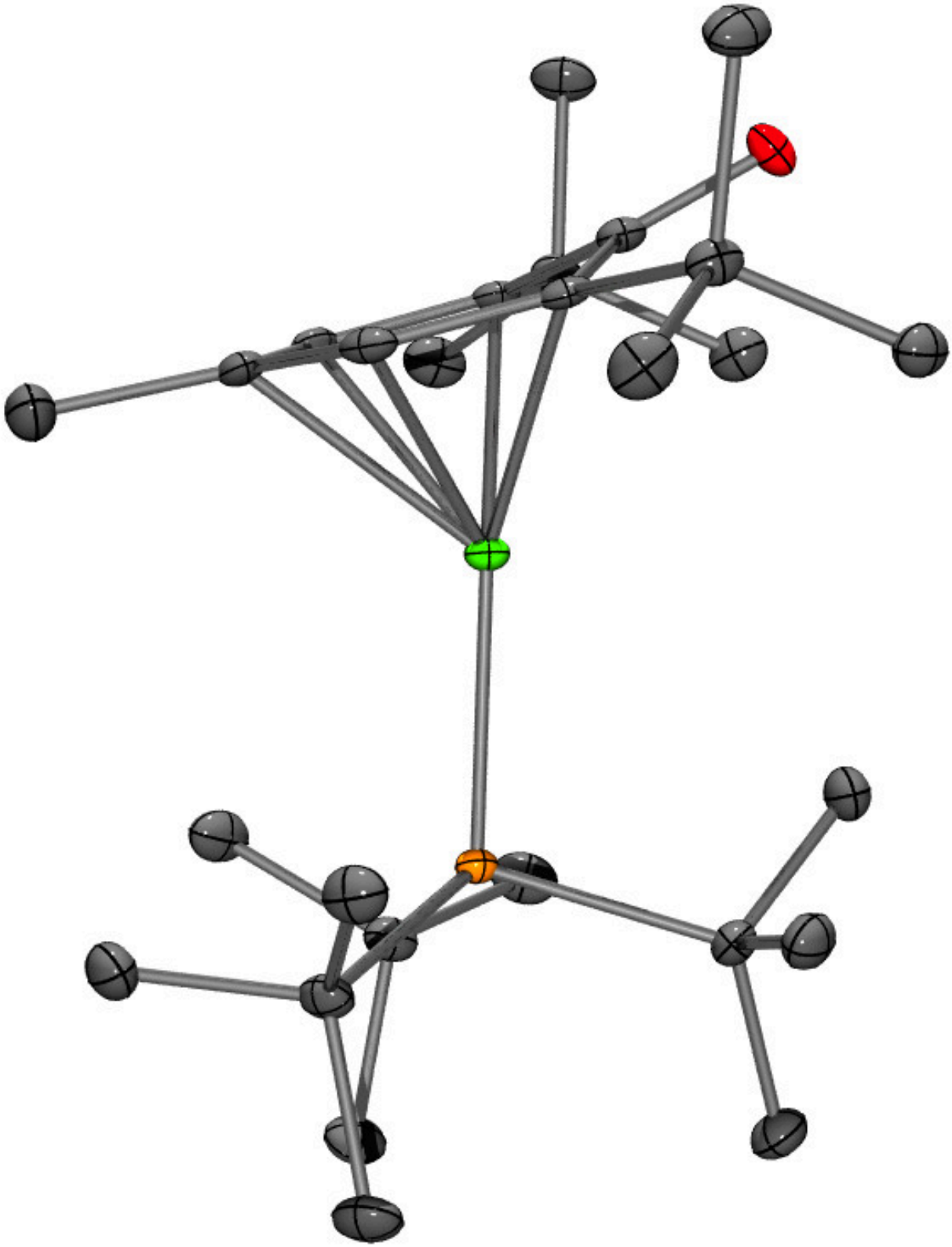

ORTEP diagram for compound **8**.

X-RAY DATA TABLES

Compound **3**:

Empirical formula	C42 H62 N3 Ni Si	
Formula weight	695.75	
Temperature	100(2) K	
Wavelength	0.71073 Å	
Crystal system	Monoclinic	
Space group	P2(1)/n	
Unit cell dimensions	a = 10.4100(4) Å	a= 90º.
	b = 18.0926(7) Å	b= 99.612(2)º.
	c = 22.1319(8) Å	g = 90º.
Volume	4109.9(3) $Å^3$	
Z	4	
Density (calculated)	1.124 Mg/m^3	
Absorption coefficient	0.531 mm^{-1}	
F(000)	1508	
Crystal size	0.19 x 0.15 x 0.07 mm^3	
Theta range for data collection	1.46 to 27.55º.	
Index ranges	-13<=h<=13, -23<=k<=23, -28<=l<=28	
Reflections collected	62759	
Independent reflections	9320 [R(int) = 0.0439]	
Completeness to theta = 25.00º	100.0 %	
Absorption correction	Semi-empirical from equivalents	
Max. and min. transmission	0.9637 and 0.9058	
Refinement method	Full-matrix least-squares on F^2	
Data / restraints / parameters	9320 / 0 / 439	
Goodness-of-fit on F^2	1.024	
Final R indices [I>2sigma(I)]	R1 = 0.0374, wR2 = 0.0837	
R indices (all data)	R1 = 0.0559, wR2 = 0.0922	
Largest diff. peak and hole	0.363 and -0.314 $e.Å^{-3}$	

Compound **4**:

Empirical formula	C27 H53 N Ni P Si	
Formula weight	509.47	
Temperature	100(2) K	
Wavelength	0.71073 Å	
Crystal system	Monoclinic	
Space group	P2(1)/c	
Unit cell dimensions	a = 8.6401(5) Å	a= 90º.
	b = 14.7417(9) Å	b= 92.321(3)º.
	c = 23.2643(14) Å	g = 90º.
Volume	2960.7(3) $Å^3$	
Z	4	

Density (calculated)	1.143 Mg/m^3
Absorption coefficient	0.764 mm^{-1}
F(000)	1116
Crystal size	0.13 x 0.12 x 0.12 mm^3
Theta range for data collection	1.64 to 31.50º.
Index ranges	-12<=h<=10, -17<=k<=21, -33<=l<=31
Reflections collected	40981
Independent reflections	8851 [R(int) = 0.0297]
Completeness to theta = 25.00º	100.0 %
Absorption correction	Semi-empirical from equivalents
Max. and min. transmission	0.9139 and 0.9072
Refinement method	Full-matrix least-squares on F^2
Data / restraints / parameters	8851 / 0 / 306
Goodness-of-fit on F^2	1.046
Final R indices [I>2sigma(I)]	R1 = 0.0462, wR2 = 0.1300
R indices (all data)	R1 = 0.0579, wR2 = 0.1385
Largest diff. peak and hole	0.894 and -0.428 $e.Å^{-3}$

Compound **5**:

Empirical formula	C24 H47 N Ni P Si	
Formula weight	467.40	
Temperature	100(2) K	
Wavelength	0.71073 Å	
Crystal system	Monoclinic	
Space group	P2(1)/n	
Unit cell dimensions	a = 11.9515(5) Å	a= 90º.
	b = 13.9669(5) Å	b= 102.4770(10)º.
	c = 16.9287(7) Å	g = 90º.
Volume	2759.09(19) $Å^3$	
Z	4	
Density (calculated)	1.125 Mg/m^3	
Absorption coefficient	0.814 mm^{-1}	
F(000)	1020	
Crystal size	0.10 x 0.08 x 0.01 mm^3	
Theta range for data collection	1.91 to 25.37º.	
Index ranges	-14<=h<=14, -16<=k<=12, -20<=l<=18	
Reflections collected	13644	
Independent reflections	4989 [R(int) = 0.0423]	
Completeness to theta = 25.00º	98.7 %	
Absorption correction	Semi-empirical from equivalents	
Max. and min. transmission	0.9919 and 0.9230	
Refinement method	Full-matrix least-squares on F^2	
Data / restraints / parameters	4989 / 0 / 266	
Goodness-of-fit on F^2	0.991	

Final R indices [I>2sigma(I)]	R1 = 0.0383, wR2 = 0.0751
R indices (all data)	R1 = 0.0573, wR2 = 0.0829
Largest diff. peak and hole	0.415 and -0.299 e.Å^{-3}

Compound **6**:

Empirical formula	C41 H50 N Ni P2 Si	
Formula weight	705.56	
Temperature	100(2) K	
Wavelength	0.71073 Å	
Crystal system	Triclinic	
Space group	P-1	
Unit cell dimensions	a = 10.2622(5) Å	a= 95.201(2)º.
	b = 10.9582(5) Å	b= 102.210(2)º.
	c = 18.1585(8) Å	g = 108.057(2)º.
Volume	1870.53(15) Å^3	
Z	2	
Density (calculated)	1.253 Mg/m^3	
Absorption coefficient	0.665 mm^{-1}	
F(000)	750	
Crystal size	0.09 x 0.06 x 0.06 mm^3	
Theta range for data collection	1.98 to 25.41º.	
Index ranges	-12<=h<=12, -12<=k<=13, -21<=l<=21	
Reflections collected	52301	
Independent reflections	6884 [R(int) = 0.0321]	
Completeness to theta = 25.00º	99.9 %	
Absorption correction	Semi-empirical from equivalents	
Max. and min. transmission	0.9612 and 0.9425	
Refinement method	Full-matrix least-squares on F^2	
Data / restraints / parameters	6884 / 7 / 422	
Goodness-of-fit on F^2	1.042	
Final R indices [I>2sigma(I)]	R1 = 0.0480, wR2 = 0.1072	
R indices (all data)	R1 = 0.0551, wR2 = 0.1119	
Largest diff. peak and hole	1.678 and -1.856 e.Å^{-3}	

Compound **7**:

Empirical formula	C42 H59 N2 Ni O	
Formula weight	666.60	
Temperature	100(2) K	
Wavelength	0.71073 Å	
Crystal system	Triclinic	
Space group	P-1	
Unit cell dimensions	a = 18.329(5) Å	a= 109.439(5)º.
	b = 19.847(5) Å	b= 106.744(5)º.
	c = 20.428(5) Å	g = 96.811(5)º.

Volume	6518(3) $Å^3$
Z	6
Density (calculated)	1.019 Mg/m^3
Absorption coefficient	0.475 mm^{-1}
F(000)	2166
Crystal size	0.08 x 0.06 x 0.06 mm^3
Theta range for data collection	1.43 to 26.44º.
Index ranges	-22<=h<=22, -24<=k<=24, -25<=l<=25
Reflections collected	157318
Independent reflections	26731 [R(int) = 0.0625]
Completeness to theta = 25.00º	99.9 %
Absorption correction	Semi-empirical from equivalents
Max. and min. transmission	0.9721 and 0.9630
Refinement method	Full-matrix least-squares on F^2
Data / restraints / parameters	26731 / 0 / 1288
Goodness-of-fit on F^2	1.094
Final R indices [I>2sigma(I)]	R1 = 0.0552, wR2 = 0.1287
R indices (all data)	R1 = 0.0924, wR2 = 0.1395
Largest diff. peak and hole	0.937 and -0.652 $e.Å^{-3}$

Compound **8**:

Empirical formula	C27 H50 Ni O P	
Formula weight	480.353	
Temperature	100(2) K	
Wavelength	0.71073 Å	
Crystal system	Monoclinic	
Space group	P2(1)/n	
Unit cell dimensions	a = 9.7648(7) Å	a= 90º.
	b = 16.4415(12) Å	b= 103.794(3)º.
	c = 16.7346(12) Å	g = 90º.
Volume	2609.2(3) $Å^3$	
Z	4	
Density (calculated)	1.223 Mg/m^3	
Absorption coefficient	0.821 mm^{-1}	
F(000)	1052	
Crystal size	0.10 x 0.10 x 0.08 mm^3	
Theta range for data collection	1.76 to 25.41º.	
Index ranges	-11<=h<=11, -19<=k<=19, -20<=l<=20	
Reflections collected	50067	
Independent reflections	4796 [R(int) = 0.0313]	
Completeness to theta = 25.00º	100.0 %	
Absorption correction	Semi-empirical from equivalents	
Max. and min. transmission	0.9372 and 0.9224	
Refinement method	Full-matrix least-squares on F^2	

Data / restraints / parameters	4796 / 0 / 287
Goodness-of-fit on F^2	1.044
Final R indices [I>2sigma(I)]	R1 = 0.0231, wR2 = 0.0571
R indices (all data)	R1 = 0.0264, wR2 = 0.0590
Largest diff. peak and hole	0.340 and -0.208 e.$Å^{-3}$

Chapter 5. A Bis(amido) Ligand Set That Supports Two-coordinate Chromium in the +1, +2, and +3 Oxidation States

INTRODUCTION

The first-row transition metals are unique in their ability to support very low coordination numbers over a wide range of d^n configurations. The interest in such compounds has largely been driven by attempts to understand structure and bonding for these unusual coordination geometries, and this has led to the isolation and characterization of fewer than one hundred two-coordinate, open-shell complexes.[1–11] Recently, the silyl(aryl)amido ligand –N(SiMe$_3$)DIPP (DIPP = 2,6-diisopropylphenyl) has been shown to allow access to multiple oxidation states for two-coordinate nickel, iron and cobalt complexes.[4–7] Interestingly, it cannot be used to make a strictly two-coordinate chromium complex; attempts to synthesize Cr[N(SiMe$_3$)DIPP]$_2$ led to C–H bond activation of the ligand and formation of a remarkable tetra-chromium complex containing bridging –CH$_2$(SiMe$_2$) groups (**A**, Figure 1).[6] Also, although the silylamido ligand –N(SiMe$_2$Ph)$_2$ produces a two-coordinate chromium complex in the solid state, the bis(THF) adduct of the complex is also isolated from the same reaction mixture (**B**, Figure 1).[8]

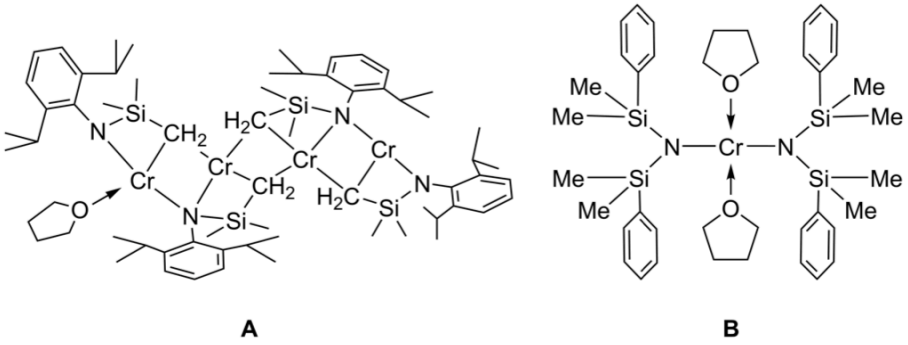

Figure 1. Previous examples of chromium complexes supported by silylamido ligands, **A**[6] and **B**.[8]

The stabilization of low-coordinate complexes is more challenging for the earlier first-row transition metals, due to their larger atomic radii and lower d^n counts. Notably, only two two-coordinate vanadium complexes have been reported and both require the presence of extremely bulky terphenyl amido ligands.[2] Similar requirements for exceptional steric bulk seem to hold for open-shell, two-coordinate chromium complexes, which have been obtained with bulky borylamido,[12,13] arylamido,[3,14] thiolato,[15] and terphenyl[16–19] ligands.[1] Although the aforementioned –N(SiMe$_3$)DIPP ligand cannot stabilize a two-coordinate Cr^{II} species, it seemed that an increase of its steric bulk would allow for isolation of such a complex. Herein, we describe the synthesis and characterization of a two-coordinate Cr^{II} complex with the sterically demanding –N(Si^{i}Pr$_3$)DIPP ligand, which also allows access to low-coordinate complexes of Cr^{I} and Cr^{III}.

RESULTS AND DISCUSSION

Cr[N(Si^{i}Pr$_3$)DIPP]$_2$ (**1**) was synthesized by a salt metathesis reaction of $CrCl_2$ with 2 equiv of K[N(Si^{i}Pr$_3$)DIPP] in THF at ambient temperature. Workup of the red reaction mixture and recrystallization from pentane and hexamethyldisiloxane (HMDSO) afforded green crystals of **1** in 60% yield. The X-ray structure of **1** (Figure 2) reveals a linear geometry about chromium with a crystallographically imposed 180° N-Cr-N bond angle and a Cr-N bond length of

2.0036(1) Å, which falls within the 1.94-2.00 Å range of distances previously reported for two-coordinate chromium bis(amido) complexes.[1,8] The solid state structure also indicates a close interaction between the chromium atom and the *ipso* carbon of the adjacent aryl ring, with a Cr-N-C_{ipso} angle of 81.59(8)° and a Cr-C_{ipso} distance of 2.2709(1) Å. This distance is shorter than Cr-C_{ipso} interactions observed for related chromium bis(amido) complexes, with $Cr[N(Ph)BMes_2]_2$ (Mes = C_6H_2-2,4,6-Me_3) having the shortest distance of 2.328(2) Å between the chromium atom and an *ipso* carbon from a –$BMes_2$ group.[1,13] The solution magnetic moment of **1**, determined by Evans's method,[20,21] is 4.9 μ_B and consistent with a high-spin d^4 configuration. Correspondingly, non-distinctive, broad, unintegratable signals are observed in the ^{1}H NMR spectrum of **1**, due to its paramagnetism.

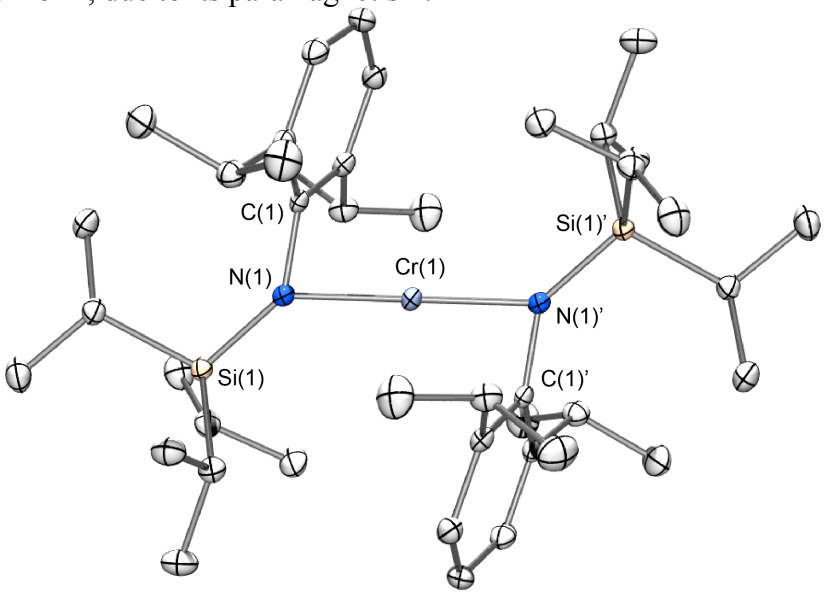

Figure 2. ORTEP diagram of **1**. Thermal ellipsoids shown at 50% probability. Hydrogen atoms are omitted for clarity.

A previous report on the ability of the -N($SiMe_3$)DIPP ligand to stabilize multiple d^n configurations and oxidation states of nickel[5] prompted an investigation of **1** by cyclic voltammetry (CV). The cyclic voltammogram of **1** reveals reversible Cr(I/II) and Cr(II/III) couples at -2.04 V ($E_{1/2}$ vs Fc/Fc^+, ip_a/ip_c = 0.95) and -0.38 V ($E_{1/2}$ vs Fc/Fc^+, ip_a/ip_c = 1.09), respectively (see Experimental section). The reversibility of these redox events suggested that the analogous two-coordinate complexes of Cr^I and Cr^{III} would be stable and chemically accessible.

Reduction of **1** with 1.1 equivs of KC_8 in diethyl ether over 30 minutes at ambient temperature, followed by recrystallization from dimethoxyethane (DME) and pentane, afforded orange crystals which were dried under reduced pressure to provide $[K(DME)_n]\{Cr[N(Si^iPr_3)DIPP]_2\}$ (**2a**) in 97% yield (Scheme 1, n = 1.5, determined by ^{1}H NMR integration against an internal standard). The X-ray structure of **2a** before desolvation under vacuum (Figure 3) reveals that the linear coordination environment of the complex is maintained, with a N-Cr-N bond angle of 175.02(1)° and Cr-N bond lengths of 2.054(3) and 2.061(3) Å, which are slightly longer than that of **1**, as expected. Interestingly, the *ipso* carbon of **2** interacts less strongly with Cr^I than with Cr^{II} (in **1**), with a Cr-C_{ipso} distance greater than 2.8 Å and Cr-N-C_{ipso} angles of 108.4(2)° and 108.5(2)° for **2a**. Additionally, unlike the analogous Ni^I species

$K\{Ni[N(SiMe_3)DIPP]_2\}$,[5] the potassium is not coordinated to the aryl groups of the amido ligands and is instead complexed by four equivalents of DME to give the outer-sphere $[K(DME)_4]^+$ cation. The solution magnetic moment of **2a**, 5.2 μ_B (by Evans's method), is lower than the expected spin-only value of 5.9 μ_B but consistent with a high-spin d^5 configuration.

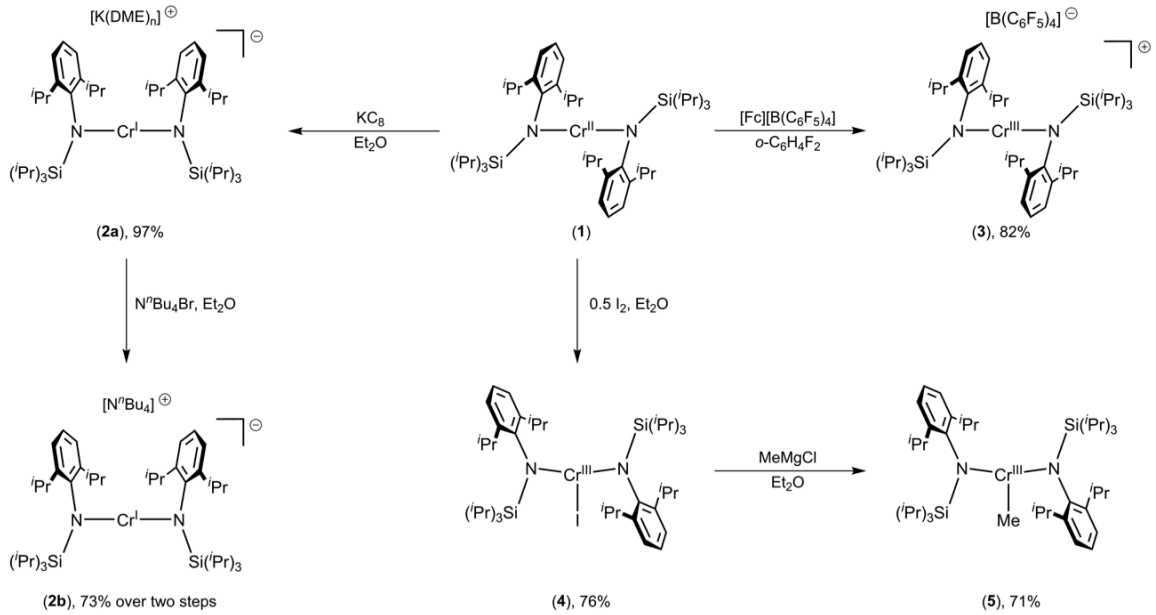

Scheme 1. Reactions of chromium bis(amido) complexes.

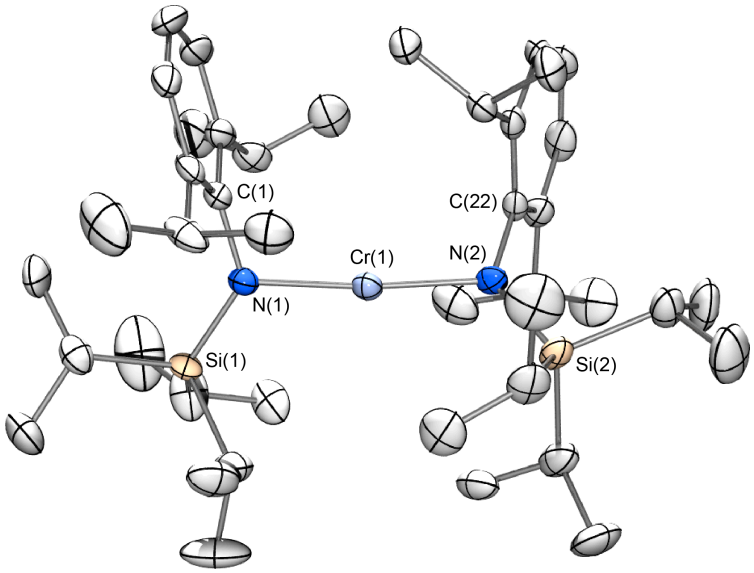

Figure 3. ORTEP diagram of **2a**. Thermal ellipsoids shown at 50% probability. Hydrogen atoms, cation, and solvent are omitted for clarity.

Compound **2a** reacted with tetrabutylammonium bromide to provide $[N^nBu_4]\{Cr[N(Si^iPr_3)DIPP]_2\}$ (**2b**), which has a geometry consistent with that of **2a** (Scheme 1,

see Appendix for details). The solution magnetic moment of **2b** is 5.7 μ_B, also consistent with a high-spin d^5 configuration. The UV-Vis spectra of **2a** and **2b** in DME are consistent with each other; despite being high-spin, the Cr^I species displays several intense absorptions with molar absorptivities ranging from 5200 to 18000 mol^{-1} L cm^{-1}, likely corresponding to ligand-to-metal charge transfer.

Reaction of **1** with ferrocenium tetrakis(pentafluorophenyl)borate over 1 hour at ambient temperature afforded dark red crystals of $\{Cr[N(Si^iPr_3)DIPP]_2\}[B(C_6F_5)_4]$ (**3**) from 1,2-difluorobenzene and HMDSO in 82% yield (Scheme 1). The complex co-crystallizes with 1,2-difluorobenzene and contains two crystallographically independent molecules of **3** within the unit cell. Both molecules are linear, having an N-Cr-N bond angle of 180.000(1)° (Figure 4, see Appendix for details). Due to a smaller atomic radius, the Cr-N bond lengths for each of the molecules of **3** are 1.872(2) and 1.869(2) Å, respectively, and notably shorter than comparable distances observed for **1**. Correspondingly, the Cr-C_{ipso} interaction is increased, such that relatively short Cr-C_{ipso} distances of 2.225(2) and 2.217(2) Å are observed. The solution magnetic moment of **3**, determined by Evans's method, is 3.8 μ_B and most consistent with a high-spin d^3 configuration. Assuming a $(d_{xy}, d_{x2-y2})^2(d_{xz}, d_{yz})^1(d_{z2})^0$ electronic configuration based on $D_{\infty h}$ symmetry, **3** might be expected to be anisotropic. However, despite being isoelectronic to the linear two-coordinate complex $V\{N(H)(C_6H_3\text{-}2,6\text{-}(C_6H_2\text{-}2,4,6\text{-}^iPr_3)_2)\}_2$,[2] **3** does not exhibit significant spin-orbit coupling. Calculations on a similar complex, $Fe[N(SiMe_3)DIPP]_2$, have shown that the nitrogen lone pairs can interact with the metal center, breaking degeneracy of the (d_{xz}, d_{yz}) pair and quenching orbital angular momentum.[22,23] In contrast to the isoelectronic vanadium complex, the cationic charge on **3** is expected to increase further the strength of the ligand field and such degeneracy-breaking interactions, such that isotropic magnetic properties would be observed for **3**.

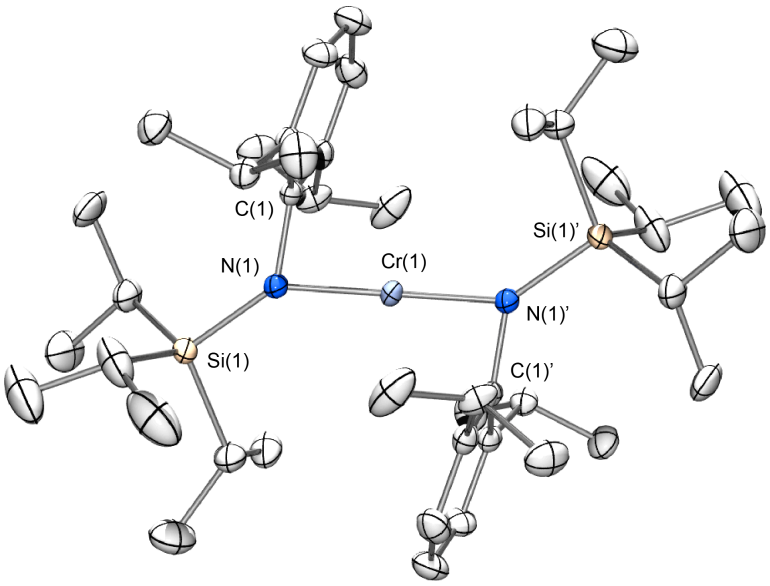

Figure 4. ORTEP diagram of **3**. Thermal ellipsoids shown at 50% probability. Hydrogen atoms, anions, and solvent are omitted for clarity. The second crystallographically independent molecule of **3** has been omitted.

Similar to what is observed for later first row transition metals ligated by -N(SiMe$_3$)DIPP,[4,6] both **1** and **3** exhibit an eclipsed configuration of the two amido groups, with C_{ipso}-NCrN-C_{ipso} dihedral angles of 180.0(1)° and 180.0(2)°, respectively. In contrast, the aryl substituents on the ligands of **2a** and **2b** adopt a *syn* conformation and are approximately staggered, with C_{ipso}-NCrN-C_{ipso} dihedral angles of 44.1(3)° and 39.8(2)°, respectively.

To further explore the oxidation chemistry associated with **1**, 0.5 equivalents of I_2 were added to **1**, to afford dark red crystals of (I)Cr[N(Si^{i}Pr$_3$)DIPP]$_2$ (**4**) from pentane in 76% yield (Scheme 1). Addition of the iodo ligand to **1** results in a trigonal planar geometry with a N-Cr-N bond angle of 139.49(7)° and shorter Cr-N bonds of 1.906(4) and 1.8889(4) Å (Figure 5). There is no significant interaction of the aryl *ipso* carbons with the chromium center, as indicated by Cr-N-C_{ipso} angles of 120.2(3) and 123.8(3)° for **4**. The solution magnetic moment of **4**, determined by Evans's method, is 3.35 μ_B and lower than the expected spin-only value of 3.87 μ_B but consistent with a d^3 configuration.

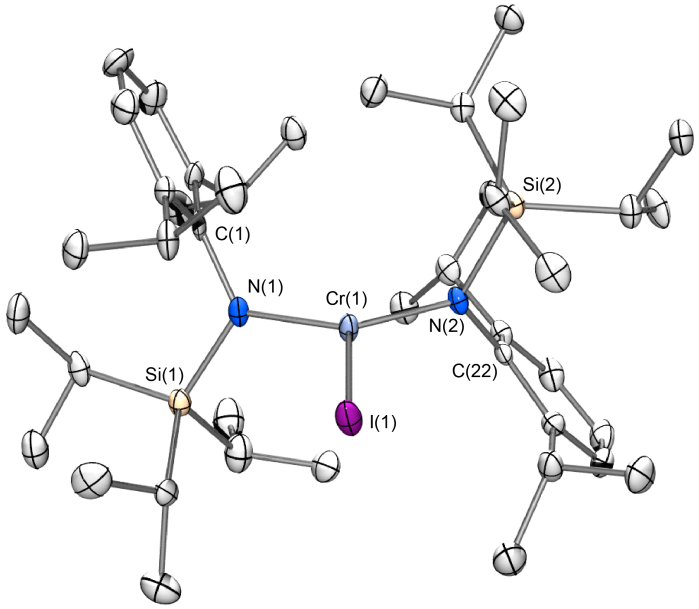

Figure 5. ORTEP diagram of **4**. Thermal ellipsoids shown at 50% probability. Hydrogen atoms are omitted for clarity.

Given the long-standing interest in Cr^{III} alkyl complexes,[24–27] **4** was examined as a possible synthetic entry to such species. Addition of methylmagnesium chloride in THF to a dark red solution of **4** in diethyl ether resulted in a color change to red-orange after five minutes. Workup of the reaction mixture and recrystallization from pentane afforded red crystals of (Me)Cr[N(Si^{i}Pr$_3$)DIPP]$_2$ (**5**) in 71% yield (Scheme 1). Complex **5** crystallizes in a unit cell nearly identical to that of **4**. The N-Cr-N bond angle of 142.89(1)° is slightly wider than that for **4**, but comparable Cr-N bond lengths of 1.906(2) and 1.893(2) Å are observed (Figure 6). Similarly, there is no significant interaction of the *ipso* carbon with the chromium center, with Cr-N-C_{ipso} angles of 122.71(2) and 118.75(2)°. The Cr-C_{Me} bond length of 2.058(3) Å is comparable to the Cr-C_{Me} distance of 2.081(3) Å observed in the β-ketiminate Cr^{II} methyl complex reported by Mindiola and coworkers, one of the few three-coordinate chromium alkyl complexes to be fully characterized.[28] The solution magnetic moment of 5 (3.57 μ_B, Evans's method) is consistent with a d^3 configuration.

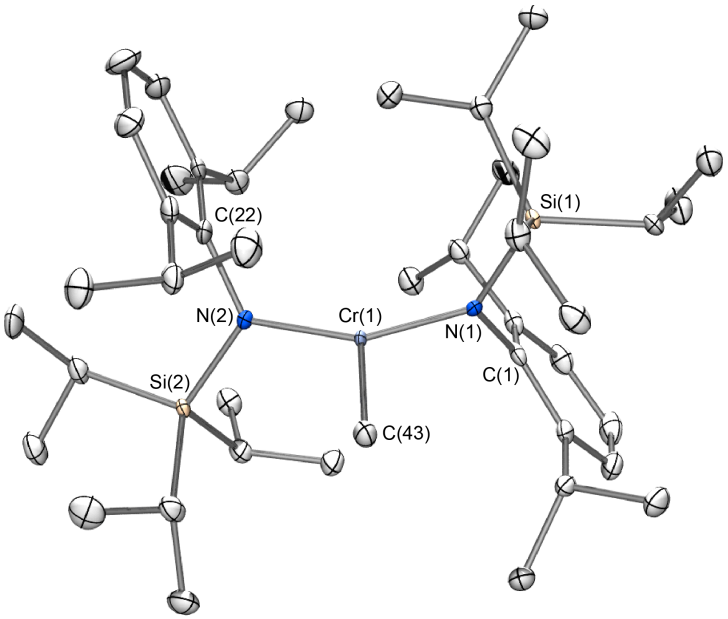

Figure 6. ORTEP diagram of **5**. Thermal ellipsoids shown at 50% probability. Hydrogen atoms are omitted for clarity. Disordered chromium and silicon atoms have been excluded.

CONCLUSION

In summary, a series of two-coordinate chromium complexes has been isolated and characterized. The ability of the –N(Si^{i}Pr$_3$)DIPP ligand to support a monomeric Cr^{II} complex, in contrast to the less bulky –N(SiMe$_3$)DIPP ligand, highlights the role of sterics in maintaining linearity for two-coordinate complexes. Furthermore, isolation of these chromium species continues to demonstrate the ability of silyl(aryl)amido ligands to support two-coordinate species of first row transition metals in a variety of oxidation states. Studies further examining the reactivity of this chromium series are currently ongoing.

EXPERIMENTAL

General Considerations. Unless otherwise noted, all experiments were conducted with dry, oxygen-free solvents using standard Schlenk techniques or in a N_2 atmosphere glovebox. Benzene-d_6 was purchased from Cambridge Isotope Laboratories and dried by vacuum distillation from Na/K alloy. Dimethoxyethane (DME) was purchased from Sigma Aldrich, dried by vacuum distillation from K/benzophenone, and stored over 3 Å molecular sieves. Unless otherwise noted, reagents were obtained from commercial suppliers and used as received. Potassium hydride was purchased as a dispersion in mineral oil from Sigma Aldrich and washed with pentane before use. Tetrabutylammonium tetrakis(pentafluorophenyl)borate,[29] Benzyl potassium,[30] potassium graphite,[31] and ferrocenium tetrakis(pentafluorophenyl)borate[32] were prepared by standard literature procedures. The abbreviation "DIPP" refers to a 2,6-diisopropylphenyl moiety and "DME" refers to dimethoxyethane.

Analytical Methods. All ^{1}H NMR spectra were collected at ambient temperature (ca. 21 °C) on Bruker AVB-400, AVQ-400, AV-500, or AV-600 NMR spectrometers, each equipped with a 5 mm BB probe, and referenced to the residual proteo-solvent signals. Solution magnetic susceptibilities were determined by ^{1}H NMR spectroscopy using Evans's method.[20] For Evans's method measurements using only proteo-solvent, a sealed insert containing DMSO-d_6 was also included for a lock signal. IR spectra were collected on a Bruker Alpha-P FR-IR Spectrometer equipped with a "Platinum" Attenuated Total Reflection sample module. Solution UV-Vis spectra were collected using a Varian Cary 300 series spectrophotometer. Melting points were determined on a Mel-Temp II melting point apparatus. Elemental analyses were performed by the UC Berkeley College of Chemistry Microanalytical Facility.

Cyclic Voltammetry Experiments. Cyclic voltammetry experiments were conducted at ambient temperature in a Vacuum Atmospheres glovebox. Measurements employed a Bio-Logic SP-200 potentiostat with a standard three-electrode configuration. The working electrode was a 3mm diameter glassy carbon electrode purchased from ALS. Silver wire was used as a quasi-reference electrode and sublimed ferrocene was used as an internal potential reference. The counter electrode was a 1/8 inch diameter graphite rod purchased from Electron Microscopy Sciences. The glassy carbon electrode was polished with 1 μm alumina prior to each use. The graphite rod was cleaned with acetone and dried prior to each use. Analyses of **1** were performed in a 0.1 M solution of tetrabutylammonium tetrakis(pentafluorophenyl)borate in 1,2-difluorobenzene with an analyte concentration of 1 mM at a scan rate of 100 mV/s. Solution resistance was corrected by applying *i*R compensation for each measurement. All potential values are reported as $E_{1/2}$ for reversible events and E_p for irreversible events.

X-ray Diffraction Experiments. Single crystal X-ray diffraction experiments were carried out at the UC Berkeley CHEXRAY crystallographic facility. Measurements of all compounds were performed on a Bruker APEX-II CCD area detector using Mo Kα radiation (λ = 0.71073 Å) monochromated using QUAZAR multilayer mirrors. Crystals were kept at 100(2) K throughout collection. Data collection, refinement, and reduction were performed with Bruker APEX2 software (v. 2013.4). All structures were solved using SIR97. Structures **1**, **2a**, **3**, **4**, and **5** were refined with SHELXL-97 with refinement of F^2 against all reflections by full-matrix least squares, while structures **2b** was refined with SHELXL-2013 with refinement of F^2 against all reflections by full-matrix least squares. In all models, non-hydrogen atoms were refined anisotropically, and hydrogen atoms were included at the geometrically-calculated positions and refined using a riding model. Specific details can be found below, in section 4 of this document and in the included crystallographic information files.

Experimental Details:

Compound	Detector Distance (mm)	Image Width (°)	Exposure Time (s)
1	40	0.5	10 s
2a	50	0.5	20 s
2b	40	0.5	30 s
3	40	0.5	10 s
4	60	0.5	30 s
5	40	0.5	30 s

Synthesis of HN(Si^{i}Pr$_3$)DIPP. To a 250 mL Chemglass Air-Free Teflon-stoppered flask was added 2,6-diisopropylaniline (5.3 mL, 28 mmol) and 30 mL of THF. The solution was placed in an ice bath, and to the stirred solution was added *n*BuLi (1.6 M in hexanes, 18.4 mL, 29.4 mmol), dropwise *via* syringe. The yellow solution was removed from the ice bath and stirred for 20 min. To the stirred solution was then slowly added a solution of triisopropylsilyl chloride (6.0 mL, 28 mmol) in 10 mL of THF, *via* syringe. The solution was stirred for 23 h in a 75 °C oil bath. After allowing the reaction to cool to ambient temperature, the volatile materials were removed under reduced pressure. The resulting residue was distilled under 90 °C/ 0.05 mmHg to give a clear, light orange oil (7.3 g, 78%). ^{1}H NMR (400 MHz, C_6D_6, 20 °C) δ 7.05-7.16 (m, 3 H, C_6H_3), 3.56 (sep, 2 H, $CH(CH_3)_2$), 2.43 (b s, 1 H, N-*H*), 1.23 (d, 12 H, $CH(CH_3)_2$), 1.17-1.26 (m, 3 H, $CH(CH_3)_2$), 1.10 (d, J_{HH} = 7.1 Hz, 18 H, $CH(CH_3)_2$). ^{13}C NMR data in C_6D_6 were consistent with values reported in the literature.[33]

K[N(Si^{i}Pr$_3$)DIPP]. To a 20 mL scintillation vial was added benzyl potassium (0.351, 2.7 mmol) and 6 mL of diethyl ether. To a 4 mL, 1 dram vial was added HN(Si^{i}Pr$_3$)DIPP (0.900 g, 2.7 mmol), and 2 mL of diethyl ether. Both vials were placed in a -30 °C freezer and allowed to cool for 30 min. Upon removal of both vials from the freezer, the suspension of benzyl potassium was stirred and the solution of HN(Si^{i}Pr$_3$)DIPP] was added dropwise. The contents of 4 mL vial were washed with an additional 2 mL of diethyl ether and the resulting solution in diethyl ether was then added to the 20 mL scintillation vial. The reaction mixture was stirred at ambient temperature for 70 min. The mixture was filtered and concentrated to a solid. The solid was washed with pentane (3 x 5 mL) and dried *in vacuo* to give an off-white powder (0.725, 72%), which was used without further purification.

Cr[N(Si^{i}Pr$_3$)DIPP]$_2$ (1). To a 20 mL scintillation vial was added chromium(II) chloride (0.100 g, 0.81 mmol) and 4 mL of THF. To a 4 mL, 1 dram vial was added K[N(Si^{i}Pr$_3$)DIPP] (0.610 g, 1.64 mmol) and 2 mL of THF, forming a clear, light yellow solution. Both vials were placed in a -30 °C freezer and allowed to cool for 10 min. Upon removal of both vials from the freezer, the suspension of chromium(II) chloride was stirred and the solution of K[N(Si^{i}Pr$_3$)DIPP] was added dropwise. The contents of 4 mL vial were washed with an additional 2 mL of THF and the resulting solution in THF was then added to the 20 mL scintillation vial. The reaction mixture was stirred at ambient temperature for 1 h. The red solution was concentrated under reduced pressure to a green and orange solid, which was extracted into 10 mL of pentane. The pentane extract was filtered, then concentrated under reduced pressure to a volume of 4 mL, and placed in a -30 °C freezer for several h, to yield 0.263 g (45%) of Cr[N(Si^{i}Pr$_3$)DIPP]$_2$ (**1**) as green, block-like crystals which were isolated by decantation and dried *in vacuo*. The supernatant was collected and the volatile components were removed under reduced pressure. A second crystallization was set up in an identical fashion using the resulting residue with a minimal amount of hexamethyldisiloxane, yielding an additional 0.096 g of **1**. Total yield: 0.349 g (60%). The ^{1}H NMR spectrum of **1** in C_6D_6 contains non-distinctive, broad and unintegrable signals, attributed to the paramagnetism of **1**; μ_{eff} = 4.92 μ_B (C_6D_6, 19.2 °C, Evans's method). IR (neat solid, cm^{-1}) 2863 m, 929 m, 879 s, 766 s, 766 s, 722 m, 669 m. UV-Vis (DME) λ_{max} (ε): 437 nm (5.4 × 10^3 mol^{-1} L cm^{-1}). Mp: 77-80 °C (color change from green to red), 137-140 °C (decomposition). Anal. Calcd. for $C_{42}H_{76}N_2CrSi_2$: C,

70.33%, H, 10.68%, N, 3.91%. Found: C, 70.55%, H, 10.42%, N, 3.81%. Crystals suitable for single crystal X-ray diffraction studies were obtained from the workup described above.

$[K(DME)_n]\{Cr[N(Si^iPr_3)DIPP]_2\}$ (2a). To a 20 mL scintillation vial was added **1** (0.200 g, 0.279 mmol) and 10 mL of diethyl ether. The solution was placed in a -30 °C freezer and allowed to cool for 20 min. Upon removal of the vial from the freezer, the solution was stirred and potassium graphite (0.042 g, 0.307 mmol) was added as a solid. The reaction mixture was stirred at ambient temperature for 30 min. The mixture was filtered and concentrated to a red solid under reduced pressure. The solid was dissolved in 1 mL of DME, upon which was layered 9 mL of pentane. The layered solution was placed in a -30 °C freezer overnight, yielding orange crystals which were isolated by decantation and dried in vacuo, resulting in a 0.242 g (0.270 mmol, 97%) of $[K(DME)_{1.5}]\{Cr[N(Si^iPr_3)DIPP]_2\}$ (MW 891.53) as an orange solid. The relative amount of residual DME was determined after each workup by ^{1}H NMR spectroscopy, using hexamethylbenzene as an internal standard. Apart from residual DME, the ^{1}H NMR spectrum of **2a** in C_6D_6 contains non-distinctive, broad and unintegrable signals, attributed to the paramagnetism of **2a**; $\mu_{eff} = 5.2\ \mu_B$ (C_6D_6, 20 °C, Evans's method). UV-Vis (DME) λ_{max} (ε): 244 (1.8×10^4), 282 (7.2×10^3), 330 (5.7×10^3), 429 (5.2×10^3) nm (mol^{-1} L cm^{-1}). Anal. Calcd. for $C_{42}H_{76}N_2CrKSi_2 \cdot 1.4C_4H_{10}O_2$: C, 64.78%, H, 10.30%, N, 3.17%. Found: C, 64.46%, H, 10.41%, N, 2.96%. Crystals suitable for single crystal X-ray diffraction studies were obtained from the workup described above.

$[N^nBu_4]\{Cr[N(Si^iPr_3)DIPP]_2\}$ (2b). To a 20 mL scintillation vial was added **1** (0.200 g, 0.279 mmol) and 8 mL of diethyl ether. The solution was placed in a -30 °C freezer and allowed to cool for 30 min. Upon removal of the vial from the freezer, the solution was stirred and potassium graphite (0.042 g, 0.307 mmol) was added as a solid. The reaction mixture was stirred at ambient temperature for 30 min. Tetrabutylammonium bromide (0.090 g, 0.279 mmol) was then added directly to the stirring reaction. The mixture was stirred for an additional 1 h at ambient temperature. The mixture was filtered, and the filtrate was concentrated to a volume of 4 mL. The solution was placed in a -30 °C freezer for two days, affording 0.196 g (73%) of $[N^nBu_4]\{Cr[N(Si^iPr_3)DIPP]_2\}$ (**2b**) as orange crystals, which were isolated by decantation and dried *in vacuo*. The ^{1}H NMR spectrum of **2b** in C_6D_6 contains non-distinctive, broad and unintegrable signals, attributed to the paramagnetism of **2b**; $\mu_{eff} = 5.74\ \mu_B$ (THF, 20 °C, Evans's method). UV-vis (DME) λ_{max} (ε): 243 (1.8×10^4), 282 (8.8×10^3), 330 (7.4×10^3), 427(6.3×10^3) nm (mol^{-1} L cm^{-1}). UV-Vis (toluene) λ_{max} (ε): 327 (1.0×10^4), 424 (7.2×10^3) nm (mol^{-1} L cm^{-1}). Anal. Calcd. for $C_{58}H_{112}N_3CrSi_2$: C, 72.59%, H, 11.76%, N, 4.38%. Found: C, 72.32%, H, 11.90%, N, 4.25%. Crystals suitable for single crystal X-ray diffraction studies were obtained from the workup described above.

$\{Cr[N(Si^iPr_3)DIPP]_2\}[B(C_6F_5)_4]$ (3). To a 20 mL scintillation vial was added **1** (0.100 g, 0.140 mmol) and 4 mL of 1,2-difluorobenzene, to produce an orange solution. The solution was placed in a -30 °C freezer and allowed to cool for 50 min. Upon removal of the vial from the freezer, the solution was stirred and ferrocenium tetrakis(pentafluorphenyl)borate) (0.121 g, 0.140 mmol) in 4 mL of 1,2-difluorobenzene was added dropwise. The reaction was stirred at ambient temperature for 1 h. The volatile components of the reaction mixture were removed under reduced pressure and the resulting residue was washed with 5 portions of 2 mL of pentane, until the pentane from washing was no longer visibly yellow. The residue was dissolved in 1,2-

difluorobenzene, and the resulting solution was filtered and then concentrated to a volume of 2 mL, upon which was layered 8 mL of hexamethyldisiloxane. The layered solution was placed in a -30 °C freezer for two days, yielding 0.161 g (82%) of {Cr[N(Si^{i}Pr$_3$)DIPP]$_2$}[B(C$_6$F$_5$)$_4$] (**3**) as very dark red crystals, which were isolated by decantation and dried in vacuo. The ^{1}H NMR spectrum of **3** in C$_6$D$_6$ contains non-distinctive, broad and unintegrable signals, attributed to the paramagnetism of **3**; μ_{eff} = 3.83 μ_B (THF, 20 °C, Evans's method). UV-Vis (DME) λ_{max} (ε): 355 (5.1×10^3), 391 (5.1×10^3) nm (mol^{-1} L cm^{-1}). Anal. Calcd. for $C_{66}H_{76}N_2BCrF_{20}Si_2$: C, 56.77%, H, 5.49%, N, 2.01%. Found: C, 56.49%, H, 5.38%, N, 1.75%. Crystals suitable for single crystal X-ray diffraction studies were obtained from the workup described above.

(I)Cr[N(Si^{i}Pr$_3$)DIPP]$_2$ (4). To a stirred solution of **1** (0.389 g, 0.542 mmol) in 10 mL of diethyl ether was added dropwise a solution of iodine (0.069 g, 0.271 mmol) in 4 mL of diethyl ether. The reaction was stirred for 2 h at ambient temperature and then concentrated to a solid under reduced pressure. The solid was dissolved in pentane, and the resulting solution was filtered and the pentane was removed under reduced pressure to afford a red solid. Crystallization from pentane at -30 °C afforded 0.264 g (58%) of (I)Cr[N(Si^{i}Pr$_3$)DIPP]$_2$ (**4**) as dark red crystals, which were isolated by decantation and dried *in vacuo*. The supernatant was collected and the volatile components were removed under reduced pressure. Subsequent recrystallizations were set up in an identical fashion, yielding an additional 0.084 g of **4**. Total yield: 0.348 g (76%). The ^{1}H NMR spectrum of **4** in C$_6$D$_6$ contains non-distinctive, broad and unintegrable signals, attributed to the paramagnetism of **4**; μ_{eff} = 3.35 μ_B (C$_6$D$_6$, 26 °C, Evans's method). UV-Vis (DME) λ_{max} (ε): 286 (1.5×10^4), 355 (6.5×10^3), 480 (1.4×10^4) nm (mol^{-1} L cm^{-1}). Anal. Calcd. for $C_{42}H_{76}N_2CrISi_2$: C, 59.76%, H, 9.08%, N, 3.32%. Found: C, 59.92%, H, 9.34%, N, 3.41%. Crystals suitable for single crystal X-ray diffraction studies were obtained from the workup described above.

(Me)Cr[N(Si^{i}Pr$_3$)DIPP]$_2$ (5). To a 20 mL scintillation vial was added **4** (0.084 g, 0.100 mmol) and 4 mL of diethyl ether. The solution was placed in a -30 °C freezer allowed to cool for 10 min. Upon removal of the vial from the freezer, the solution was stirred and methylmagnesium chloride (0.1 M in THF, 1.00 mL, 0.100 mmol) was added dropwise *via* syringe. The reaction was stirred for 2 h at ambient temperature and then concentrated to a red-orange solid under reduced pressure. The solid was triturated with 6 mL of pentane and dried *in vacuo*. The solid was dissolved in pentane, and the resulting solution was filtered and re-concentrated to a solid. Recrystallization from pentane at -30 °C afforded 0.052 g (71%) of (Me)Cr[N(Si^{i}Pr$_3$)DIPP]$_2$ (**5**) as red crystals, which were isolated by decantation and dried *in vacuo*. The ^{1}H NMR spectrum of **5** in C$_6$D$_6$ contains non-distinctive, broad and unintegrable signals, attributed to the paramagnetism of **5**; μ_{eff} = 3.57 μ_B (C$_6$D$_6$, 26 °C, Evans's method). UV-Vis (DME) λ_{max} (ε): 244 (1.7×10^4), 340 (7.6×10^3), 450 (4.7×10^3) nm (mol^{-1} L cm^{-1}). Anal. Calcd. for $C_{43}H_{79}N_2CrSi_2$: C, 70.53%, H, 10.87%, N, 3.83%. Found: C, 70.27%, H, 11.21%, N, 3.69%. Crystals suitable for single crystal X-ray diffraction studies were obtained from the workup described above.

REFERENCES

(1) Power, P. P. *Chem. Rev.* **2012**, *112*, 3482–3507.

(2) Boynton, J. N.; Guo, J.-D.; Fettinger, J. C.; Melton, C. E.; Nagase, S.; Power, P. P. *J. Am. Chem. Soc.* **2013**, *135*, 10720–10728.
(3) Huang, Y.-L.; Lu, D.-Y.; Yu, H.-C.; Yu, K.; Hsu, C.-W.; Kuo, T.-S.; Lee, G.-H.; Wang, Y.; Tsai, Y.-C.; *Angew. Chem. Int. Ed.* **2012**, *51*, 7781–7785.
(4) Lipschutz M. I.; Tilley, T. D. *Chem. Commun.* **2012**, *48*, 7146–7148.
(5) Lipschutz, M. I.; Yang, X.; Chatterjee, R.; Tilley, T. D. *J. Am. Chem. Soc.* **2013**, *135*, 15298–15301.
(6) Lin, C.-Y.; Guo, J.-D.; Fettinger, J. C.; Nagase, S.; Grandjean, F.; Long, G. J.; Chilton, N. F.; Power, P. P. *Inorg. Chem.* **2013**, *52*, 13584–13593.
(7) Lin, C.-Y.; Fettinger, J. C.; Grandjean, F.; Long, G. J.; Power, P. P. *Inorg. Chem.* **2014**, *53*, 9400-9406.
(8) König, S. N.; Schädle, C.; Maichle-Mössmer, C.; Anwander, R. *Inorg. Chem.*, **2014**, *53*, 4585–4597.
(9) Ung, G.; Rittle, J.; Soleilhavoup, M.; Bertrand, G.; Peters, J. C. *Angew. Chem. Int. Ed.* **2014**, *53*, 8427–8431.
(10) Mondal, K. C.; Roy, S.; De, S.; Parameswaran, P.; Dittrich, B.; Ehret, F.; Kaim, W.; Roesky, H. W. *Chem. Eur. J.* **2014**, *20*, 11646–11649.
(11) Samuel, P. P.; Mondal, K. C.; Amin Sk, N.; Roesky, H. W.; Carl, E.; Neufeld, R.; Stalke, D.; Demeshko, S.; Meyer, F.; Ungur, L.; Chibotaru, L. F.; Christian, J.; Ramachandran, V.; van Tol, J.; Dalal, N. S. *J. Am. Chem. Soc.* **2014**, *136*, 11964–11971.
(12) Bartlett, R. A.; Chen, H.; Power, P. P. *Angew. Chem. Int. Ed. Engl.* **1989**, *28*, 316–317.
(13) Chen, H.; Bartlett, R. A.; Olmstead, M. M.; Power, P. P.; Shoner, S. C. *J. Am. Chem. Soc.*, **1990**, *112*, 1048–1055.
(14) Boynton, J. N.; Merrill, W. A.; Reiff, W. M.; Fettinger, J. C.; Power, P. P. *Inorg. Chem.* **2012**, *51*, 3212–3219.
(15) Nguyen, T.; Panda, A.; Olmstead, M. M.; Richards, A. F.; Stender, M.; Brynda, M.; Power, P. P. *J. Am. Chem. Soc.* **2005**, *127*, 8545–8552.
(16) Nguyen, T.; Sutton, A. D.; Brynda, M.; Fettinger, J. C.; Long, G. J.; Power, P. P. *Science* **2005**, *310*, 844–847.
(17) Wolf, R.; Ni, C.; Nguyen, T.; Brynda, M.; Long, G. J.; Sutton, A. D.; Fischer, R. C.; Fettinger, J. C.; Hellman, M.; Pu, L.; Power, L. *Inorg. Chem.* **2007**, *46*, 11277–11290.
(18) Wolf, R.; Brynda, M.; Ni, C.; Long, G. J.; Power, P. P. *J. Am. Chem. Soc.* **2007**, *129*, 6076–6077.
(19) Lei, H.; Guo, J.-D.; Fettinger, J. C.; Nagase, S.; Power, P. P. *J. Am. Chem. Soc.* **2010**, *132*, 17399–17401.
(20) Evans, D. F. *J. Chem. Soc. Resumed*, **1959**, 2003–2005.
(21) Live D. H.; Chan, S. I. *Anal. Chem.*, **1970**, *42*, 791–792.
(22) Zadrozny, J. M.; Atanasov, M.; Bryan, A. M.; Lin, C.-Y.; Rekken, B. D.; Power, P. P.; Neese, F.; Long, J. R. *Chem. Sci.* **2013**, *4*, 125–138.
(23) Atanasov, M.; Zadrozny, J. M.; Long, J. R.; Neese, F. *Chem. Sci.* **2013**, *4*, 139–156.
(24) Theopold, K. H. *Acc. Chem. Res.* **1990**, *23*, 263–270.
(25) Liang, Y.; Yap, G. P. A.; Rheingold, A. L.; Theopold, K. H. *Organometallics* **1996**, *15*, 5284–5286.
(26) Heintz, R. A.; Leelasubcharoen, S.; Liable-Sands, L. M.; Rheingold, A. L.; Theopold, K. H. *Organometallics* **1998**, *17*, 5477–5485.

(27) MacAdams, L. A.; Buffone, G. P.; Incarvito, C. D.; Rheingold, A. L.; Theopold, K. H. *J. Am. Chem. Soc.* **2005**, *127*, 1082–1083.
(28) Fan, H.; Adhikari, D.; Saleh, A. A.; Clark, R. L.; Zuno-Cruz, F. J.; Sanchez Cabrera, G.; Huffman, J. C.; Pink, M.; Mindiola, D. J.; Baik, M.-H. *J. Am. Chem. Soc.* **2008**, *130*, 17351–17361.
(29) LeSuer, R. J.; Buttolph, C.; Geiger, W. E. *Anal. Chem.* **2004**, *76*, 6395–6401.
(30) Bailey, P. J.; Coxall, R. A.; Dick, C. M.; Fabre, S.; Henderson, L. C.; Herber, C.; Liddle, S. T.; Loroño-González, D.; Parkin, A.; Parsons, S. *Chem. Eur. J.* **2003**, *9*, 4820–4828.
(31) Bergbreiter, D. E.; Killough, J. M. *J. Am. Chem. Soc.* **1978**, *100*, 2126–2134.
(32) O'Connor, A. R.; Nataro, C.; Golen, J. A.; Rheingold, A. L. *J. Organomet. Chem.* **2004**, *689*, 2411–2414.
(33) Shen, B.; Ying, L.; Chen, J.; Luo, Y. *Inorganica Chim. Acta* **2008**, *361*, 1255–1260.

Chapter 5 Appendix

CYCLIC VOLTAMMOGRAM

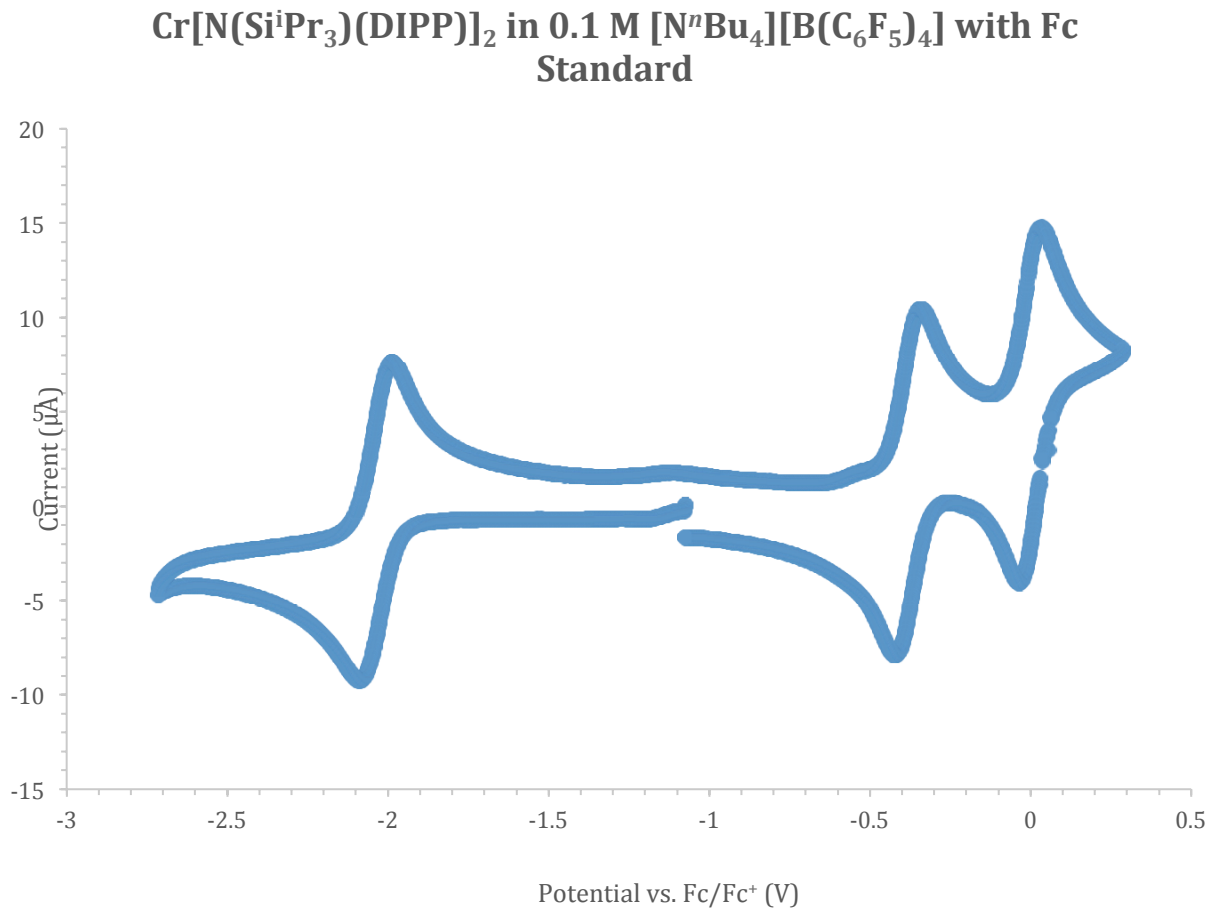

ENLARGED ORTEP DIAGRAMS

Carbon atoms are shown in light gray, chromium in light blue, silicon in yellow and nitrogen in dark blue in all of the following diagrams.

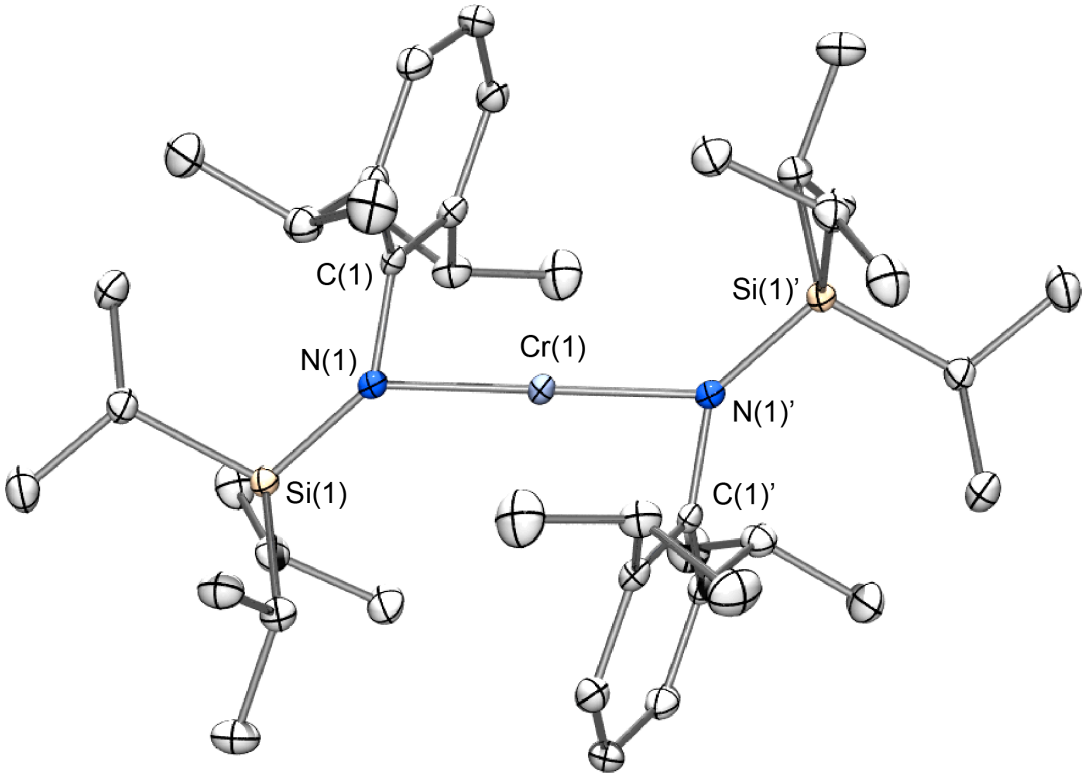

ORTEP diagram of Cr[N(Si^{i}Pr$_3$)DIPP]$_2$ (**1**). Hydrogen atoms have been omitted for clarity. Thermal ellipsoids shown at 50% probability. Selected bond distances [Å], angles [°], and torsions [°]: Cr(1)–N(1): 2.0036(12), C(1)–N(1): 1.402(2), N(1)–Si(1): 1.7146(13), Cr(1)–C(1): 2.2709(14), N(1)–Cr(1)–N(1)': 180.00(8), C(1)– N(1)–Cr(1): 81.59(8), Si(1)–N(1)–Cr(1): 137.87(8), C(1)–N(1)–N(1)'–C(1)': 180.0(1).

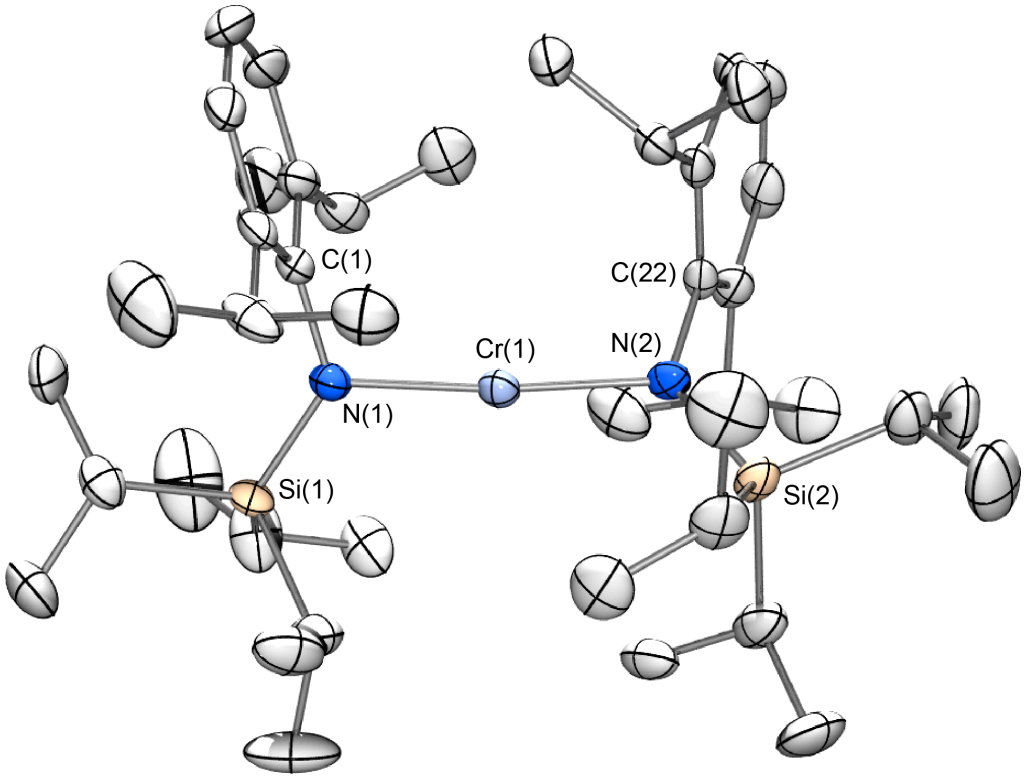

ORTEP diagram of $[K(DME)_4]\{Cr[N(Si^iPr_3)DIPP]_2\}$ (**2a**). Hydrogen atoms and potassium cation coordinated by DME have been omitted for clarity. Thermal ellipsoids shown at 50% probability. Selected bond distances [Å], angles [°], and torsions [°]: Cr(1)–N(1): 2.054(3), Cr(1)–N(2): 2.061(3), C(1)–N(1): 1.416(5), C(22)–N(2): 1.425(5), N(1)–Si(1): 1.703(3), N(2)–Si(2): 1.697(3), Cr(1)–C(1): 2.840(5), Cr(1)–C(22): 2.854(3), N(1)–Cr(1)–N(2): 175.02(13), C(1)–N(1)–Cr(1): 108.4(2), C(22)–N(2)–Cr(1): 108.5(2), Si(1)–N(1)–Cr(1): 123.67(18), Si(2)–N(2)–Cr(1): 125.79(17), C(1)–N(1)–N(2)–C(22): ±44.1(3).

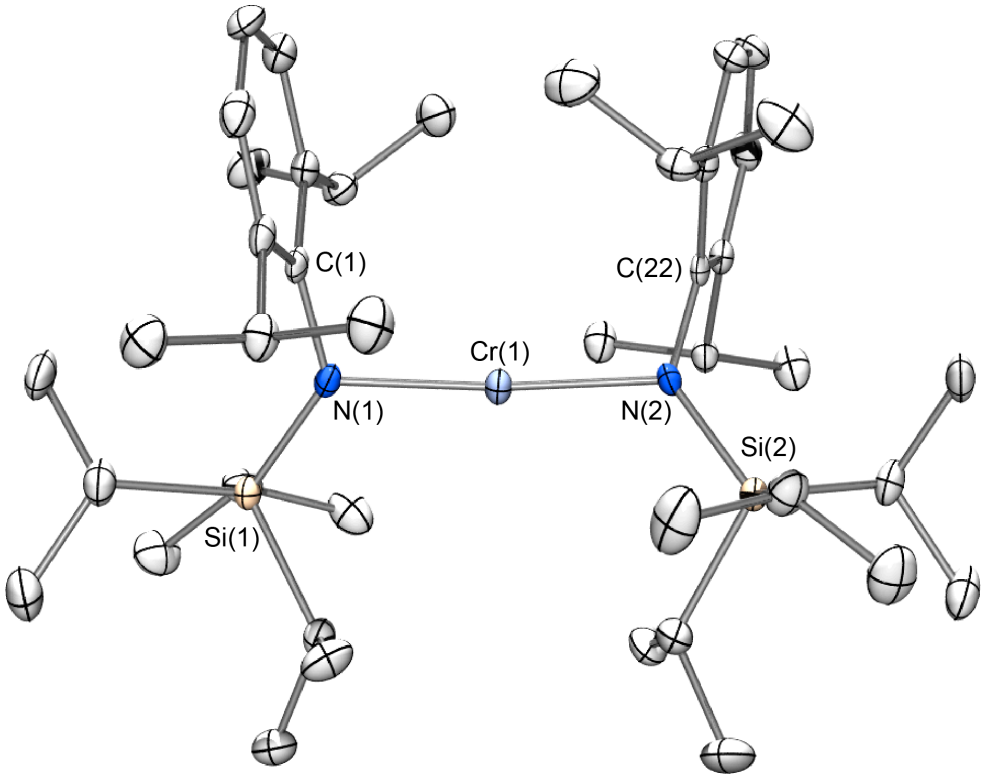

ORTEP diagram of $[N^{n}Bu_4]\{Cr[N(Si^{i}Pr_3)DIPP]_2\}$ (**2b**). Hydrogen atoms and tetrabutylammonium cation have been omitted for clarity. Thermal ellipsoids shown at 50% probability. Selected bond distances [Å], angles [°], and torsions [°]: Cr(1)–N(1): 2.051(2), Cr(1)–N(2): 2.047(2), C(1)–N(1): 1.405(3), C(22)–N(2): 1.407(3), N(1)–Si(1): 1.699(2), N(2)–Si(2): 1.703(2), Cr(1)–C(1): 2.836(3), Cr(1)–C(22): 2.789(3), N(1)–Cr(1)–N(2): 175.63(9), C(1)–N(1)–Cr(1): 108.86(16), C(22)–N(2)–Cr(1): 106.19(16), Si(1)–N(1)–Cr(1): 122.64(12), Si(2)–N(2)–Cr(1): 123.86(12), C(1)–N(1)–N(2)–C(22): ±39.8(2).

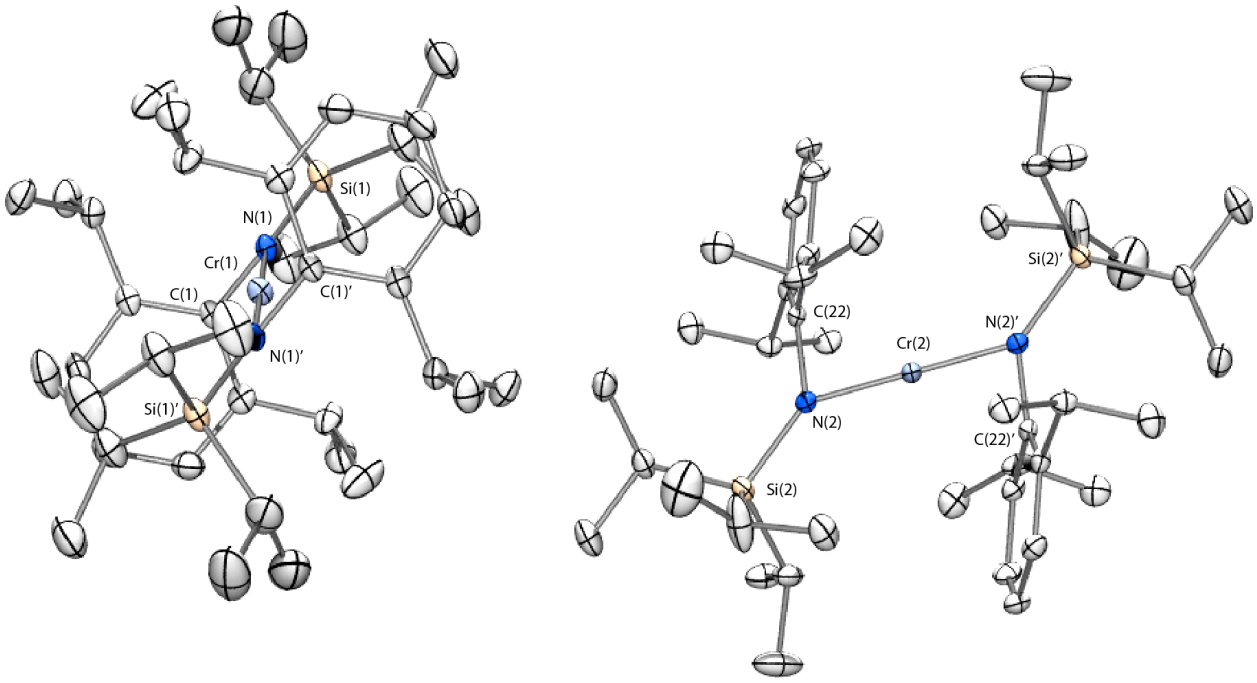

ORTEP diagram of $\{Cr[N(Si^{i}Pr_3)DIPP]_2\}[B(C_6F_5)_4]$ (**4**). Hydrogen atoms have been omitted for clarity. Solvent and $B(C_6F_5)_4$ anions have been excluded. Thermal ellipsoids shown at 50% probability. Selected bond distances [Å], angles [°], and torsions [°]: Cr(1)–N(1): 1.872(2), Cr(2)–N(2): 1.869(2), C(1)–N(1): 1.433(3), C(22)–N(2): 1.433(3), N(1)–Si(1): 1.796(2), N(2)–Si(2): 1.785(2), Cr(1)–C(1): 2.225(2), Cr(2)–C(22): 2.217(2), N(1)–Cr(1)–N(1)': 180.000(1), N(2)–Cr(2)–N(2)': 180.0, C(1)–N(1)–Cr(1): 83.48(14), C(22)–N(2)–Cr(2): 83.24(13), Si(1)–N(1)–Cr(1): 142.58(12), Si(2)–N(2)–Cr(2): 141.09(12), C(1)–N(1)–N(1)'–C(1)': 180.0(2), C(22)–N(2)–N(2)'–C(22)': 180.0(2).

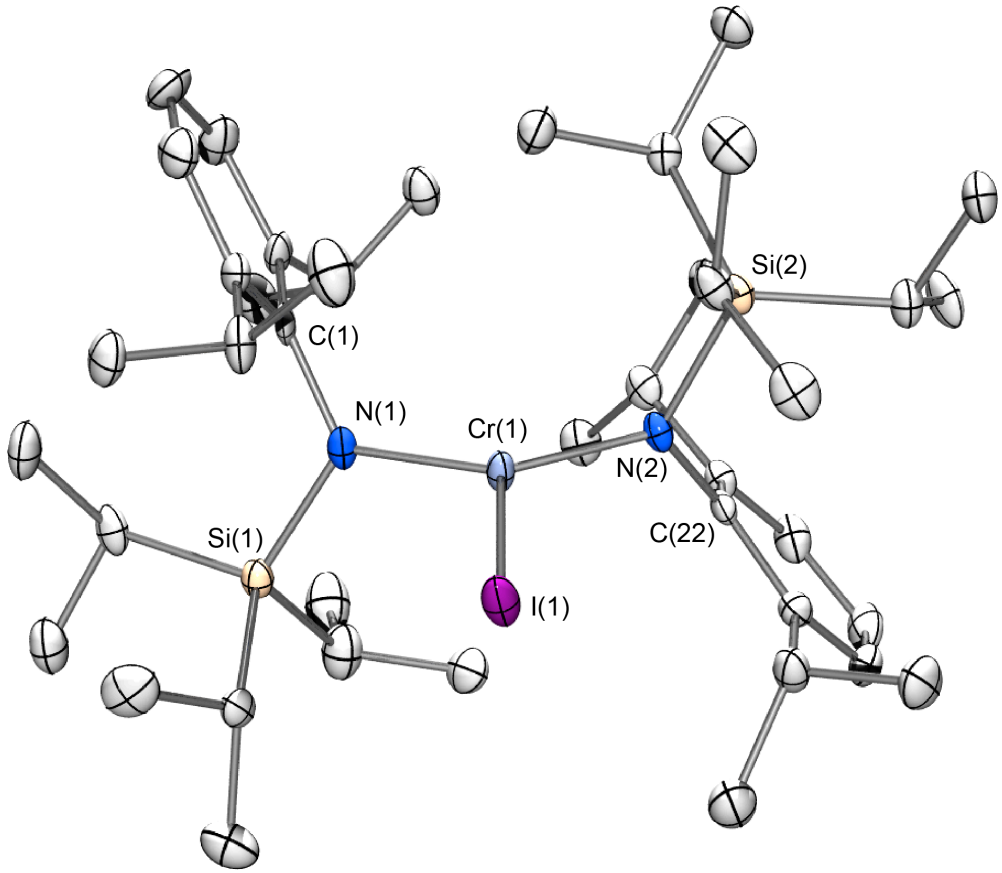

ORTEP diagram of (I)Cr[N(Si^{i}Pr$_3$)DIPP]$_2$ (**4**). Hydrogen atoms have been omitted for clarity. Thermal ellipsoids shown at 50% probability. Selected bond distances [Å], angles [°], and torsions [°]: Cr(1)–N(1): 1.906(4), Cr(1)–N(2): 1.889(4), Cr(1)–I(1): 2.5929(8), C(1)–N(1): 1.457(6), C(22)–N(2): 1.465(6), N(1)–Si(1): 1.808(4), N(2)–Si(2): 1.815(4), Cr(1)–C(1): 2.924(5), Cr(1)–C(22): 2.965(5), N(1)–Cr(1)–N(2): 139.49(17), N(1)–Cr(1)–I(1): 110.31(12), N(2)–Cr(1)–I(1): 110.19(12), C(1)–N(1)–Cr(1): 120.2(3), C(22)–N(2)–Cr(1): 123.8(3), Si(1)–N(1)–Cr(1): 121.2(2), Si(2)–N(2)–Cr(1): 120.1(2), C(1)–N(1)–N(2)–C(22): ±136.5(4).

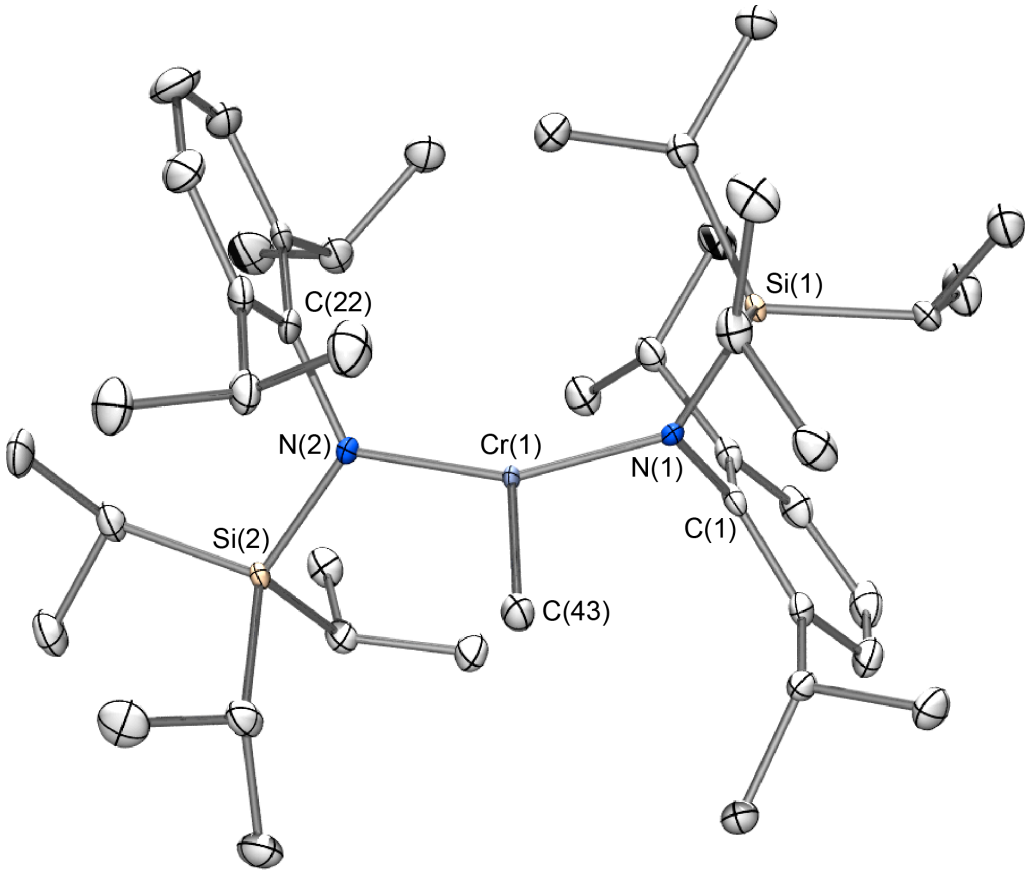

ORTEP diagram of (Me)Cr[N(Si^{i}Pr$_3$)DIPP]$_2$ (**5**). Hydrogen atoms have been omitted for clarity. Disordered chromium and silicon atoms have been excluded. Thermal ellipsoids shown at 50% probability. Selected bond distances [Å], angles [°], and torsions [°]: Cr(1)–N(1): 1.893(2), Cr(1)–N(2): 1.906(2), Cr(1)–C(43): 2.058(3), C(1)–N(1): 1.458(4), C(22)–N(2): 1.460(4), N(1)–Si(1): 1.793(3), N(2)–Si(2): 1.783(3), Cr(1)–C(1): 2.949(3), Cr(1)–C(22): 2.905(3), N(1)–Cr(1)–N(2): 142.89(11), N(1)–Cr(1)–C(43): 107.92(12), N(2)–Cr(1)–C(43): 109.14(12), C(1)–N(1)–Cr(1): 122.71(19), C(22)–N(2)–Cr(1): 118.75(19), Si(1)–N(1)–Cr(1): 120.45(14), Si(2)–N(2)–Cr(1): 121.61(13), C(1)–N(1)–N(2)–C(22): ±138.2(2).

Compound **1**:

Empirical formula	C42 H76 Cr N2 Si2
Formula weight	717.23
Temperature	100(2) K
Wavelength	0.71073 Å
Crystal system	Triclinic
Space group	P-1
Unit cell dimensions	a = 10.6605(3) Å α = 98.9810(10)°. b = 10.8266(3) Å β = 104.6850(10)°. c = 11.4767(3) Å γ = 118.9100(10)°.
Volume	1059.18(5) $Å^3$
Z	1
Density (calculated)	1.124 Mg/m^3
Absorption coefficient	0.356 mm^{-1}
F(000)	394
Crystal size	0.09 x 0.09 x 0.06 mm^3
Theta range for data collection	1.94 to 31.24°.
Index ranges	-13<=h<=15, -15<=k<=13, -14<=l<=16
Reflections collected	24671
Independent reflections	5882 [R(int) = 0.0420]
Completeness to theta = 25.00°	99.4 %
Absorption correction	Semi-empirical from equivalents
Max. and min. transmission	0.9790 and 0.9687
Refinement method	Full-matrix least-squares on F^2
Data / restraints / parameters	5882 / 0 / 224
Goodness-of-fit on F^2	1.021
Final R indices [I>2sigma(I)]	R1 = 0.0405, wR2 = 0.0852
R indices (all data)	R1 = 0.0675, wR2 = 0.0950
Largest diff. peak and hole	0.365 and -0.302 $e.Å^{-3}$

Compound **2a**:

Empirical formula	C58 H116 Cr K N2 O8 Si2
Formula weight	1116.81
Temperature	100(2) K
Wavelength	0.71073 Å
Crystal system	Orthorhombic
Space group	P2(1)2(1)2(1)
Unit cell dimensions	a = 15.8187(7) Å a= 90°. b = 17.0756(8) Å b= 90°. c = 25.0015(13) Å g = 90°.
Volume	6753.2(6) $Å^3$
Z	4
Density (calculated)	1.098 Mg/m^3

Absorption coefficient	0.313 mm^{-1}
F(000)	2452
Crystal size	0.11 x 0.10 x 0.01 mm^3
Theta range for data collection	1.44 to 30.70°.
Index ranges	-10<=h<=22, -19<=k<=22, -31<=l<=32
Reflections collected	54941
Independent reflections	16443 [R(int) = 0.0409]
Completeness to theta = 25.00°	100.0 %
Absorption correction	Semi-empirical from equivalents
Max. and min. transmission	0.9969 and 0.9664
Refinement method	Full-matrix least-squares on F^2
Data / restraints / parameters	16443 / 158 / 677
Goodness-of-fit on F^2	1.037
Final R indices [I>2sigma(I)]	R1 = 0.0729, wR2 = 0.1814
R indices (all data)	R1 = 0.0961, wR2 = 0.1995
Absolute structure parameter	0.00
Largest diff. peak and hole	1.261 and -0.615 e.$Å^{-3}$

Compound **2b**:

Empirical formula	C58 H112 Cr N3 Si2
Formula weight	959.68
Temperature	100(2) K
Wavelength	0.71073 Å
Crystal system	Monoclinic
Space group	P 21/n
Unit cell dimensions	a = 14.7215(4) Å α = 90°. b = 28.4194(8) Å β = 90.949(2)°. c = 14.8687(4) Å γ = 90°.
Volume	6219.9(3) $Å^3$
Z	4
Density (calculated)	1.025 Mg/m^3
Absorption coefficient	0.257 mm^{-1}
F(000)	2132
Crystal size	0.100 x 0.100 x 0.040 mm^3
Theta range for data collection	1.558 to 25.376°.
Index ranges	-17<=h<=17, -30<=k<=34, -17<=l<=17
Reflections collected	36473
Independent reflections	11368 [R(int) = 0.0567]
Completeness to theta = 25.000°	99.8 %
Absorption correction	Semi-empirical from equivalents
Max. and min. transmission	0.942 and 0.828
Refinement method	Full-matrix least-squares on F^2
Data / restraints / parameters	11368 / 0 / 601
Goodness-of-fit on F^2	1.013

Final R indices [I>2sigma(I)]	R1 = 0.0574, wR2 = 0.1120
R indices (all data)	R1 = 0.1036, wR2 = 0.1308
Extinction coefficient	n/a
Largest diff. peak and hole	1.353 and -0.480 e.Å^{-3}

Compound **3**:

Empirical formula	C69 H77 B Cr F21 N2 Si2
Formula weight	1452.32
Temperature	100(2) K
Wavelength	0.71073 Å
Crystal system, space group	Triclinic
Space group	P-1
Unit cell dimensions	a = 13.4838(8) Å α = 67.150(3) deg. b = 15.8748(9) Å β = 89.637(3) deg. c = 18.4544(10) Å γ = 69.398(3) deg.
Volume	3368.3(3) Å^3
Z	2
Calculated density	1.432 Mg/m^3
Absorption coefficient	0.307 mm^{-1}
F(000)	1502
Crystal size	0.13 x 0.06 x 0.02 mm
Theta range for data collection	1.49 to 25.45 deg.
Limiting indices	-16<=h<=15, -19<=k<=19, -22<=l<=22
Reflections collected / unique	55268 / 12395 [R(int) = 0.0321]
Completeness to theta = 25.00	100.0 %
Absorption correction	Semi-empirical from equivalents
Max. and min. transmission	0.9939 and 0.9612
Refinement method	Full-matrix least-squares on F^2
Data / restraints / parameters	12395 / 0 / 897
Goodness-of-fit on F^2	1.032
Final R indices [I>2sigma(I)]	R1 = 0.0494, wR2 = 0.1204
R indices (all data)	R1 = 0.0600, wR2 = 0.1282
Largest diff. peak and hole	2.339 and -0.829 e.Å^{-3}

Compound **4**

Empirical formula	C42 H76 Cr I N2 Si2
Formula weight	844.13
Temperature	100(2) K
Wavelength	0.71073 Å
Crystal system	Monoclinic
Space group	P2(1)/c
Unit cell dimensions	a = 11.0285(5) Å α= 90°.

	b = 23.0870(10) Å β= 90.515(3)°.
	c = 17.0353(7) Å γ = 90°.
Volume	4337.3(3) $Å^3$
Z	4
Density (calculated)	1.293 Mg/m^3
Absorption coefficient	1.061 mm^{-1}
F(000)	1788
Crystal size	0.04 x 0.03 x 0.01 mm^3
Theta range for data collection	1.76 to 25.43°.
Index ranges	-13<=h<=13, 0<=k<=27, 0<=l<=20
Reflections collected	7912
Independent reflections	7912 [R(int) = 0.0808]
Completeness to theta = 25.00°	99.1 %
Absorption correction	Semi-empirical from equivalents
Max. and min. transmission	0.9895 and 0.9588
Refinement method	Full-matrix least-squares on F^2
Data / restraints / parameters	7912 / 0 / 453
Goodness-of-fit on F^2	1.050
Final R indices [I>2sigma(I)]	R1 = 0.0523, wR2 = 0.0978
R indices (all data)	R1 = 0.0854, wR2 = 0.1047
Largest diff. peak and hole	0.977 and -0.583 $e.Å^{-3}$

Compound **5**

Empirical formula	C43 H79 Cr N2 Si2
Formula weight	732.26
Temperature	100(2) K
Wavelength	0.71073 Å
Crystal system	Monoclinic
Space group	P2(1)/c
Unit cell dimensions	a = 11.0453(7) Å a= 90°.
	b = 23.1010(16) Å b= 90.156(3)°.
	c = 16.8139(10) Å g = 90°.
Volume	4290.2(5) $Å^3$
Z	4
Density (calculated)	1.134 Mg/m^3
Absorption coefficient	0.353 mm^{-1}
F(000)	1612
Crystal size	0.09 x 0.09 x 0.02 mm^3
Theta range for data collection	1.50 to 25.41°.
Index ranges	-13<=h<=13, -27<=k<=27, -20<=l<=20
Reflections collected	47476
Independent reflections	7802 [R(int) = 0.0811]
Completeness to theta = 25.00°	99.4 %
Absorption correction	Semi-empirical from equivalents

Max. and min. transmission	0.9930 and 0.9689
Refinement method	Full-matrix least-squares on F^2
Data / restraints / parameters	7802 / 0 / 468
Goodness-of-fit on F^2	1.067
Final R indices [I>2sigma(I)]	R1 = 0.0515, wR2 = 0.1176
R indices (all data)	R1 = 0.0607, wR2 = 0.1222
Largest diff. peak and hole	0.517 and -0.375 e.$Å^{-3}$

Chapter 6. Synthesis, Characterization and Alkyne Trimerization Catalysis of a Heteroleptic Two-Coordinate Fe^{I} Complex

INTRODUCTION

Two-coordinate transition metal complexes have attracted considerable interest due to their novel structural and electronic properties.[1] In particular, previous investigations have focused on the structural consequences of two-coordination, and the potential of these complexes as single molecule magnets.[1,2] More recently, studies on their reactivity have revealed a number of noteworthy transformations.[3] Because such species are almost exclusively associated with earth-abundant first row metals, the potential of these compounds to serve as inexpensive, active catalysts for important reactions is of particular interest.[4] This possibility is supported by recent reports of two-coordinate complexes as catalysts for olefin hydrosilylation,[5] carbon-carbon cross-coupling[6] and dinitrogen reduction.[7] Progress in this area has inspired the development of new ligand frameworks and synthetic methods to widen the scope of available compounds and explore the effect of different ligands and oxidation states on chemical reactivity.[8,9,10]

With few exceptions, open-shell two-coordinate compounds have been limited to homoleptic complexes in either the M^{II} or, less commonly, the M^0 oxidation state.[1] Complexes in the M^I or M^{III} oxidation states are very rare and are occasionally synthesized *via* reduction of M^{II} or oxidation of M^0 complexes.[2a,3a,9] Recently, a general method for the preparation of two-coordinate Ni^I complexes was reported.[10] Since numerous such complexes are known, their properties and reactivity are the most thoroughly investigated for M^I compounds.[11] However, little is known about monovalent, two-coordinate complexes of other metals because general methods for their preparation have not been established.

Though only a handful of two-coordinate Fe^I species are known, they have attracted a great deal of attention.[2a,9b,12] Such Fe^I complexes have been shown to possess exceptional magnetic blocking behavior[2a,13] and one such complex was recently reported to be catalytically active for N_2 reduction.[7] All known two-coordinate Fe^I complexes are homoleptic and have been derived from reduction of Fe^{II} derivatives,[2a,9b,12c] resulting in $[FeX_2]^-$ species, or by oxidation of an Fe^0 complex to a $[FeL_2]^+$ species.[12a,12b] No heteroleptic two-coordinate Fe^I complexes have been reported and the chemistry and catalytic activity of such compounds are unexplored. Given our success in preparing unsymmetrical two-coordinate Ni^I complexes of the L–Ni–X type, we sought to develop an analogous route to the corresponding Fe^I derivatives. Herein, we report the synthesis, physical properties and catalytic activity of the first heteroleptic, two-coordinate Fe^I complex IPr–Fe–N(SiMe$_3$)DIPP (**1**; IPr = 1,3-bis(2,6-diisopropylphenyl)imidazol-2-ylidene; DIPP = 2,6-^{i}Pr$_2$-C$_6$H$_3$).

RESULTS AND DISCUSSION

Synthesis of heteroleptic two-coordinate Fe^I complexes. Recently, this laboratory described a general synthetic method for the preparation of neutral two-coordinate Ni^I complexes of the type L – Ni – N(SiMe$_3$)DIPP, from the easily prepared Ni^I bis(amido) complex K{Ni[N(SiMe$_3$)DIPP]$_2$} (**2**).[10] Protonation of **2** with a weak acid in the presence of various bulky L-donors results in loss of HN(SiMe$_3$)DIPP and trapping of the resulting Ni^I fragment by L to give a neutral, heteroleptic, two-coordinate Ni^I complex. This methodology seemed applicable to the synthesis of related Fe^I complexes, especially given Power's contemporaneous report of an anionic Fe^I bis(amido) complex analogous to **2**, [K(18-crown-6)]{Fe[N(SiMe$_3$)DIPP]$_2$} (**3**).[9b] However, treatment of **3** with NEt$_3$·HCl in Et$_2$O at -30 °C in the presence of 1 equiv of IPr resulted only in formation of the Fe^{II} complex Fe[N(SiMe$_3$)DIPP]$_2$ (**4**), which was observed by

^{1}H NMR spectroscopy (due to the paramagnetism of **4**, a yield could not be accurately determined). Thus, in this system protonation of the iron complex leads to oxidation of **3** to **4** and formation of H_2 (by ^{1}H NMR spectroscopy), rather than elimination of HN(SiMe$_3$)DIPP. Development of a different synthetic route to neutral, two-coordinate Fe^{I} complexes was therefore required.

The successful strategy outlined in Scheme 1 is based on a one-pot reaction sequence involving protonation, ligand substitution, and then reduction, rather than the reduction, protonation, and ligand substitution order employed for nickel. Compound **4** was treated with 1 equiv of NEt$_3$•HCl at ambient temperature, followed by addition of a THF solution of IPr and then addition of 1.1 equiv of KC_8. Workup and recrystallization from toluene/hexamethyldisiloxane gave **1** in 77% overall yield as thin red plates, which desolvate under vacuum. Compound **1** is indefinitely stable in the solid state at ambient temperatures and shows no signs of decomposition after several months (by ^{1}H NMR spectroscopy).

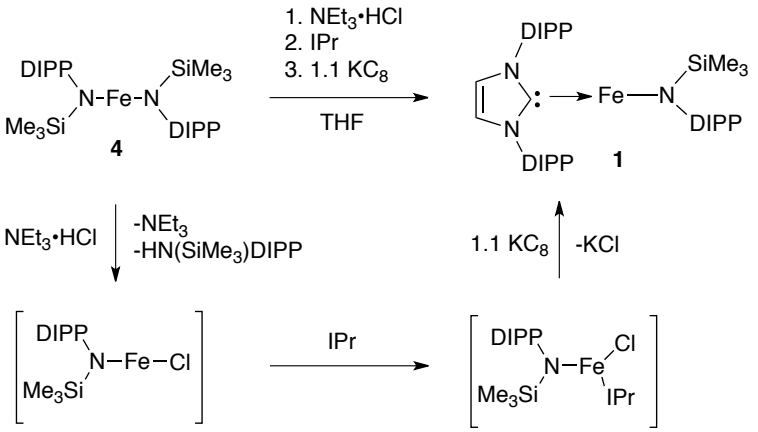

Scheme 1. Synthesis of compound **1**.

Efforts to isolate the presumed intermediates in this reaction, ClFe[N(SiMe$_3$)DIPP] (probably dimeric) and (IPr)ClFe[N(SiMe$_3$)DIPP], led only to mixtures thought to contain these compounds. After addition of NEt$_3$•HCl to **4** in benzene-d_6, analysis of the reaction mixture by ^{1}H NMR spectroscopy indicated the complete consumption of **4**, and the presence of HN(SiMe$_3$)DIPP as well as a new paramagnetic compound, presumed to be ClFe[N(SiMe$_3$)DIPP] (see Appendix). After 22 h, a tan precipitate (presumably $FeCl_2$) was observed and the NMR spectrum revealed the regeneration of **4**, along with the previously observed HN(SiMe$_3$)DIPP and the same new, paramagnetic product. Attempts to isolate ClFe[N(SiMe$_3$)DIPP] resulted only in mixtures containing the new iron complex and **4**. These observations suggest that in solution, ClFe[N(SiMe$_3$)DIPP] disproportionates to **4** and $FeCl_2$ (Scheme 2).

Attempts to isolate (IPr)ClFe[N(SiMe$_3$)DIPP] were based on the reaction of **4** with NEt$_3$•HCl, followed by IPr in THF. Workup of the reaction mixture gave mixtures of **4**, the putative (IPr)ClFe[N(SiMe$_3$)DIPP], free IPr, and [(IPr)$FeCl_2$]$_2$ (identified by its previously reported ^{1}H NMR spectrum).[14] From this reaction mixture, crystals of (IPr)ClFe[N(SiMe$_3$)DIPP] were obtained from a toluene-pentane solvent mixture. This complex was characterized by single crystal X-ray diffraction (see Appendix). These observations suggest that (IPr)ClFe[N(SiMe$_3$)DIPP] disproportionates in solution to the mixture of compounds shown in

Scheme 2.

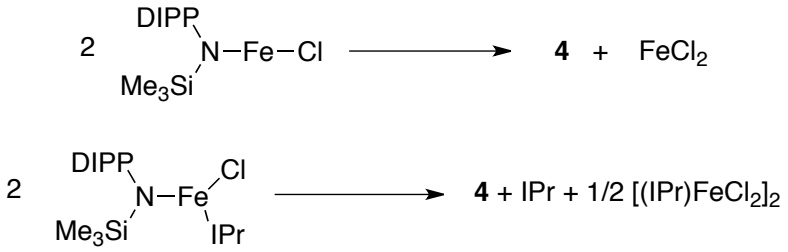

Scheme 2. Proposed disproportional decomposition pathways of synthetic intermediates for compound **1**.

Reduction of 1 to an Fe(0) complex. Reports from this laboratory and others have shown that two-coordinate M^{II} bis(amido) complexes of Cr, Fe, Co and Ni are redox active, such that corresponding anionic (M^{I}) and cationic (M^{III}) analogues are accessible and isolable.[3a,9] Given the generality of this chemical property, over a variety of metals and *d*-electron counts, it was of interest to explore the redox properties of the two-coordinate, neutral Fe^{I} complex **1**.

Treatment of **1** with 1.5 equivs of potassium graphite in Et_2O gave dark red, needle-shaped crystals of paramagnetic K{(η^6-IPr)Fe-N(SiMe$_3$)DIPP] (**5**) in 87% yield after subsequent workup and recrystallization (Scheme 3). Analysis of **5** by single crystal X-ray diffraction (*vide infra*) revealed that the complex results from an unexpected ligand rearrangement in which the IPr ligand is no longer bound *via* the carbenyl carbon. Instead, IPr serves as a p-bonded ligand *via* η^6-coordination of a DIPP substituent to the Fe center. This redox-induced ligand rearrangement, and the unusual structure of this complex, present interesting questions regarding the electronic structure and oxidation state of **5**. For this reason, compounds **1** and **5** were studied by ^{57}Fe Mössbauer spectroscopy.

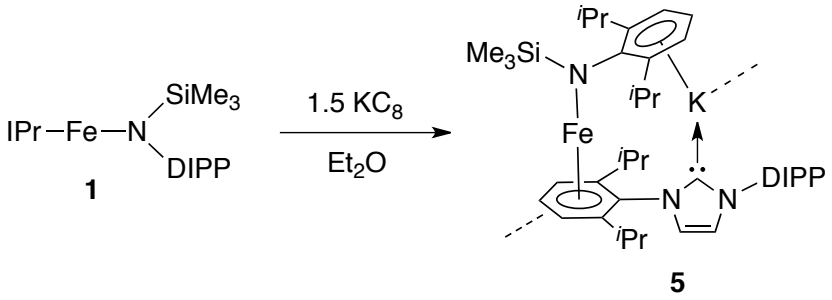

Scheme 3. Reduction of **1** to **5**. Dashed lines indicate intermolecular bonding in the solid state.

Mössbauer Spectroscopy of 1 and 5. The ^{57}Fe Mössbauer spectrum of compound **1** displays a sextet pattern, with an isomer shift of δ = 0.387 mm/s and quadrupole splitting of ΔE_q = -2.253 mm/s at 5 K (Figure 1). This spectrum closely resembles that of [K(crypt-222)]{Fe[C(SiMe$_3$)$_3$]$_2$},[2a,13] which also displays a sextet spectrum with similar parameters (δ = 0.410 mm/s, ΔE_q = −2.557 mm/s). However, this spectrum differs substantially from that of [(CAAC)$_2$Fe][BAr$^F_{24}$],[12c] which displays a doublet at 5 K. This difference in Mössbauer spectra for the latter two complexes was attributed to the bond angles at iron, since the coordination geometry for [K(crypt-222)]{Fe[C(SiMe$_3$)$_3$]$_2$} is essentially linear (bond angle of 179°)[2a] while

$[(CAAC)_2Fe][BAr^F{}_{24}]$, is bent with a C–Fe–C bond angle of approximately 165°.[12c] This is consistent with the observations for **1**, which possesses a C–Fe–N bond angle of 176.94(6)°.

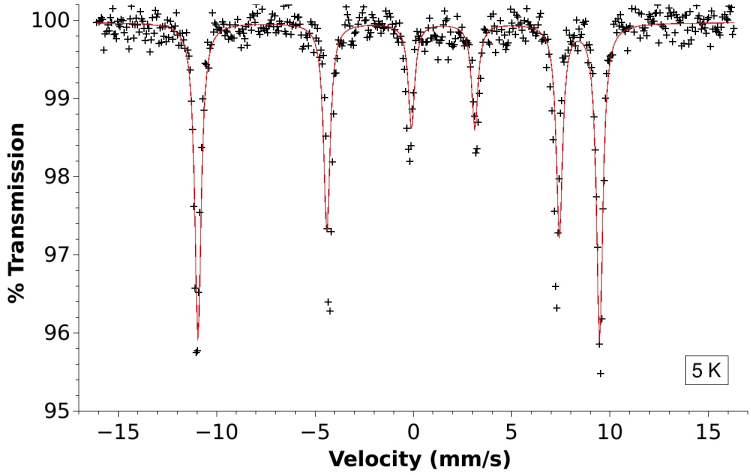

Figure 1. Zero-field ^{57}Fe Mössbauer spectrum of compound **1** acquired at 5 K. The red line corresponds to a least-square fit with an isomer shift of $\delta = 0.387$ mm/s, and quadrupole splitting of $\Delta E_q = -2.253$ mm/s.

Unlike **1**, compound **5** displays a Mössbauer spectrum that features a doublet at 5 K with a markedly different isomer shift of $\delta = 0.812$ mm/s, indicating substantially higher electron density at the metal center and suggesting a reduction at Fe rather than reduction of the ligand (Figure 2). This significant increase in the isomer shift parameter suggests that the oxidation state of Fe in **5** is zero.

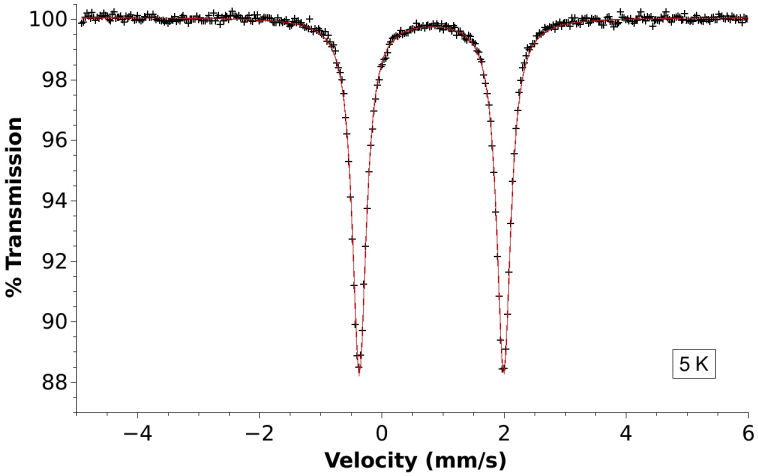

Figure 2. Zero-field ^{57}Fe Mössbauer spectrum of compound **5** acquired at at 5 K. The red line corresponds to a least-square fit with an isomer shift of $\delta = 0.812$ mm/s and a quadrupole splitting of $\Delta E_q = 2.364$ mm/s.

Solution Magnetic Properties of 1 and 5. The differences in Mössbauer parameters mentioned above, and their correlation with coordination geometry, is consistent with reported

magnetic properties for two-coordinate Fe^{I} complexes. The bent complex $[(CAAC)_2Fe][BAr^{F}_{24}]$ has a magnetic moment of 4.3 μ_B, which is modestly higher than the spin-only value of 3.87 μ_B (by the Evans method[21]) expected for an S = 3/2 complex, reflecting some degree of magnetic anisotropy due to spin-orbit coupling. In comparison, the linear complexes [K(crypt-222)]{$Fe[C(SiMe_3)_3]_2$} (179°) and [K(18-crown-6)]{$Fe[N(SiMe_3)_2]_2$} (180°) exhibit magnetic moments of 5.2 and 5.12 μ_B, respectively, indicating stronger spin-orbit coupling interactions.[2a,12a]

Compound **1** follows the trend of linearity leading to higher anisotropy, with a magnetic moment of 4.97 μ_B. To help gauge the importance of a two-coordinate ligand field to the observed magnetic anisotropy, a simple, three-coordinate isocyanide adduct of **1**, IPr–Fe(XylNC)–$N(SiMe_3)$DIPP (**6**), was prepared (see Experimental Section). Analysis of **6** by Evans's method shows that the additional ligand diminishes the spin-orbit coupling, resulting in a markedly lower magnetic moment of 4.06 μ_B which is close to the spin-only value of 3.87 μ_B.

Analysis of **5** by Evans's method led to the observation of magnetic anisotropy in a non-two-coordinate compound, with an observed moment of 3.94 μ_B. This value is lower than that for **1**, which is consistent with additional pairing of electrons, but substantially higher than the spin-only value of 2.83 μ_B expected for an S = 1 ion. Since compound **5** is not two-coordinate, the origin of its increased magnetic moment is currently unclear.

Structural Properties. The X-ray crystal structures of compounds **1**, **5** and **6** are shown in Figures 3-5. Two-coordinate **1** possesses a linear geometry with a N–Fe–C_{NHC} bond angle of 176.94(6)°. The Fe–N and Fe–C_{NHC} bond lengths of 1.890(2) and 2.014(2) Å are unremarkable and similar to the values reported for related Fe^{I} compounds reported in the literature.[9b,12b,12c]

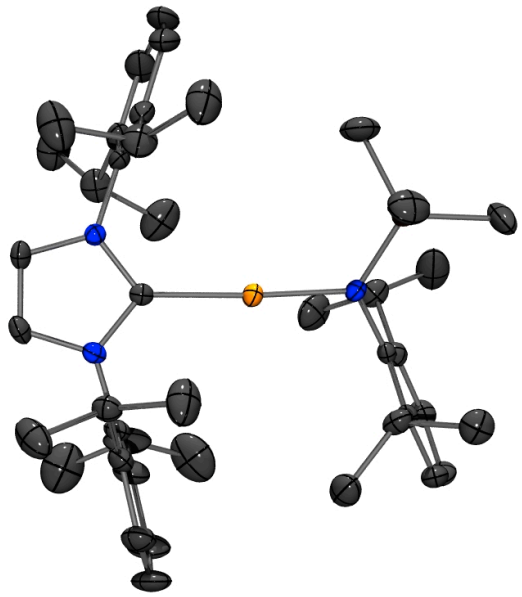

Figure 3. ORTEP diagram of **1**. Thermal ellipsoids shown at 50% probability. Carbon atoms are shown in dark grey, nitrogen in blue, iron in orange and silicon in red. Selected bond lengths (Å) and angles (deg): Fe–N, 1.890(2); Fe–C, 2.014(2); N–Fe–C, 176.94(6).

Reduction to Fe^{0} results in lengthening of the Fe–N bond in **5** to 1.962(2) Å. The

reorganization of the IPr ligand in **5** results in an interaction between the carbenyl carbon of IPr and the potassium ion, with a C–K distance of 2.877(3) Å. This is similar to the C–K bond lengths reported for the $[IPr–K–IPr]^+$ ion,[15] suggesting that there is a bonding interaction between the potassium ion and the carbenyl carbon. The new η^6-interaction between the Fe center and the DIPP moiety of the IPr ligand results in notable lengthening of the C–C bonds within the ring as compared to the unbound DIPP moiety (1.423 Å av. vs. 1.388 Å av., respectively). This degree of bond lengthening is on par with that observed in other examples of Fe^0–aryl complexes, and is attributable to π-back-bonding from the electron-rich Fe center to the aryl ring.[16]

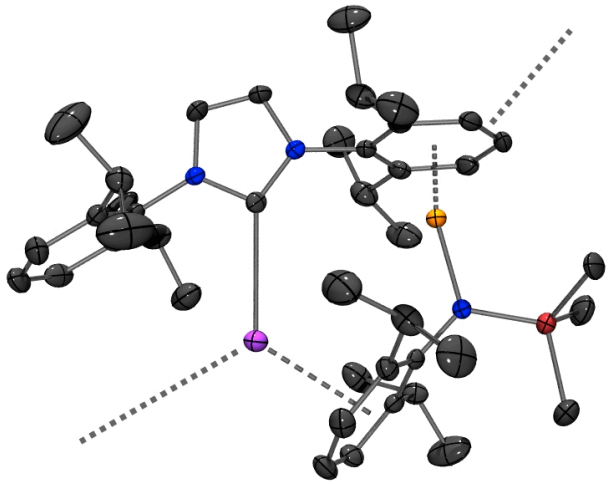

Figure 4. ORTEP diagram of **5**. Thermal ellipsoids shown at 50% probability. Carbon atoms are shown in dark grey, nitrogen in blue, iron in orange, potassium in purple and silicon in red. Selected bond lengths (Å): Fe–N, 1.962(2); C–K, 2.877(3).

Addition of the XylNC ligand to the coordination sphere of Fe results in an approximately trigonal planar geometry in **6**, accompanied by the expected lengthening of the Fe–N (1.933(2) Å) and Fe–C_{NHC} (2.076(2) Å) bonds due to steric crowding. The C–N–C bond angle of the XylNC ligand is somewhat bent at nitrogen (160.8(2)°), with a slightly lengthened N-C triple bond of 1.192(2) Å (vs. 1.160 Å in the unbound molecule[17]), reflecting π-donation from the Fe center.

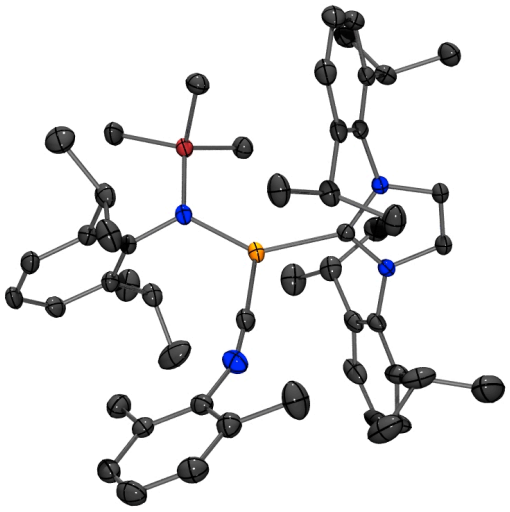

Figure 5. ORTEP diagram of **6**. Thermal ellipsoids shown at 50% probability. Carbon atoms are shown in dark grey, nitrogen in blue, iron in orange, and silicon in red. Selected bond lengths (Å) and angles (deg): Fe–N, 1.933(2); Fe–C_{NHC}, 2.076(2); Fe–C_{XylNC}, 1.856(2); XylN–C, 1.192(2); C_{Ar}–N–C, 160.8(2).

Catalytic Cyclotrimerization of Alkynes. Recent studies on the chemistry of two-coordinate, first-row metal complexes of Ni[3a] and Fe[12a] show that these compounds are capable of two-electron substrate activations mediated by a M^{I} to M^{III} oxidation state change. Such redox processes are generally thought to be difficult for first-row transition metal complexes, but are associated with key steps in many important catalytic cycles involving second- and third-row metals. Thus, an important goal for development of catalysts based on more abundant metals is to establish useful, two-electron reaction steps for these metals. For this reason, it was of interest to examine the efficacy of **1** as a catalyst for reactions in which formal two-electron redox processes are presumed to play a key role.

The cyclotrimerization of alkynes is an efficient and atom-economical method for the preparation of functionalized arenes. Such trimerization reactions are thought to proceed via a metalocyclopentadiene intermediate, the formation of which involves a formal two-electron oxidation of the metal center to form a new C-C bond (Scheme 4).[18] Similar reactions can also be used to produce unsymmetrical arenes, aromatic heterocycles and many other cyclic structures.[19] While known catalysts for this reaction are based on rhodium and cobalt, examples of catalysis by iron are rare.[20] The potential for two-coordinate compounds to mediate two-electron redox processes, and the dearth of examples of iron catalysts for this reaction type, prompted an examination of **1** as a catalyst for the cyclotrimerization of alkynes.

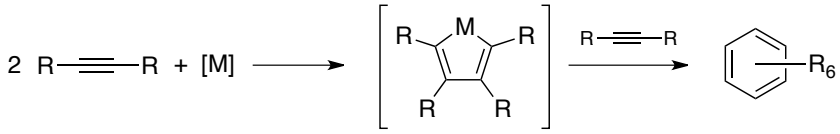

Scheme 4. Mechanism for alkyne trimerization.

Complex **1** is competent as a catalyst for cyclotrimerizations at fairly low loadings and under mild conditions (Scheme 5). Reaction of **1** with 50 equivs of 2-butyne in benzene-d_6 over 3 hours at ambient temperature resulted in the quantitative formation of hexamethylbenzene (by ^{1}H NMR spectroscopy). The trimerization of 20 equivs of 1-phenyl-1-proyne resulted in complete conversion of the starting material over 6 h, and a mixture of the 1,3,5- and 1,2,4-substituted trimethyltriphenylbenzenes in 31 and 69% yields, respectively. Compound **1** was also found to catalyze the trimerization of a terminal alkyne, in the conversion of 50 equiv of 3-methyl-1-butyne to 1,3,5-triisopropylbenzene (80%) and 1,2,4-triisopropylbenzene (10%), over 2 h. Accompanying these trimerization products was a colorless, gummy precipitate that was found to be insoluble in benzene, THF and DMSO. Due to the insolubility of this substance, we tentatively suggest that it is derived from polymerization of 3-methyl-1-butyne.

In an effort to further understand the role of **1** in the catalytic cycle, particularly as an on-cycle intermediate or a precatalyst, the post-catalytic reaction mixture was examined. At higher catalyst loadings in the trimerization of 2-butyne (10 mol %), by far the most prominent Fe-containing compound observed in the post catalytic mixture was **1**, with small quantities of other paramagnetic species also observed. Observation of the reaction mixture during catalysis indicates that all of **1** is initially consumed, and that the **1** observed in the post-catalytic reaction mixture is reformed from catalytically active intermediates. As the loading is lowered (5 mol % and 2 mol %), the amount of **1** observed in the post-catalytic mixture decreases and the amount of other paramagnetic species increases, suggesting some degree of decomposition of the catalyst. This decomposition is a greater factor in the catalysis of 1-phenyl-1-proyne and 3-methyl-1-butyne, where only small amounts of **1** are observed post-catalysis.

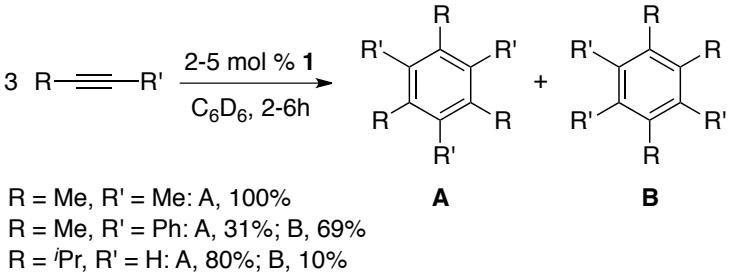

Scheme 5. Catalytic cyclotrimerization of various alkynes by compound **1**.

While trimerization reactions with simple alkyl- and aryl-substituted alkynes are efficient, substrates bearing bulky substituents or electron-withdrawing groups may be problematic. Thus, no reaction was observed between **1** and 50 equiv of bis(trimethylsilyl)acetylene in benzene-d_6 at 105 °C over 24 h. In addition, the exposure of **1** to 50 equiv of dimethylactylenedicarboxylate at ambient temperature over 24 hours resulted in the sole formation of a gummy precipitate which was found to be insoluble in benzene, THF and DMSO, and is presumably polymeric.

Despite the limited scope of the trimerization catalysis reported here, the two-coordinate Fe^{I} framework of **1** offers numerous opportunities for catalyst modification *via* exchanges of the L- and X-type ligands that support the Fe center. The methodology for the preparation of **1** may in principle be extended to other L-type ligands with different steric profiles and donor properties. The amido ligand could then be used as a handle for the introduction of different X-type ligands, as in the case of an analogous series of Ni^{I} complexes.[10] Attempts to introduce

different ligands in this manner and to fully explore reductive-coupling catalysis with **1** and its derivatives are currently underway.

CONCLUSION

The synthesis, spectroscopic properties, and catalytic activity of the rare two-coordinate Fe^{I} complex IPr–Fe–N($SiMe_3$)DIPP (**1**) have been described. This complex is the first example of a heteroleptic two-coordinate Fe^{I} complex as well as the first neutral example of such a complex. Like other two-coordinate complexes, **1** was found to be redox active, in accepting an electron to form the Fe^{0} complex K{(η^6-IPr)Fe–N($SiMe_3$)DIPP] (**5**). Compound **1** was also found to be a competent catalyst for the cyclotrimerization of both internal and terminal alkynes to form arenes at modest loadings under mild conditions. Exploration of the scope and mechanism of this reaction, as well as attempts to improve activity via ligand modification, are currently underway.

EXPERIMENTAL

General Considerations. Unless otherwise stated, all reactions and manipulations were carried out in a MBraun Lab Master DP glovebox or using standard Schlenk techniques under a nitrogen atmosphere. Pentane, toluene, and hexamethyldisiloxane were purchased from Sigma Aldrich. Diethyl ether was purchased from Honeywell and tetrahydrofuran was purchased from Macron Chemicals. Pentane, toluene, tetrahydrofuran and diethyl ether were dried and degassed using a JC Meyers Phoenix SDS solvent purification system. Hexamethyldisiloxane was dried by stirring over potassium metal for 2 days and degassed by four freeze-pump-thaw cycles. C_6D_6 was purchased from Cambridge Isotope Laboratories, dried over Na/K alloy and then degassed by four freeze-pump-thaw cycles. All NMR spectra were collected at ambient temperature (ca. 22°C) on Bruker AVB-400, AV-500, AV-600 or AVQ-400 NMR spectrometers, each equipped with a 5 mm BB probe, and referenced to the residual proteo solvent signals. Solution magnetic susceptibilities were determined by ^{1}H NMR spectroscopy using Evans's method.[21] Elemental analyses were performed by the UC Berkeley College of Chemistry Microanalytical facility. The abbreviation "DIPP" refers to a 2,6-diisopropylphenyl moiety. The abbreviation "IPr" refers to the N-heterocyclic carbene N,N'-1,3-bis(2,6-diisopropylphenyl)imidazol-2-ylidene. The abbreviation "HMDSO" refers to hexamethyldisiloxane. NEt_3•HCl was purchased from Sigma Aldrich and sublimed before use. Xylyl isocyanide was purchased from Sigma Aldrich and sublimed before use. $FeCl_2$ was purchased from Strem Chemical and used as received. Dimethylacetylenedicarboxylate was purchased from Sigma Aldrich and used as received. IPr,[22] LiN($SiMe_3$)DIPP,[23] and potassium graphite[24] were prepared according to standard literature procedures. Fe[N($SiMe_3$)DIPP]$_2$ was prepared using a modified procedure from the literature (detailed below).[25]

X-ray Diffraction Experiments. Single crystal X-ray diffraction experiments were carried out at UC Berkeley CHEXRAY crystallographic facility. Measurements of compounds **1**, **5**, **6** and (IPr)Cl-Fe[N($SiMe_3$)DIPP] were performed on a Bruker APEX-II CCD area detector. Measurements for **1**, **5** and (IPr)Cl-Fe[N($SiMe_3$)DIPP] used Mo Kα radiation (λ = 0.71073 Å) monochromated using QUAZAR multilayer mirrors. Measurements for **6** used Cu Kα radiation

(λ = 1.54178) monochromated using HELIOS multilayer mirrors. Specific details of each experiment can be found below, in section 3 at the end of this document and in the included crystallographic information files.

Experimental Details:

	Detector Distance	Image Width	Exposure Time
Compound **1**	40 mm	0.5°	20 s
Compound **5**	40 mm	0.5°	20 s
Compound **6**	60 mm	1.0°	5 s
(IPr)Cl-Fe[N($SiMe_3$)DIPP]	40 mm	0.5º	20 s

Mössbauer Spectroscopy. Zero-field, ^{57}Fe Mössbauer spectra were recorded in constant acceleration spectrometer (See Co Edina, MN) between room temperature and 5 K in a Janis Research Co. cryostat (Willmington, MA). Collected spectra were analyzed using the WMOSS software package (See Co., Medina, MN). Isomer shifts are reported relative to α-iron (27 μm foil) at room temperature. Samples were prepared by mixing Boron Nitride (BN) with finely ground crystalline samples of Fe complexes. Powder mixture was placed in nylon washer wrapped in Kapton® tape under inert atmosphere prior to introduction into the spectrometer in air.

Compound **1**: At 5 K, Mössbauer spectrum of Fe(I) exhibited a sextet pattern with isomer shift, δ, of 0.387 mm/s and quadrupole splitting, ΔEq, of -2.253 mm/s. The sextet pattern broadens at 50 K and collapses into a doublet at 75 K with δ of 0.417 mm/s and ΔEq of 0.888 mm/s. The non-ideal fit of the spectrum at 5 K may due to the non-linearity of the source motion outside the calibrated range. (Line 2 and 5 too wide and line 3 and 4 too narrow).

Compound **5**: The spectra of Fe(0) at variable temperature only show a doublet pattern. At 5 K, it has a δ of 0.812 mm/s and ΔEq of 2.364 mm/s. The increase in the value of isomer shift from 0.387 mm/s in **1** to 0.812 mm/s in **5** indicates reduction of the iron center. Comparing δ at 75 K (0.417 mm/s of **1** and 0.800 mm/s of **5)**, the more positive isomer shift indicates reduction at the iron center.

Catalytic Trimerization of Alkynes. Catalytic substrates where weighed in 20 mL scintillation vials along with a known quantity of $Si(SiMe_3)_4$, used as an internal standard. This mixture was dissolved in approx. 0.7 mL of d_6-benzene and to this solution was added a known quantity of catalyst. The whole solution was then transferred to a J-young NMR tube and monitored by ^{1}H NMR. In the case of 2-butyne, which is highly volatile, four drops were added to a d_6-benzene solution containing a known quantity of of $Si(SiMe_3)_4$ and the quantity of 2-butyne was determined by integration against the internal standard prior to the addition of catalyst. Yields were determined by integration of product peaks against the internal standard. The products of catalysis, hexamethylbenzene,[26] 1,2,4-trimethyl-3,5,6-triphenylbenzene,[27] 1,3,5-trimethyl-2,4,6-triphenylbenzene,[27] 1,3,5-triisopropylbenzene[27] and 1,2,4-triisopropylbenzene[27] were identified by comparison of their ^{1}H NMR spectra to values previously reported in the literature.

IPr–Fe–N(SiMe$_3$)DIPP (1). To a 20 mL scintillation vial was added Fe[N(SiMe$_3$)DIPP]$_2$ (**4**) (0.430 g, 0.78 mmol) and 4 mL of tetrahydrofuran (THF), to form a light yellow solution. To this stirred solution was added NEt$_3$•HCl (0.107 g, 0.78 mmol). Over the course of 10 min, the solution changed color from light yellow to tan and the NEt$_3$•HCl dissolved. To the stirred, tan solution was added a solution of IPr (0.30 g, 0.78 mmol) in 4 mL of THF, dropwise over the course of one minute, causing a color change from light tan to golden yellow. This yellow solution was stirred for an additional five min, then potassium graphite (0.116 g, 0.86 mmol, 1.1 equiv) was added, causing an immediate color change to dark red along with the formation of black graphite. The resulting mixture was stirred for 15 min, and then stirring was ceased and the mixture was allowed to settle. The mixture was then filtered through a pipette fitted with a glass fiber filter into a 20 mL scintillation vial, the red filtrate was placed under vacuum, and the volatile components of the mixture were removed under vacuum. The resulting red residue was washed with two portions of 2 mL of HMDSO and dried under vacuum. This residue was then dissolved in 8 mL of toluene and layered with 12 mL of HMDSO and placed in a -30 °C freezer for 12 h to yield 0.37 g (68%) of **1** as long, narrow, red plates which were isolated by decantation and dried under vacuum until fully desolvated, requiring approximately 2 h to reach constant mass. The supernatant was dried under vacuum and the residue was recrystallized and isolated in an identical fashion using 1.5 mL of toluene and 7 mL of HMDSO, yielding an additional 0.048 g of **1**, bringing the total yield to 0.414 (77%). Where possible, ^{1}H NMR shifts are assigned to specific protons by integration. ^{1}H NMR (500 MHz, C_6D_6, 20ºC) δ 89.01 (2H), 59.17 (2H), 46.48 (4H), 34.38 (2H), 29.77 (6H, amido-NAr-CH(C*H$_3$*)), 13.94 (1H, amido-N-*para*-Ar-*H*), 8.65 (12H, NHC-NAr-CH(C*H$_3$*)), -6.53 (9H, -Si(C*H$_3$*)$_3$), -14.73 (2H), -19.27 (4H), -75.37 (12H, NHC-NAr-CH(C*H$_3$*), overlapping with adjacent signal), -76.27 (6H, amido-NAr-CH(C*H$_3$*), overlapping with adjacent signal). μ_{eff} = 4.97 μ_B (C_6D_6, 20°C, Evans's method). Anal. Calcd. for $C_{42}H_{62}FeN_3Si$: C, 72.80%; H, 9.02%; N, 6.06%. Found: C, 72.55%; H, 8.78%; N, 6.16%. Crystals suitable for single crystal X-ray diffraction studies were obtained from the workup described above.

Fe[N(SiMe$_3$)DIPP]$_2$ (4). Modified synthetic procedure: to a 20 mL scintillation vial was added $FeCl_2$ (0.526 g, 4.15 mmol) and 4 mL of Et_2O to produce a suspension. To the stirred suspension at ambient temperature was added a solution of LiN(SiMe$_3$)DIPP (2.00 g, 7.86 mmol, 1.9 equiv) in 10 mL of Et_2O, causing the mixture to turn dark brown. The mixture was stirred for 16 h, and then the volatile components were removed under vacuum. Once visibly dry, the residue was dried under vacuum for 2 additional h, during which time the color of the residue changed from brown/tan to orange (note: this extra drying is essential for consistently preparing pure product). To the resulting residue was added 8 mL of pentane and the mixture was stirred for 15 min, allowed to settle, and was then filtered through a pipette equipped with a glass fiber filter into a 20 mL scintillation vial. The filtrate was placed in the -30 °C freezer for 12 h, yielding 1.44 g of **4** (66%) as red/orange crystals, which were isolated by decantation and dried under vacuum. The supernatant was dried under vacuum and the residue was recrystallized in an identical fashion using 2 mL of pentane to yield an additional 0.42 g of **4**, bringing the total yield to 1.86 g (85%). ^{1}H NMR (400 MHz, C_6D_6, 20ºC) δ 64.15, 51.33, 36.43, -54.92.

K[(η^6-IPr)Fe–N(SiMe$_3$)DIPP] (5). To a 20 mL scintillation vial was added **1** (0.200 g, 0.289 mmol) and 6 mL of Et_2O, to give a red solution. To the stirred solution was added potassium graphite (0.058 g, 0.43 mmol, 1.5 equiv), causing an immediate color change from red

to dark red/orange along with the formation of black graphite. The mixture was stirred for 30 min, then stirring was ceased and the mixture was allowed to settle. The mixture was then filtered through a pipette fitted with a glass fiber filter into a 20 mL scintillation vial and the volatile components were removed under vacuum. The resulting residue was dissolved in 5 mL of toluene and the solution was layered with 15 mL of pentane and placed in a -30 °C freezer for 12 h, yielding 0.142 g of **5** (68%) as long, dark red needle-shaped crystals which were isolated by decantation and dried under vacuum. The supernatant was dried under vacuum, and recrystallized and isolated in an identical fashion using 2 mL of toluene and 10 mL of pentane, yielding an additional 0.041 g of **5**, bringing the total yield to 0.183 g (87%). Note: compound **5** dissolves rather slowly in toluene, so several min of agitation are required to dissolve the residue for recrystallization. The ^{1}H NMR spectrum of **5** in benzene-d_6 varies greatly with concentration, which we attribute to the presence of various oligomers capped by benzene (see X-ray crystal structure for polymeric structure of **5**). μ_{eff} = 3.94 μ_B (C_6D_6, 20°C, Evans's method). Anal. Calcd. for $C_{42}H_{62}FeKN_3Si$: C, 68.91%; H, 8.54%; N, 5.74%. Found: C, 69.24%; H, 8.45%; N, 6.12%. Crystals suitable for single crystal X-ray diffraction studies were obtained from the workup described above.

IPr–Fe(CNXyl)–N(SiMe$_3$)DIPP (6). To a 20 mL scintillation vial was added **1** (0.108 g, 0.156 mmol) and 2 mL of Et_2O, to form a red solution. To this solution was added a solution of xylyl isocyanide (0.0205 g, 0.156 mmol) in 2 mL of Et_2O causing an immediate color change from red to very dark orange. The volatile components of the mixture were immediately removed under vacuum and the resulting residue was dissolved in 2 mL of Et_2O and layered with 8 mL of HMDSO. This mixture was placed in the -30 °C freezer for 12 h, yielding 0.104 g of **6** (81%) as dark orange crystals which were isolated by decantation and dried under vacuum. The ^{1}H NMR spectrum of **6** contains numerous broad and overlapping peaks from 4-7.25 ppm, so assigning shifts to individual peaks and integration of these peaks is not possible. All clearly visible characteristic peaks of **6**: ^{1}H NMR (500 MHz, C_6D_6, 20 °C) δ 63.57, 48.62, 28.07, 12.97, 8.54, 4.55, 3.05, -8.50, -24.05, -54.11. μ_{eff} = 4.06 μ_B (C_6D_6, 20°C, Evans's method). Anal. Calcd. for $C_{51}H_{71}FeN_4Si$: C, 74.33%; H, 8.68%; N, 6.80%. Found: C, 74.01%; H, 8.88%; N, 6.85%. Crystals suitable for single crystal X-ray diffraction studies were obtained from the workup described above.

ClFe[N(SiMe$_3$)DIPP]. To a 20 mL scintillation vial was added Fe[N(SiMe$_3$)DIPP]$_2$ (**4**) (0.014 g, 0.025 mmol), NEt_3•HCl (0.04 g, 0.029 mmol) and 1 mL of benzene-d_6, forming an orange/red solution. The mixture was allowed to stand for 30 min, during which the solution changed from orange/red to light orange and most of the NEt_3•HCl dissolved. The solution was transferred to a J-young NMR tube and analyzed by ^{1}H NMR spectroscopy, which revealed HN(SiMe$_3$)DIPP as well as a new paramagnetic compound, presumed to be ClFe[N(SiMe$_3$)DIPP] (NMR shifts reported below). After 22 h, a tan precipitate (presumably $FeCl_2$) was observed and the NMR spectrum revealed the regeneration of **4**, along with the previously observed HN(SiMe$_3$)DIPP and the previously observed paramagnetic shifts assigned to ClFe[N(SiMe$_3$)DIPP]. ^{1}H NMR (500 MHz, C_6D_6, 20ºC) δ 58.24, 28.89, -6.60, -45.98, -56.91.

(IPr)Cl-Fe[N(SiMe$_3$)DIPP]. To a 20 mL scintillation vial was added Fe[N(SiMe$_3$)DIPP]$_2$ (**4**) (0.430 g, 0.778 mmol) and 4 mL of tetrahydrofuran (THF), forming a light yellow solution. To this stirring solution was added NEt_3•HCl (0.107 g, 0.777 mmol). Over

the course of 10 min, the solution changed color from light yellow to tan and the NEt_3•HCl went into solution. To this stirring, tan solution was added a solution of IPr (0.303 g, 0.780 mmol) in 4 mL of THF, dropwise, over the course of one minute, causing a color change from light tan to golden yellow. This yellow solution was stirred for an additional five min, then the volatile components were removed under vacuum. Analysis of the resulting residue by ^{1}H NMR revealed a mixture of **4**, free IPr, (IPr)$FeCl_2$, and additional shifts assigned to (IPr)Cl-Fe[N($SiMe_3$)DIPP]. The residue was dissolved in 4 mL of toluene, layered with 8 mL of pentane and placed in the -30ºC freezer overnight, yielding crystals of **4**, (IPr)$FeCl_2$, and (IPr)Cl-Fe[N($SiMe_3$)DIPP]. Crystals of (IPr)Cl-Fe[N($SiMe_3$)DIPP] suitable for X-ray diffraction studies were obtained from this mixture of crystals. ^{1}H NMR (500 MHz, C_6D_6, 20ºC) δ 61.80, 25.94, 20.84, 3.00, -8.29, -14.23, -18.61, -19.36, -31.69, -57.98.

REFERENCES

(1) Power, P. P. *Chem. Rev.* **2012**, *112*, 3482.
(2) (a) Zadrozny, J. M.; Xiao, D. J.; Atanasov, M.; Long, G. J.; Grandjean, F.; Neese, F.; Long, J. R. *Nat. Chem.* **2013**, *5*, 577. (b) Boynton, J. N.; Guo, J.-D.; Fettinger, J. C.; Melton, C. E.; Nagase, S.; Power, P. P. *J. Am. Chem. Soc.* **2013**, *135*, 10720. (c) Bryan, A. M.; Merrill, W. A.; Reiff, W. M.; Fettinger J. C.; Power, P. P. *Inorg. Chem.* **2012**, *51*, 3366. (d) Boynton, J. N.; Merrill, W. A.; Reiff, W. M.; Fettinger J. C.; Power, P. P. *Inorg. Chem.* **2012**, *51*, 3212. (e) Ni, C.; Stich, T.A.; Long G. J.; Power, P. P. *Chem. Commun.* **2010**, *46*, 4466. (f) Merrill, W. A.; Stich, T. A.; Brynda, M.; Yeagle, G. J.; Fettinger, J. C.; De Hont, R.; Reiff, W. M.; Schulz, C. E.; Britt, R. D.; Power, P. P. *J. Am. Chem. Soc.* **2009**, *131*, 12693.
(3) (a) Lipschutz, M. I.; Yang, X.; Chatterjee, R.; Tilley, T. D. *J. Am. Chem. Soc.* **2013**, *135*, 15298. (b) Laskowski, C. A.; Morello, G. R.; Saouma, C. T.; Cundari, T. R.; Hillhouse, G. L. *Chem. Sci.* **2013**, *4*, 170. (c) Laskowski, C. A.; Miller, A. J. M.; Hillhouse, G. L.; Cundari, T. R. *J. Am. Chem. Soc.* **2011**, *133*, 771. (d) Iluc, V. M.; Hillhouse, G. L. *J. Am. Chem. Soc.* **2010**, *132*, 11890. (e) Iluc, V. M.; Hillhouse, G. L. *J. Am. Chem. Soc.* **2010**, *132*, 15148. (f) Andersen, J. S.; Iluc, V. M.; Hillhouse, G. L. *Inorg. Chem.* **2010**, *49*, 10203. (g) Laskowski, C. A.; Hillhouse, G. L. *J. Am. Chem. Soc.* **2008**, *130*, 13846.
(4) *Catalysts Without Precious Metals*; Bullock, R. M., Eds.; Wiley-VCH: Weinheim, Germany, 2010.
(5) Lipschutz, M. I.; Tilley, T. D. *Chem. Commun.* **2012**, *48*, 7146.
(6) Lipschutz, M. I.; Tilley, T. D. *Angew. Chem. Int. Ed.* **2014**, *53*, 7290.
(7) Ung, G.; Peters, J. C. *Angew. Chem. Int. Ed.* **2015**, *54*, 532.
(8) (a) Jones, C.; Hicks, J. *Organometallics* **2015**, doi: 10.1021/om501233f. (b) Hicks, J.; Hoyer, C. E.; Moubaraki, B.; Li Manni, G.; Carter, E.; Murphy, D. M.; Murray, K. S.; Gagliardi, L.; Jones, C. *J. Am. Chem. Soc.* **2014**, *136*, 5283. (c) König, S. N.; Schälde, C.; Maichle-Mössmer; Anwander, R. *Inorg. Chem.* **2014**, *53*, 4584. (d) Boynton, J. N.; Guo, J.-D.; Fettinger, J. C.; Melton, C. E.; Nagase, S.; Power, P. P. *J. Am. Chem. Soc.* **2013**, *135*, 10720.
(9) (a) Cai, I. C.; Lipschutz, M. I.; Tilley, T. D. *Chem. Commun.* **2014**, *50*, 13062. (b) Lin, C.-Y.; Fettinger, J. C.; Grandjean, F.; Long, G. J.; Power, P. P. *Inorg. Chem.* **2014**, *53*, 9400.
(10) Lipschutz, M. I.; Tilley, T. D. *Organometallics* **2014**, *33*, 5566.
(11) (a) Wu, J.; Nova, A.; Balcells, D.; Brudwig, G. W.; Dai, W.; Guard, L. M.; Hazari, N.; Lin, P.-H.; Pokhrel, R.; Takese, M. K. *Chem. Eur. J.* **2014**, *20*, 5327. (b) Laskowski, C. A.; Bungum, D. J.; Baldwin, S. M.; Del Ciello, S. A.; Iluc, V. M.; Hillhouse, G. L. *J. Am. Chem.*

Soc. **2013**, *135*, 18272. (c) Laskowski, C. A.; Morello, G. R.; Saouma, C. T.; Cundari, T. R.; Hillhouse, G. L. *Chem. Sci.* **2013**, *4*, 170. (d) Hruszkewycz, D. P.; Wu, J.; Green, J. C.; Hazari, N.; Schmeter, T. J. *Organometallics* **2012**, *31*, 470. (e) Iluc, V. M.; Hillhouse, G. L. *J. Am. Chem. Soc.* **2010**, *132*, 11890. (f) Laskowski, C. A.; Hillouse, G. L. *J. Am. Chem. Soc.* **2008**, *130*, 13846. (g) Dibble, B. R.; Sigman, M. S.; Arif, A. M. *Inorg. Chem.* **2005**, *44*, 3774. (h) Kitiachvili, K. D.; Mindiola, D. J.; Hillhouse, G. L. *J. Am. Chem. Soc.* **2004**, *126*, 10554. (i) Melenkivitz, R.; Mindiola, D. J.; Hillhouse, G. L. *J. Am. Chem. Soc.* **2002**, *124*, 3846. (j) Mindiola, D. J.; Hillhouse, G. L. *J. Am. Chem. Soc.* **2001**, *123*, 4623. (k) Bach, I.; Goddard, R.; Kopiske, C.; Seevogel, K.; Pörschke, K.-R. *Organometallics* **1999**, *18*,10.

(12) (a) Werncke, C. G.; Bunting, P. C.; Duhayon, C.; Long, J. R.; Bontemps, S.; Sabo-Etienne, S. *Angew. Chem. Int. Ed.* **2015**, *54*, 245. (b) Mo, Z.; Ouyang, Z.; Wang, L.; Fillman, K. L.; Neidig, M. L.; Deng, L. *Org. Chem. Front.* **2014**, *1*, 1040. (c) Ung, G.; Rittle, J.; Soleilhavoup, M.; Bertrand, G.; Peters, J. C. *Angew. Chem. Int. Ed.* **2014**, *53*, 8427.

(13) Zadrozny, J. M.; Xiao, D. J.; Long, J. R.; Atanasov, M.; Neese F.; Grandjean, F.; Long, G. J. *Inorg. Chem.* **2013**, *52*, 13123.

(14) Przyojski, J. A.; Arman, H. D.; Tonzetich, Z. J. *Organometallics* **2012**, *31*, 3264.

(15) Hill, M. S.; Kociok-Köhn, G.; MacDougall, D. J. *Inorg. Chem.* **2011**, *50*, 5234.

(16) (a) Nakajima, Y.; Ozawa F. *Organometallics*, **2012**, *31*, 2009. (b) Radonovich, L. J.; Eyring, M. W.; Groshens, T. J.; Klabunde K. J. *J. Am. Chem. Soc.* **1982**, *104*, 2816.

(17) Mathieson, T.; Schier, A.; Schmidbaur, H. *J. Chem. Soc., Dalton Trans.* **2001**, 1196.

(18) (a) Agenet, N.; Gandon, V.; Vollhardt, K. P. C.; Malacria, M.; Aubert, C. *J. Am. Chem. Soc.* **2007**, *129*, 8860. (b) Saito, S.; Yamamoto, Y. *Chem. Rev*. **2000**, *100*, 2901.

(19) (a) Young, D. D.; Deiters, A. *Angew. Chem. Int. Ed.* **2007**, *46*, 5187. (b) Tanaka, K.; Suzuki, N.; Nishida, G. *Eur. J. Org. Chem.* **2006**, *17*, 3917. (c) McCormick, M. M.; Duong, H. A.; Zuo, G.; Louie, J. *J. Am. Chem. Soc.* **2005**, *127*, 5030. (d) Gutnov, A.; Heller, B.; Fischer, C.; Drexler, H.-J.; Spannenberg, A.; Sundermann, B.; Sundermann C. *Angew. Chem. Int. Ed.* **2004**, *43*, 3795. (e) Yamamoto, Y.; Arakawa, T.; Ogawa, R.; Itoh, K. *J. Am. Chem. Soc.* **2003**, *125*, 12143.

(20) (a) Casitas, A.; Krause, H.; Goddard, R.; Fürstner, A. *Angew. Chem. Int. Ed.* **2014**, *54*, 1521. (b) Frazier, B. A.; Williams, V. A.; Wolczanski, P. T.; Bart, S. C.; Meyer, K.; Cundari, T. R.; Lobkovsky, E. B. *Inorg. Chem.* **2013**, *52*, 3295.

(21) Evans, D. F. *J. Chem. Soc.*, **1959**, 2003.

(22) Jafarpour, L.; Stevens, E. D.; Nolan, S. P. *J. Organomet. Chem.,* **2000**, *606*, 49.

(23) Chao, Y.-W.; Wexler, P. A.; Wigley, D. E. *Inorg. Chem.* **1989**, *28*, 3860.

(24) Bergbreiter, D. E.; Killough, J. M. *J. Am. Chem. Soc.* **1978**, *100*, 2126.

(25) Zadrozny, J. M.; Atanasov, M.; Bryan, A. M.; Lin, C.-Y.; Rekken, B. D.; Power, P. P.; Neese, F.; Long, J. R. *Chem. Sci.* **2013**, *4*, 125.

(26) Fulmer, G. R.; Miller, A. J. M.; Sherden, N. H.; Gottlieb, H. E.; Nudelman, A.; Stoltz, B. M.; Bercaw, J. E.; Goldberg, K. I. *Organometallics* **2010**, *29*, 2176.

(27) Hilt, G.; Vogler, T.; Hess, W.; Galbiati, F. *Chem. Commun.* **2005**, *1474.*

Chapter 6 Appendix

ADDITIONAL ORTEP DIAGRAMS

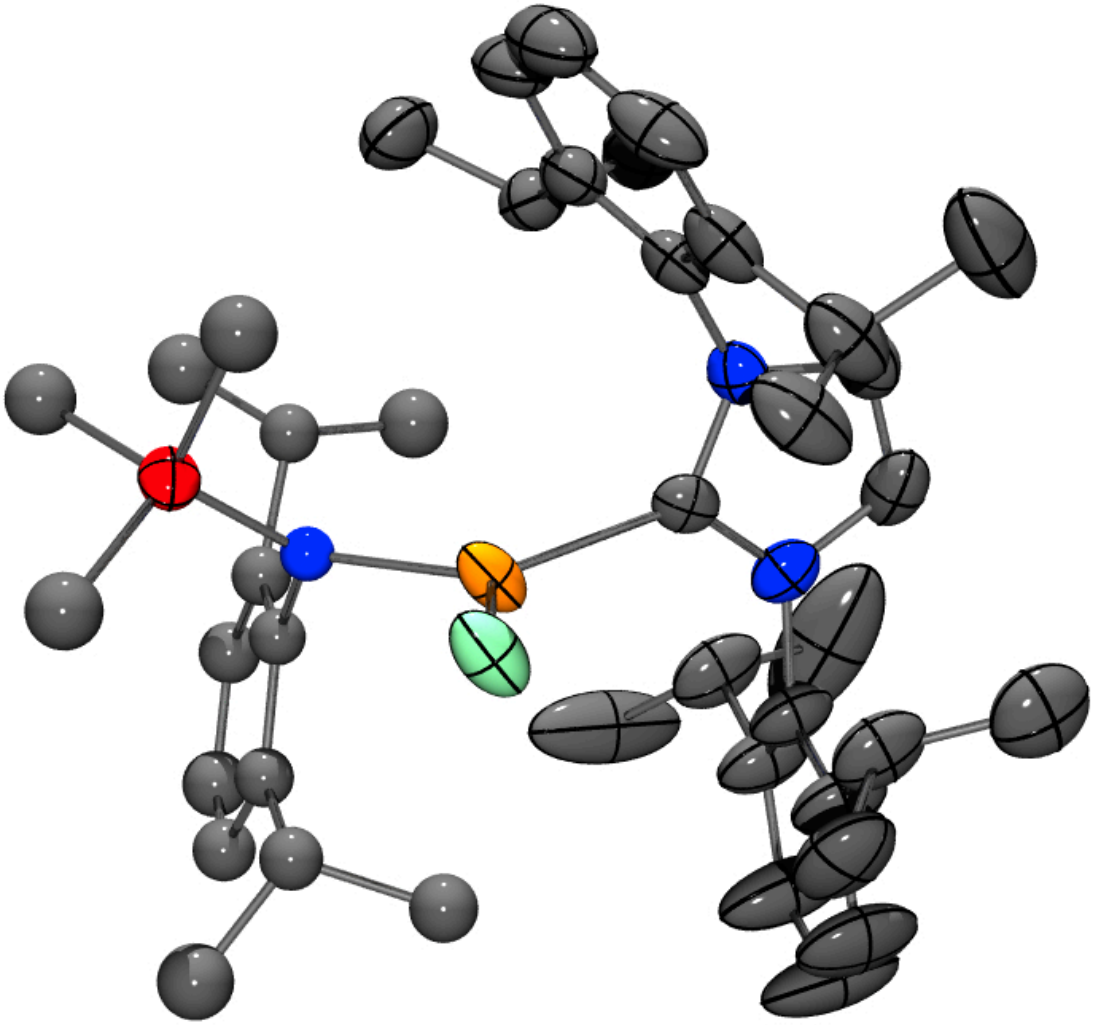

ORTEP diagram of (IPr)Cl-Fe[N($SiMe_3$)DIPP], with carbon atoms shown in dark grey, nitrogen in blue, silicon in red, iron in orange and chlorine in turquoise. The asymmetric unit contains two crystallographically independent molecules, each of which suffers from a partial molecule disorder of an entire ligand.

X-RAY DATA TABLES

Compound **1**:

Empirical formula	C42 H62 Fe N3 Si	
Formula weight	692.89	
Temperature	100(2) K	
Wavelength	0.71073 Å	
Crystal system	Monoclinic	
Space group	P2(1)/n	
Unit cell dimensions	a = 13.5867(10) Å	a= 90º.
	b = 18.2296(14) Å	b= 93.663(4)º.
	c = 17.4115(12) Å	g = 90º.
Volume	4303.7(5) $Å^3$	
Z	4	
Density (calculated)	1.069 Mg/m^3	
Absorption coefficient	0.407 mm^{-1}	
F(000)	1500	
Crystal size	0.13 x 0.11 x 0.05 mm^3	
Theta range for data collection	1.62 to 25.39º.	
Index ranges	-16<=h<=16, -21<=k<=21, -20<=l<=21	
Reflections collected	65639	
Independent reflections	7894 [R(int) = 0.0298]	
Completeness to theta = 25.00º	100.0 %	
Absorption correction	Semi-empirical from equivalents	
Max. and min. transmission	0.9879 and 0.9415	
Refinement method	Full-matrix least-squares on F^2	
Data / restraints / parameters	7894 / 0 / 439	
Goodness-of-fit on F^2	1.055	
Final R indices [I>2sigma(I)]	R1 = 0.0311, wR2 = 0.0752	
R indices (all data)	R1 = 0.0371, wR2 = 0.0783	
Largest diff. peak and hole	0.281 and -0.251 $e.Å^{-3}$	

Compound **5**:

Empirical formula	C42 H62 Fe K N3 Si	
Formula weight	731.99	
Temperature	100(2) K	
Wavelength	0.71073 Å	
Crystal system	Monoclinic	
Space group	P2(1)/c	
Unit cell dimensions	a = 11.0373(5) Å	a= 90º.
	b = 23.9854(9) Å	b= 102.689(2)º.
	c = 18.3141(8) Å	g = 90º.
Volume	4730.0(3) $Å^3$	
Z	4	
Density (calculated)	1.028 Mg/m^3	

Absorption coefficient	0.459 mm^{-1}
F(000)	1576
Crystal size	0.11 x 0.09 x 0.03 mm^3
Theta range for data collection	1.70 to 25.43º.
Index ranges	-13<=h<=13, -28<=k<=28, -22<=l<=20
Reflections collected	37820
Independent reflections	8622 [R(int) = 0.0369]
Completeness to theta = 25.00º	99.2 %
Absorption correction	Semi-empirical from equivalents
Max. and min. transmission	0.9864 and 0.9512
Refinement method	Full-matrix least-squares on F^2
Data / restraints / parameters	8622 / 0 / 448
Goodness-of-fit on F^2	1.023
Final R indices [I>2sigma(I)]	R1 = 0.0527, wR2 = 0.1402
R indices (all data)	R1 = 0.0640, wR2 = 0.1461
Largest diff. peak and hole	1.268 and -0.389 e.$Å^{-3}$

Compound **6**:

Empirical formula	C51 H71 Fe N4 Si	
Formula weight	824.06	
Temperature	100(2) K	
Wavelength	1.54178 Å	
Crystal system	Monoclinic	
Space group	P2(1)/n	
Unit cell dimensions	a = 12.1510(6) Å	a= 90º.
	b = 21.9509(11) Å	b= 95.241(3)º.
	c = 17.7959(9) Å	g = 90º.
Volume	4726.8(4) $Å^3$	
Z	4	
Density (calculated)	1.158 Mg/m^3	
Absorption coefficient	3.071 mm^{-1}	
F(000)	1780	
Crystal size	0.09 x 0.08 x 0.02 mm^3	
Theta range for data collection	3.20 to 68.43º.	
Index ranges	-14<=h<=14, -26<=k<=26, -21<=l<=21	
Reflections collected	89904	
Independent reflections	8662 [R(int) = 0.0443]	
Completeness to theta = 67.00º	99.7 %	
Absorption correction	Semi-empirical from equivalents	
Max. and min. transmission	0.9411 and 0.7696	
Refinement method	Full-matrix least-squares on F^2	
Data / restraints / parameters	8662 / 0 / 531	
Goodness-of-fit on F^2	0.890	
Final R indices [I>2sigma(I)]	R1 = 0.0311, wR2 = 0.0822	

R indices (all data)	R1 = 0.0349, wR2 = 0.0854
Largest diff. peak and hole	0.394 and -0.331 e.Å^{-3}

(IPr)Cl-Fe[N(SiMe$_3$)DIPP]

Empirical formula	C42 H62 Cl Fe N3 Si	
Formula weight	728.34	
Temperature	100(2) K	
Wavelength	0.71073 Å	
Crystal system	Triclinic	
Space group	P-1	
Unit cell dimensions	a = 13.2902(10) Å	a= 105.593(4) º.
	b = 16.1855(12) Å	b= 105.549(4)º.
	c = 22.2958(16) Å	g = 90.749(4)º.
Volume	4431.7(6) Å^3	
Z	4	
Density (calculated)	1.092 Mg/m^3	
Absorption coefficient	0.457 mm^{-1}	
F(000)	1568	
Crystal size	0.14 x 0.11 x 0.06 mm^3	
Theta range for data collection	0.99 to 25.46º.	
Index ranges	-16<=h<=16, -19<=k<=19, -25<=l<=26	
Reflections collected	74466	
Independent reflections	16283 [R(int) = 0.0452]	
Completeness to theta = 25.00º	99.9 %	
Absorption correction	Semi-empirical from equivalents	
Max. and min. transmission	0.9731 and 0.9388	
Refinement method	Full-matrix least-squares on F^2	
Data / restraints / parameters	16283 / 15 / 857	
Goodness-of-fit on F^2	1.082	
Final R indices [I>2sigma(I)]	R1 = 0.0800, wR2 = 0.2095	
R indices (all data)	R1 = 0.1018, wR2 = 0.2235	
Largest diff. peak and hole	1.139 and -1.105 e.Å^{-3}	